NON-DESTRUCTIVE EVALUATION OF WOOD UTILITY POLES USING COMPUTED AXIAL TOMOGRAPHY IMAGING

A Thesis
presented to
the Faculty of the Graduate School
at the University of Missouri-Columbia

In Partial Fulfillment
of the Requirements for the Degree

Master of Science

---

by
HOWARD DAVID THOMAS

Dr. Hani Salim, Thesis Supervisor

DECEMBER, 2006

The undersigned, appointed by the dean of the Graduate School, have examined the thesis entitled

NON-DESTRUCTIVE EVALUATION OF WOOD UTILITY POLES USING COMPUTED AXIAL TOMOGRAPHY IMAGING

presented by Howard David Thomas,

a candidate for the degree of master of Civil Engineering,

and hereby certify that, in their opinion, it is worthy of acceptance.

Dr. Hani Salim

Dr. James Baldwin

Dr. William H. Miller

All praise be to God the Father, His Son the Lord Jesus Christ and the Holy Spirit. All that I am and ever hope to be I owe to them. God the Father created me for His glory; Jesus His Son saved me and assured me an eternity in heaven with them by His death, burial and resurrection; and the Holy Spirit drew me into my personal relationship with them and provides guidance to me everyday. Every good and precious blessing that I have comes from them.

The most treasured earthly blessing that I have is a family that has lovingly supported me throughout my entire life. Each one of them has played an important role in forming who I am today; therefore I am dedicating this thesis to each one of them. Specifically I would like to thank my mother, father, grandmother, wife and daughters. Each of my parents provided me with a Christian model and they sacrificed to provide me with the love, support, training and encouragement that I needed to become a successful adult. My grandmother was always there to help me with whatever was at hand, whether it be homework, chores or providing me an after school snack. I value all of the time I have been able to spend with her throughout my life. My wife and daughters have willing sacrificed time with me so that I could see this long journey to completion. Without their love and encouragement, I would not have been able to continue. Thank you so much, you are the most precious treasure that I have.

ACKNOWLEDGEMENTS

I would like to acknowledge and thank the following people without whom I would have been unable to complete this research work and the ensuing thesis project. Firstly, Dr. William Miller, the person who conceived, designed and developed the prototype Nuclear Resonance Imaging Scanner that was being tested for this research project and Dr. James Baldwin who was my supervisor for the research work was and also my graduate school and thesis advisor when the research work was performed. Dr. Miller and Dr. Baldwin worked together to write the research plan for this work; obtain the necessary funding to perform the research; and supervise the testing and data collection. Dr. Baldwin assisted me greatly in the development of the predictive models that were used in the research. He provided me with much guidance during my graduate school course work and the work required for this research project. He also served as an example of the type of person I should be and how I should conduct myself as a Professional Engineer. Secondly, I would like to thank Mr. Richard Oberto, Research Electronic Technician. He provided essential help for this project by fabricating and assisting with the set up and trouble shooting of the instrumentation used for the testing. He also was a good friend during my time in graduate school. Lastly, I would like to acknowledge and thank Dr. Hani Salim my current thesis advisor and Ms. Jennifer Keyzer-Andre the Graduate Secretary in the Civil and Environmental Engineering Department. Without their help and support, I would have never been able to receive the necessary approval for the extension of the deadline required for the completion of this work. Every time that I needed something, Jennifer was so helpful in providing the needed assistance and Dr. Salim provided me with an incredible amount of helpful advice and encouragement this semester as I was writing and preparing to defend this thesis. I thank each of you again for everything that you did to assist me with my accomplishment of the completion of this project.

TABLE OF CONTENTS

LIST OF ILLUSTRATIONS

LIST OF TABLES

LIST OF ABBREVIATIONS

NON-DESTRUCTIVE EVALUATION OF WOOD UTILITY POLES USING COMPUTED AXIAL TOMOGRAPHY IMAGING

Howard David Thomas

Dr. Hani Salim, Thesis Advisor

ABSTRACT

Of the more than 130 million wooden utility poles in service, there are approximately 2 million that are replaced annually. A quick, yet accurate non-destructive method of evaluation of the in-service poles could provide substantial savings by reducing both the number of replacements and the number of failures. Research has been conducted to determine the possible use of Computerized Axial Tomography or CAT Imaging for pole evaluation. This involved correlating actual physical strengths determined by destructive testing with predicted strengths that were calculated using basic laws of material behavior and the cross-sectional scan image of wood density values that were measured using the prototype CAT scanner. The statistical analysis of the correlation between the measured and predicted strengths used a data set of 31 pole specimens.

A predictive model was developed assuming several different relationships between wood density and the assumed stress vs. strain diagrams. The predictive model also made adjustments for areas of decay and the average moisture content of the wood specimens. The most accurate predictive model developed had average error of estimate of approximately 24% and a coefficient of variation for the difference between the measured and predicted values of approximately 21%.

CHAPTER 1 – INTRODUCTION

1.1 Explanation of Problem

1.1.1 Purpose of Investigation

In 1980, the Electric Power Research Institute (EPRI) estimated that during the next 20 years more than 40 million wooden utility poles, worth more than $20 billion (in 1980 dollars) would be employed in the construction and maintenance of electrical transmission and distribution lines [1]. It was also estimated that of the 130 million poles then in service, approximately two million would require replacement annually at a cost of between $500 and $1,000 (in 1980 dollars) per pole. It is easy to see from these cost figures, that if you were able to reduce the number of utility poles that are being replaced unnecessarily; a substantial savings in the maintenance cost of utility lines could be realized. A non-destructive method of testing the poles that could more accurately determine if replacement was required would achieve this result. The purpose of this research was to develop a non-destructive analytical method which uses the density scans taken with a Computerized Axial Tomography (CAT) scanner to predict the strength of wooden utility poles and then develop and verify a statistical correlation for the analytical method using full scale destructive testing of actual wooden utility poles.

1.1.2 Background Information

Dr. William H. Miller [2,3,4], of the Nuclear Engineering Department at the University of Missouri-Columbia developed a prototype device for the non-destructive evaluation (NDE) of utility poles using CAT technology. CAT scans have long been

used by the medical profession to precisely produce 3-D images of internal structures without the need for harmful interior exploration. Therefore, this technology can be used to successfully predict the strength of the wooden utility poles based on the internal scan images that measure density.

The prototype device created a cross sectional scan image of a pole. This scan image contains values for the relative density of the wood at specific locations in the cross section. The research reported herein involves the correlation of these scan images with the actual physical strength of the poles. This correlation can be developed if the strength parameters of the wood for any given point can be related to the measured density of the wood at that same point. Once the strength parameters have been determined at every spatial location within the cross section, bending moment equations can be used to predict the strength of the pole.

1.1.3 Reasons for a Non-Destructive Test

The EPRI states in Technical Brief – RP 1352, "A practical, accurate device for determining the strength properties of new and in-service wood poles would be a useful tool to reduce the cost of new lines and increase the service life of existing lines [5]." The monetary savings resulting from a reliable non-destructive testing method for utility poles would be realized by several different means. The service life of some poles would be extended. These are the poles that by current methods of testing would be deemed unacceptable and be replaced, but after reliable testing would be found to have adequate strength and therefore additional life. On the other hand, poles that would need

replacement would be detected. This would result in a reduction in the quantity of unexpected pole failures, which would provide safer, more reliable service for the consumer and also save the utility companies money by reducing lost revenues caused by the down-time of lines and expensive emergency repairs. In addition, material use could be optimized for new poles by providing a more accurate estimate of a poles actual strength. The stronger poles could be used in situations that warrant more load capacity and the weaker poles would be used in lower loading conditions.

1.1.4 Current Methods to Predict Strength

A visual inspection for signs of decay and damage is the most basic inspection technique employed. This inspection technique is combined with all other methods of inspection. The American National Standard Institute (ANSI) has set minimum standards for the quality of new poles based on visual inspection. Many of the ANSI code requirements were established based on years of experience and observations, however few of the characteristics have ever been directly correlated to pole strength. In his paper titled, “Innovative Strength Testing Using Non-Destructive Evaluation (NDE) Devices”, Dr. Jozsef Bodig presents the following data. Figure 1 [6] reproduced from his lecture notes, plots pole bending strength versus maximum sum of knot diameter in a one-foot interval of pole length. The maximum sum of knot diameter in a one-foot interval of pole length is an ANSI criteria used to determine pole acceptance or rejection for in service use. As can be seen from this figure, several of the poles that did not meet ANSI requirements were stronger than other poles that did meet the ANSI requirements.

Douglas-Fir Poles

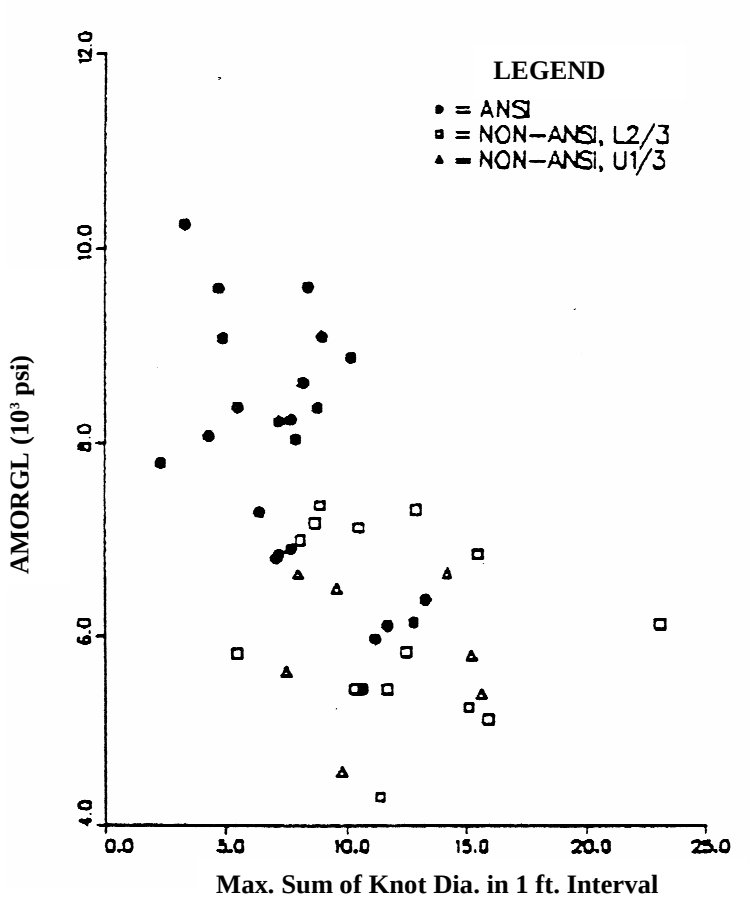

Figure 1 Relationship between Modulus of Rupture at Groundline Based on ANSI 05.1 Class Dimensions (AMORGL) and Maximum Sum of Knot Diameter in a One-Foot Interval

This illustrates the inherent difficulties of accurately predicting the acceptance of poles for use in service based solely a visual inspection.

After visual inspection, the oldest, simplest, and still the most frequently used method of inspection is referred to as tapping. Tapping involves lightly impacting the pole with a hammer and judging its durability by the sound made. A sound pole is indicated by a sharp ringing sound while a dull thud or deadened sound indicates decay. Although useful for locating decay, this test is highly subjective, does not predict strength and is therefore unreliable for determining if replacement is necessary. Boring is another simple test often performed on the poles. It involves drilling a hole into the wood to locate any areas of decay. It is physically damaging to the pole but not much more reliable than "tapping" for determining the need for pole replacement.

Some of the more refined methods used for testing are the Pilodyne Wood Tester, the Pol-Tek device, Shigometry, X-Ray Radiography, and Ultrasonics. Shigometry requires boring into the pole and placing a current probe at the point of interest. The amount of decay in the wood at this point is then determined by measuring the resistance of the wood to a pulsed electric current. Not only is the boring damaging to the pole, but also any determination about the strength of the pole is made subjectively based on the extent of the decay. Decay in the poles is usually very spotty and therefore quite difficult to locate and if there are no signs of external decay, the location of internal decay is nearly impossible. Considering these limitations, it is unreasonable to expect an accurate determination of a pole's need for replacement by using this test.

The Pilodyne Wood Tester predicts the poles bending strength using an impact reading taken on the outer shell of the pole. By measuring the depth of penetration of a

steel pin impacting against the wood, a prediction is made of the poles actual bending strength. The test is able to roughly predict the poles strength but it is a much better indicator of the moisture content of the wood.

The Pole-Tek device uses sonic vibrations to detect the presence of internal decay. It has been found to work well on certain species of wood but provides unsuitable results on other species. Like most of the other tests mentioned, this method only locates areas of decay in the pole. No determination is made about the pole's strength.

X-rays can be used to non-destructively make two-dimensional images of a pole. The 2-D images locate the areas of decay in the pole in the longitudinal direction, but tell nothing about the location of decay within the cross-section. The location of decay within the cross-section has a significant effect on the pole's bending strength.

The most reliable, commercially available method currently in use for non-destructive evaluation of utility poles is a method that uses ultrasonics. With this method an ultrasonic wave is created in the pole by dropping a small pendulum against the head of a nail that was previously driven into the pole. By measuring the characteristics of the ultrasonic wave resulting from the impact, a prediction of bending strength is made. Researchers at Colorado State University performed a large number of material tests on wood utility poles to develop a statistical correlation between the bending strength of the pole and the measured characteristics of the sound wave. A new device called PoleTest was developed from this research and is currently being marketed by a company called

Engineering Data Management, Inc. (EDM). Published data indicates that the Modulus of Rupture at Ground Line (MORGL), which is a pseudo maximum fiber stress, can be predicted with a standard error of estimate (SEE) between 13% and 20% depending upon the wood species.

The PoleTest device has several inherent limitations however. Decay in the poles tends to be in localized regions. However, the PoleTest device has no means to determine the position of that decay in the pole and the bending strength of a pole is dependent upon the location of the decay in its cross section. With the PoleTest device, the strength of the pole is predicted based on one set of readings taken at only one location on the pole. Therefore the device is only able to predict one value of strength for the entire pole. This means the character of the pole is being described by an average of the sum of the parts. Even considering the drawbacks, the extensive database of actual destructive tests makes the PoleTest device currently the most reliable method for determining the strength of in-service utility poles that is commercially available. For this reason, the EDM PoleTest device was used during this research to obtain predicted values of pole strength for comparison with the predicted values from the CAT device and the actual strengths obtained from the destructive tests.

1.2 Proposed Solution to the Problem

1.2.1 Overview of CAT Technology

The application of CAT in the field of wood science has been demonstrated by several different applications. Modified CAT scanners have been used to image growth

rings, defects, and decay in living trees. It has also been proposed that CAT scanners be used to determine growth patterns in timber to optimize cutting at the mill. Utilization of CAT technology for the purpose of non-destructive evaluation of in service utility poles is a logical extension of these applications.

The CAT scanner works on a simple premise. The absorption of radiation as it passes through an object varies depending on the density of the object. The most familiar application of this phenomenon is the radiograph (commonly referred to as an X-ray). In this use, a source of X-radiation is located on one side of the object and film is placed on the other side. The radiation passes through the object in varying amounts and develops the film. This produces an image of the objects internal structure. The procedure however provides only a two-dimensional image of the object. It provides no information about how the density of the object varies with the depth. The depth is the dimension of the object in the direction of the radiation. To obtain depth information, the technique of computed axial tomography (CAT) is used. This provides a two-dimensional, cross sectional image of the object of interest as if it has been sliced open perpendicular to its axis. By obtaining the cross sectional images at various planes up and down the axis of the object, three-dimensional information is obtained.

1.2.2 Application of CAT Technology to this Problem

There is one inherent advantage that the CAT scanner has over all of the other methods currently used for evaluation. It is the only method, which can non-destructively provide the exact location of decay within the pole. The CAT scanner provides the

location of the decay within the cross section with each scan, and the pole can be scanned at any number of planes along its length. Hence, with enough scans all defects in the pole can be located. However, in practical applications, it would not be economical to complete a three dimensional image of a pole. Judgment along with visual inspection is used to determine critical areas that are probable failure sections. The sections that warrant the most serious investigation are around the pole's ground line. This area is not only subjected to the highest stresses but is also more susceptible to decay. Using the images obtained from the scans of the suspect cross sections, basic laws of material behavior can be used to predict the pole's critical bending strength.

The cross sectional images are produced by beams of radiation passing through the object along parallel lines from a radiation source to a detector. (See Figure 2) The detector measures the amount of radiation coming through the object in each of the beams. Each of these measurements along a line is known as a ray-sum. If for example, a void were present in line with one of the beams, the ray-sum would be greater considering everything else constant because more radiation would be allowed to pass through. The collection of parallel ray-sums is known as a projection. More information is needed than is provided by one projection, so the source and the detector are rotated around the object through some fixed angle, obtaining a projection for each position. The number of ray-sums taken per projection and the number of projections taken around the object affect the spatial resolution of the resulting image. The images that are used in the medical field require a high resolution (approximately 1mm).

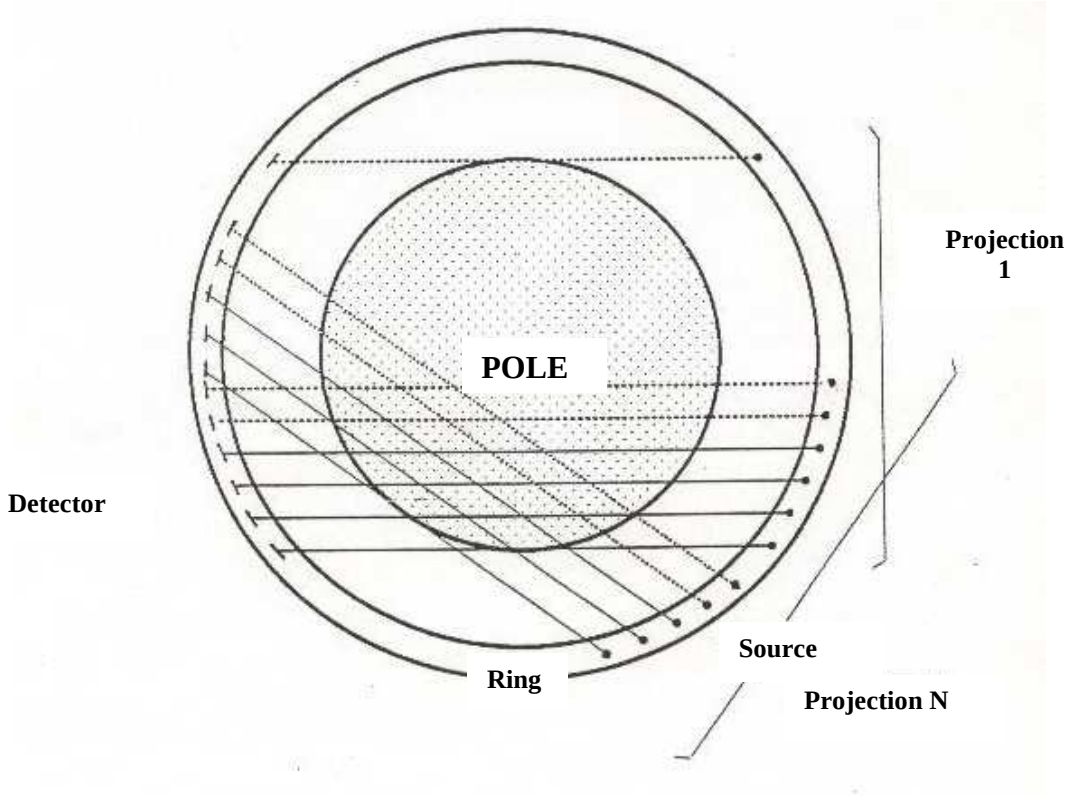

Figure 2 Scanner Schematic

To obtain images of this resolution, hundreds of thousands of ray-sums are need. The CAT scanner used for this research uses several hundred ray-sums and generates an image with a resolution of approximately 2/3 inch.

A computer then processes the data collected concerning the orientation and the magnitude of each of the ray-sums. Many mathematical calculations are made in order to produce a cross sectional image. Every digital image is composed of a 21 x 21 matrix of values representing the specific gravities of the wood in a corresponding matrix of equal

area square elements in the cross section. (See Figure 3) Therefore, each of these elements contains an average value for the specific gravity of the wood at a definite location. Since the image is always made up of the same number of elements, the dimension of each square area is a function of the pole diameter.

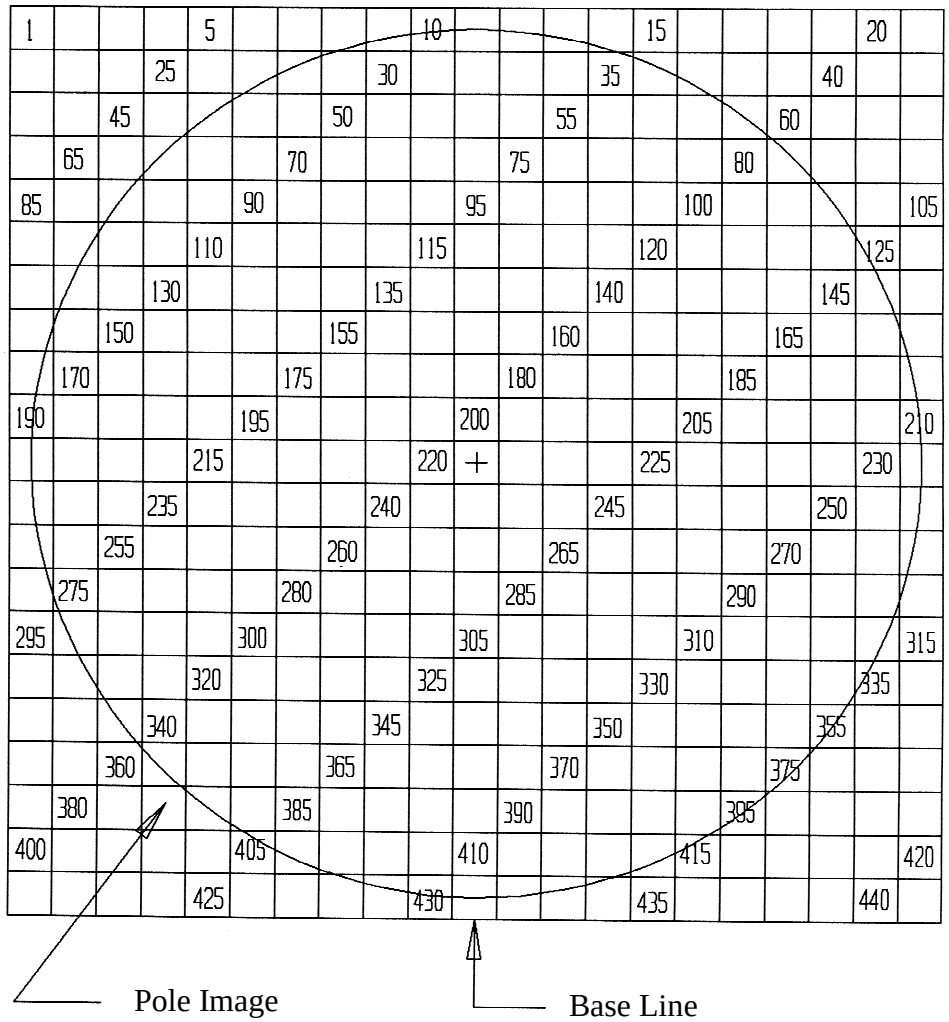

Figure 3 Scan Schematic

1.2.3 Wood Strength versus Density

Once the specific gravity for each element contained within the cross section is known, a functional relationship between specific gravity and the material properties for the wood is needed. The bending strength of a pole is calculated by summing across the whole cross section the product of the normal stress, the area and the distance from the neutral axis for each of the individual elements in the cross section. It is the relationship between the elements ultimate normal stress and its specific gravity that is needed to predict ultimate bending strength. If this connection can be made and the relationship between the wood's stress and strain is known, then with bending moment equations, the poles ultimate bending strength can be predicted.

The mechanical properties of wood are affected by many different variables, such as species, density, growth rate, orientation of the grain, and moisture content. Since it is the specific gravity or the density of the wood that is being measured with the scanner, the main interest of this research is how the woods strength properties are related to density. A growing tree has three distinct zones, the bark, a lightly colored zone just beneath the bark called the sapwood, and a darker colored inner zone called the heartwood. The growth of the tree takes place by forming new layers of cells in a thin band of tissue called the cambium layer on the outer edge of the sapwood. As the tree increases in diameter, the inner cells in the sapwood cease their function of sap conduction and food storage and form inactive hardwood.

For the past 100 years or more, data has been collected for different species of "new" (non-decayed) wood correlating the mechanical properties with its specific gravity.

These correlations are semi-empirical fits of experimental data. See Table I [7] for one set of the correlations.

Test and Property	Green		12% M.C.	
	a	*b*	*a*	*b*
Static bending				
Stress at proportional limit, psi	10,200	1.25	16,700	1.25
Modulus of rupture, psi	17,600	1.25	25,700	1.25
Modulus of elasticity, 10^6 psi	2.36	1.00	2.80	1.00
Work to ultimate load, in-lb/in.^{3}	35.6	2.00	32.4	2.00
Total work, in.-lb/in.^{3}	103	2.00	72.7	2.00
Impact bending				
Height of drop to failure, in.	114	1.75	94.6	1.75
Compression parallel to grain				
Stress at proportional limit, psi	5,250	1.00	8,750	1.00
Ultimate crushing stress, psi	6,730	1.00	12,200	1.00
Modulus of elasticity, 10^6 psi	2.91	1.00	3.38	1.00
Compression perpendicular to grain				
Stress at proportional limit, psi	3,000	2.25	4,630	2.25
Hardness				
Load on end grain, lb	3,740	2.25	4,800	2.25
Load on side grain, lb	3,420	2.25	3,770	2.25

Specific gravity of oven-dry wood, based on the volume at the moisture condition indicated.

Y	Species Group	*a*	*b*	*r*	C.V., %
E_L	S	7.3544×10^6	1.7315	0.898	16.65
	H	3.4196×10^6	1.0703	0.933	21.52
E_R	S	3.1485×10^5	9.9329×10^{-1}	0.729	18.97
	H	3.7078×10^5	1.1885	0.965	16.31
E_T	S	2.8666×10^5	1.4342	0.783	22.46
	H	2.4055×10^5	1.5917	0.988	11.23
G_{LR}	S	2.1881×10^5	7.9478×10^{-1}	0.543	24.95
	H	2.8253×10^5	1.1634	0.947	19.99
G_{LT}	S	1.8466×10^5	6.7476×10^{-1}	0.477	25.43
	H	2.2218×10^5	1.2606	0.947	21.32
G_{RT}	S	4.1156×10^4	1.5085	0.550	43.19
	H	8.1395×10^4	1.4058	0.915	28.70

Legend:
S = softwoods,
H = softwoods,
r = correlation coefficient. (All correlations significant at 1% level.)
C.V. = coefficient of variation.

Data of the Form: $Y = a D^b$
where: D = specific gravity
Y = physical property
a,b = coefficients from table

Table 1 Semi Empirical Relationships for the Mechanical Properties of Wood

It is interesting to note that the ultimate compressive stress and the modulus of elasticity are linear functions with respect to specific gravity. Typically, coefficients of variation for these semi-empirical fits range within 15% to 25%. Hence, mechanical properties of new wood are fairly well defined. For this application however, the wood in the poles under consideration is not new wood. The device will be used almost exclusively on in-service poles. These poles are exposed to a vastly varying array of surrounding atmospheric conditions that promote wood decay. Because of this, it is important to know how the decay affects the stress capacity of the wood. Toole [8,9] has researched this by subjecting like wood samples to accelerated decay in the laboratory and plotting the reductions in specific gravity and in crushing strength as functions of decay time. His research and other research done in this area indicate that small reductions in density due to decay result in much larger decreases in wood's mechanical properties. (See Figure 4)

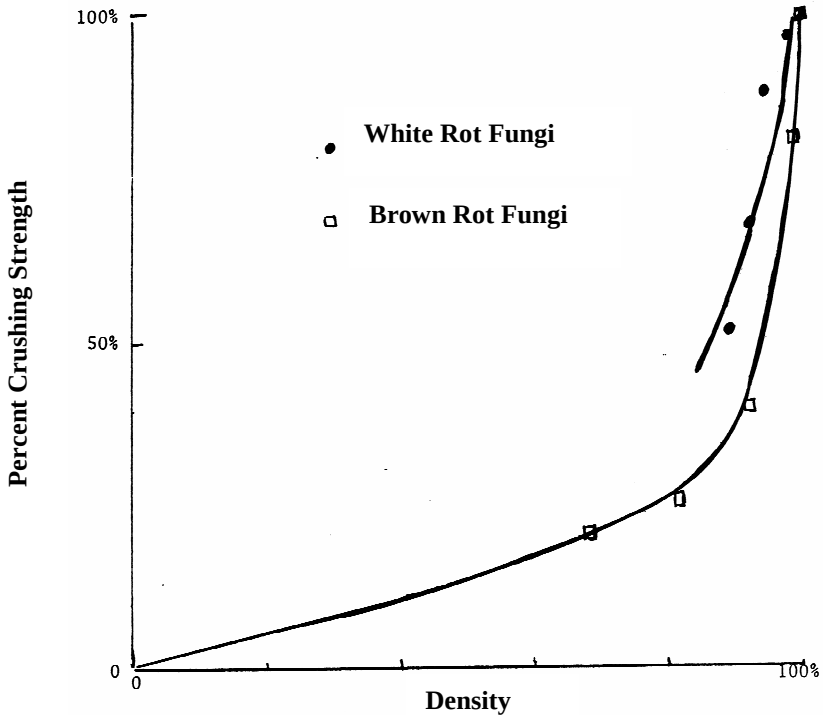

Figure 4 Percentage of Remaining Crushing Strength vs. Wood Density Due to Fungal Decay

1.2.4 Other Variables That Affect Wood Strength

The effect of moisture content on the predictive model is of interest also. Studies of strength as a function of moisture content indicate that for moisture contents below the moisture content of approximately 20%, the strength of wood increases as it becomes drier. [7,10] Above this moisture content however, the strength is relatively unaffected. (See Figure 5)

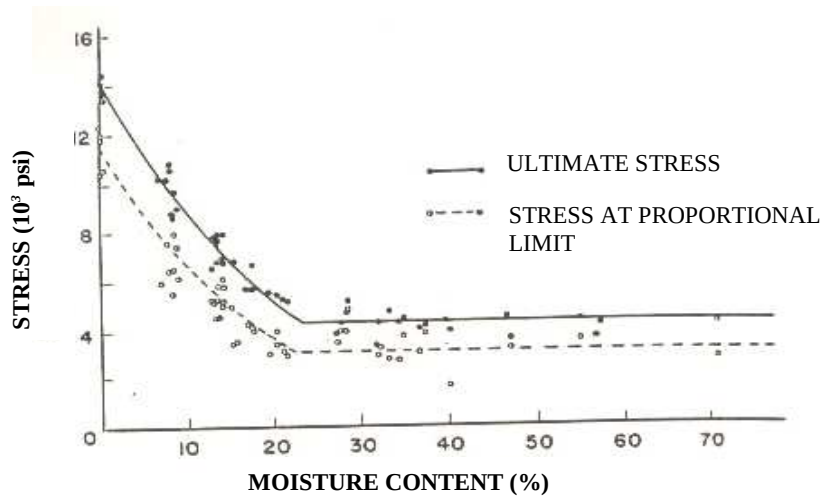

Figure 5 Relationship Between Compression Parallel to Grain Properties and Moisture Content

Since in-service poles typically have moisture contents near the saturation point at ground level (where they normally fail) this effect may not be significant. No data is available on the effect of moisture content on decayed wood. Of particular concern is the possibility of the decayed wood absorbing a relatively large quantity of water and registering an erroneously high density value. The possible error in estimating wood density accompanied by the effect of moisture content on the strength characteristics of decayed wood might constitute a possible source of error in the predictive model. To prevent this, the density values might need to be corrected for moisture content.

1.2.5 Plan of Research

The desire of this research was to develop a predictive model that could accurately predict a poles ultimate bending strength based on the scan images obtained from the prototype CAT scanner. To develop an algorithm for the predictive model, certain tasks had to be performed. These task were as follows,

1. The analytical equations to be used for the predictive model were derived. A different set of equations was derived for each trial set of assumptions to be tested. The different trial set used for the models assumed various stress versus strain relationships for the wood and also various relationships between wood density, moisture content and wood strength.
2. The testing procedure for the destructive physical test of the poles and the data collection was written.
3. An existing data collection program previously used in another civil engineering research project was modified to collect and store the data required for this testing program and calculate and store the actual ultimate strength of the pole from the test.
4. Students from the Nuclear Engineering Department scanned the poles and collected moisture content readings at seven locations for each pole. For comparison, a number of the poles were also tested with the EDM PoleTest device.
5. Destructive physical test were performed on the poles and data was measured and collected.

6. A computer program was written to calculate the predicted strength of a pole using each set of derived analytical equations from the trial set of assumptions and the scan and moisture data collected by the Nuclear Engineering Department.
7. A statistical analysis was performed for each trial set of assumptions to find which set of equations and parameters provided the best statistical correlation between actual and predicted ultimate strength. The best statistical correlation was determined by the lowest SEE.

1.3 Thesis Preview

Again, **t**he purpose of this research was to develop a non-destructive analytical method which uses the density scans taken with a CAT scanner to predict the strength of wooden utility poles and then develop and verify a statistical correlation for the analytical method using full scale destructive testing of actual wooden utility poles. A more detailed presentation on the testing and collection of the data that was required for this research project is presented in Chapter 2, followed by a detailed description of the development of the predictive model in Chapter 3. Chapter 4 presents the statistical analysis of the modeling results when compared with the results from the destructive testing and Chapter 5 provides a summary of the thesis with the conclusions and recommendations. Complete data sets of the physical destructive test data for Pole Specimens 40 and 42 are reproduced in Appendix 6.1 for reference.

CHAPTER 2 – TESTING AND COLLECTION OF DATA

2.1 Introduction

Dr. William H. Miller and Dr. James W. Baldwin developed the plan for this research project in 1986 and data collection started February 23, 1988. Funding for the research was provided by the State of Missouri through the Missouri Research Assistance Act, Missouri Public Service Company, Kansas City Power and Light, Union Electric Company (Ameren UE), Osmose Wood Preserving, Inc. and St. Joseph Light and Power. The poles used for testing were obtained from Boone Electric Cooperative in Columbia, Missouri. Most of the poles were distribution-sized poles removed from service following rejection by traditional testing methods. However, some of the poles tested were tops of poles. These top sections were sections of poles that were cut off of other poles at the small or top end of the pole instead of the large or bottom end of the pole. The poles that were top sections had a much larger occurrence of knots and other discontinuities than the other poles that were base sections.

2.2 Collection of Scan Images and Moisture Data

Nuclear Engineering students were in charge of obtaining the scan images for the poles. Each pole was scanned at seven locations. The first location was established at the poles ground-line. The ground-line for an existing pole was set at the position that the pole left the ground and for a new pole the ground-line was arbitrarily established.

Three additional scans were taken on each side of the ground-line in six-inch intervals. The following system was used for labeling the scans and scan locations. (See Figure 6)

- 00 – Groundline
- 11 – Groundline + 6”
- 12 – Groundline + 12”
- 13 – Groundline + 18”
- 01 – Groundline - 6”
- 02 – Groundline - 12”
- 03 – Groundline - 18”

Figure 6 Picture of Scan Locations

The scan files were labeled and saved individually using a combination of the pole number and the scan location number. Assuming that each scan was descriptive of the pole over a distance of six inches, the density of the pole was known over a 42" breadth. Scan locations were marked with spray paint around the circumference of the pole and a baseline was marked along the length of the pole. The baseline provided a known point of reference for the orientation of the cross-sectional scan images. Every scan image was stored separately in a sequentially formatted file. Each of the scan images was contained in a 21x21 data matrix. (See Figure 3) A graphical comparison of two scan image files from Pole 40 is shown in Figure 7 on the next page. Please note the lower densities in image 4003 and that it was the failure section during the destructive testing.

Moisture content data were also taken at each of the seven scan locations. The readings were taken in four quadrants around the circumference of the pole at depths of 0.5", 1.5", and 2.5" using a Delmhorst moisture detector. Additionally, the PoleTest device was used to predict the strengths of 22 of the 35 poles tested. Moisture content data and the strengths predicted by the PoleTest device were stored in a separate file for each pole.

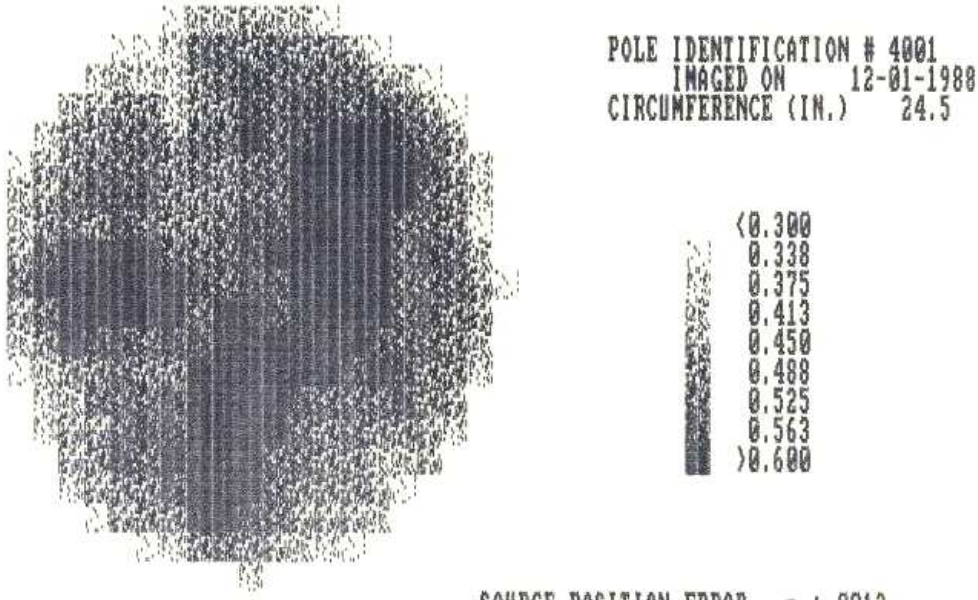

SOURCE POSITION ERROR = +.0012
DETECTOR POSITION ERROR = +.0007

(b) MIN+ MIN- MAX+ MAX- STRENGTH QUIT

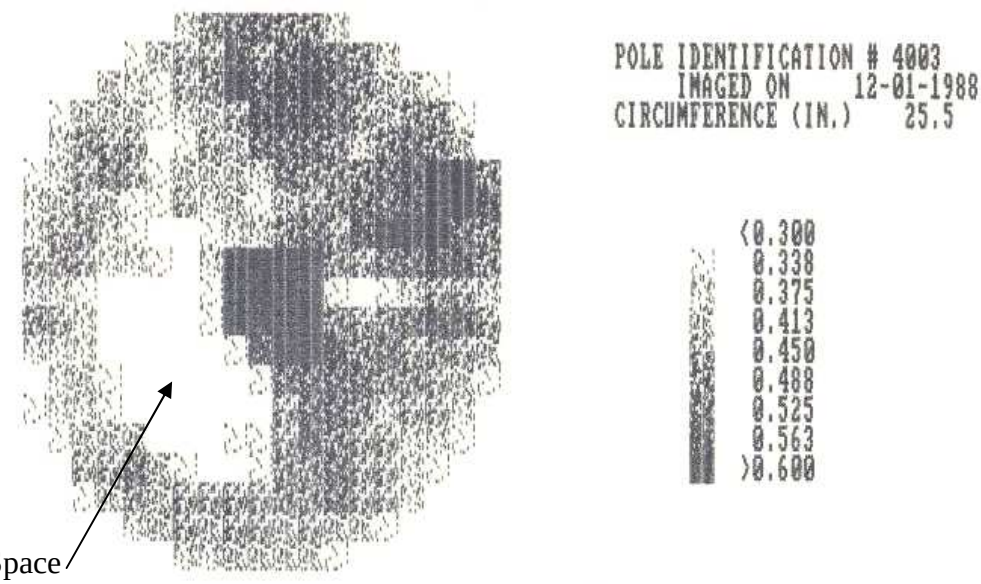

SOURCE POSITION ERROR = -.0004
DETECTOR POSITION ERROR = +.0008

(a) MIN+ MIN- MAX+ MAX- STRENGTH QUIT

Figure 7 Comparison of Scan Images (Pole 40)
(a) w/o void in cross-section
(b) w/ void in cross-section

2.3 Description of Testing Apparatus

The ASTM D1036 Machine Method of testing was used for testing the poles. In this method of testing, the pole was subjected to a simply supported, four-point loading configuration. (See Figure 8 and Figure 9)

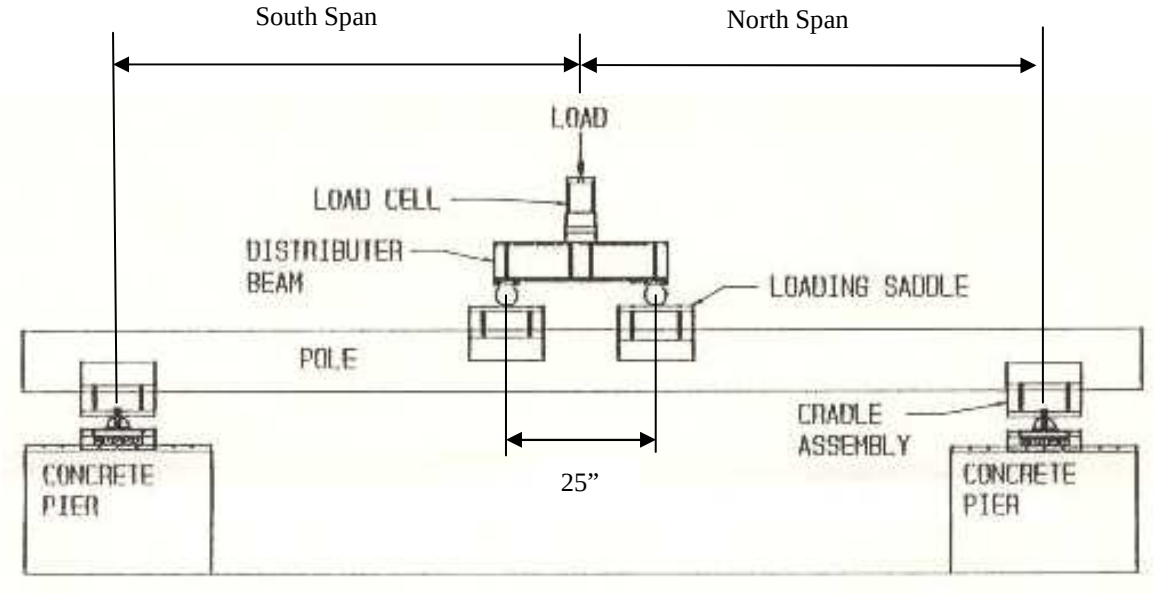

Figure 8 Drawing of Testing Apparatus

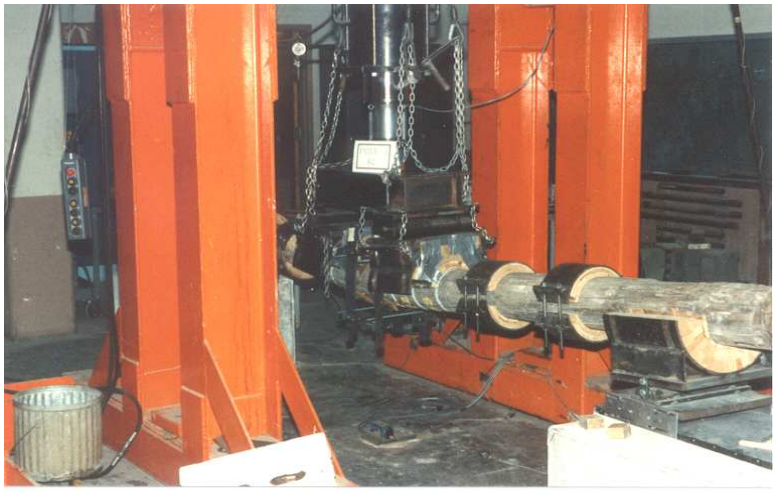

Figure 9 Picture of Testing Apparatus

The two point loads of equal magnitude were placed at an equal distance from each end support. This produced a constant moment between the two point loads. The end supports were cradles, which acted as roller supports. (See Figure 10)

Figure 10 Picture of End Support

To adjust the cradle's diameter for each individual pole, specially cut wooden blocks were used. (See Figure 11) The span length of the pole could be adjusted by repositioning the cradles, but the pole was always placed so that it extended across the full width of the cradles.

Figure 11 Picture of Adjustment Blocks

The load was applied to the pole using a manually controlled hydraulic ram, held firm by a rigid frame testing structure. (See Figure 12) The load from the ram was split into two equal point loads by a rigid distribution beam. (See Figure 8)

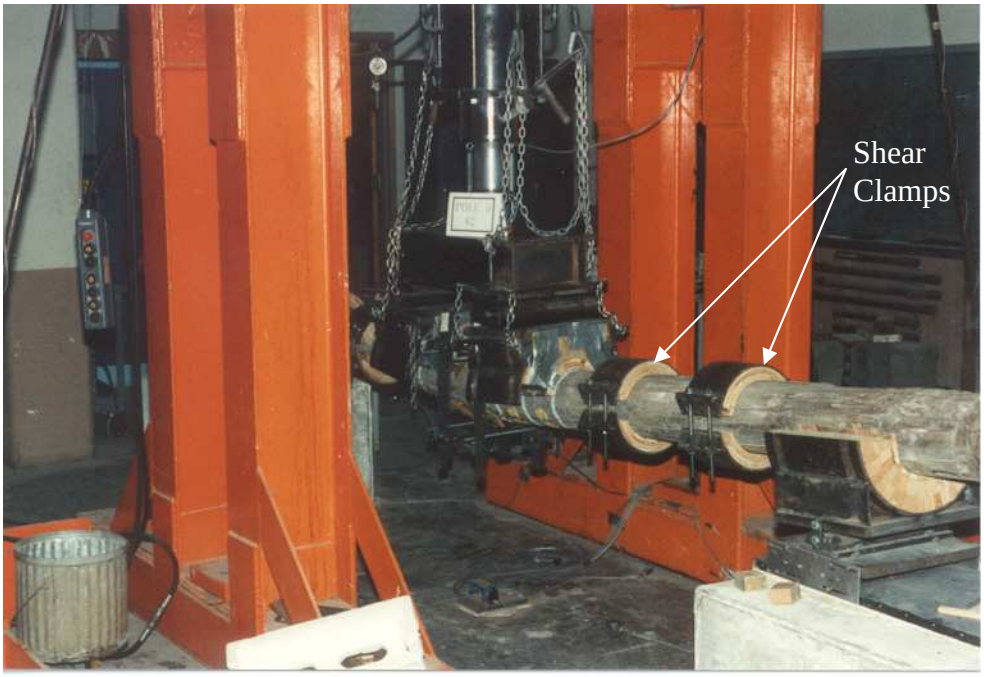

Figure 12 Picture of Rigid Frame Testing Structure

The rigid distribution beam was a rectangular flat surface with two 4" cylindrical rollers attached to the bottom. (See Figure 13) One of the cylindrical rollers was securely welded to the frame but the other was made able to move in a direction perpendicular to load along the length of the pole. This was accomplished by placing the bolts in each of the rollers ends through slotted holes. The load from the ram was centered on the top surface of the frame and was transferred by rollers to the center of a pair of saddles, which rested on the pole. (See Figure 14) The two saddles that rested on top of the pole could also be adjusted like the cradles to conform to different pole sizes.

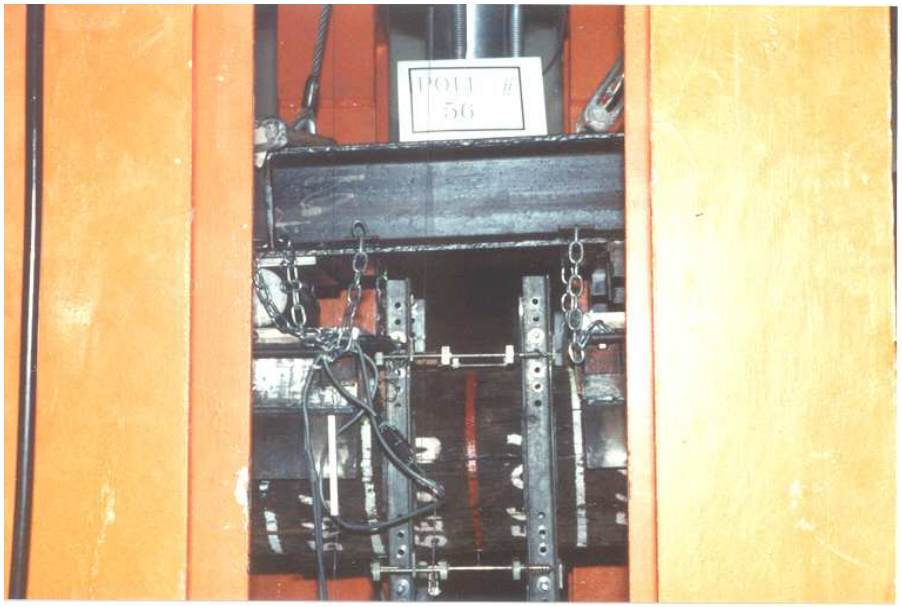

Figure 13 Picture of Rigid Distribution Beam

Figure 14 Picture of Load Saddle

2.4 Explanation of Testing Procedure

To prevent any unnecessary deviations in the test data due to variations in the testing routine, the testing procedure was kept as consistent as possible during the research. Taking into account the curvature in the pole and also the location of any areas of decay shown by the scan images, judgment was used to select a rotational orientation for the pole, which would most likely produce symmetrical bending about the vertical axis of loading. The rotational orientation of the pole was measured looking from north to south with the positive direction going counterclockwise. (See Figure 15) The cradles were adjusted to accommodate the size of the pole and the pole was placed in the cradles such that the ground-line was located directly below the load point and the pole was at the rotational orientation that would most likely result in symmetrical bending. A plumb line was used to locate the center scan image directly below the load center. The south cradle upon which the large or the below ground end of the pole always rested, was then positioned such that the south span length was a maximum. The south span length was defined as the horizontal distance from the center of the south cradle to the center of the load center. By making this a maximum, the span length was equal to the poles original in ground embedment length. The north cradle was then adjusted so that the north and the south span lengths were as close as possible to equal. (See Figure 8)

Once the pole was positioned in the cradles correctly, wedges were placed under the rollers on each end to prevent the pole from moving during the rest of the setup procedure. Next the rotation frames were put on the pole.

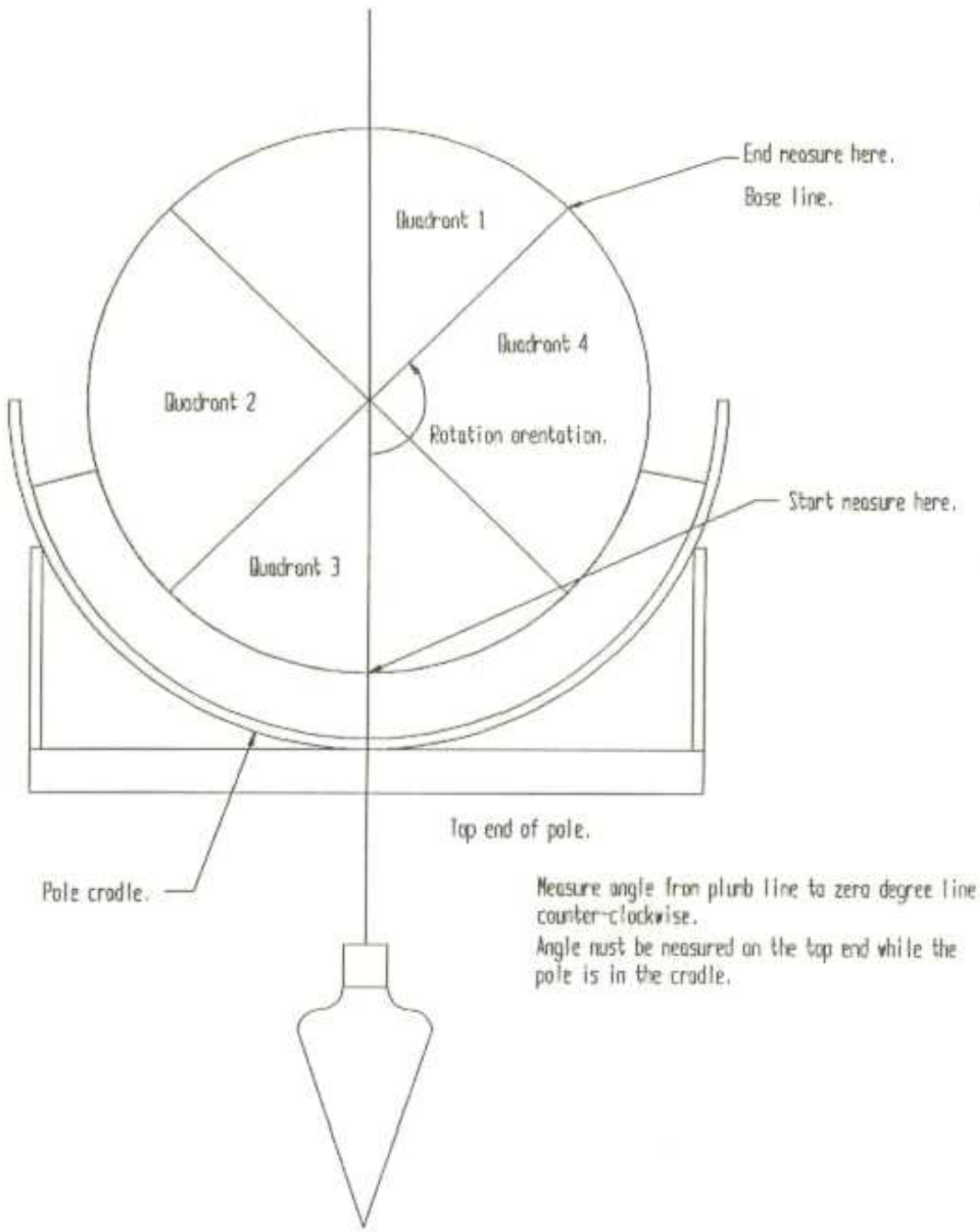

Figure 15 Measurement of Rotational Orientation of Pole (Looking South)

The frames were placed so that the 8-inch gage length was centered over the pole's ground-line. Extreme care was taken to insure that the legs of the rotation frame were plumb in both directions and that the slider arms were level. This was done so that all of the deflections being measured were perpendicular to the plane of the loading and the deflections on the each side of the neutral axis were at the same level. (See Figure 13) Upon securing the rotation frames, the ensuing step was to put on the load saddles. The size of the saddles circumference was adjusted so that they sat snugly on the pole and they were placed at an equal distance on each side of the ground-line such that the dimension between the centers of each saddle was 25 inches. A level was then used to check if they were sitting on the pole level. Shear clamps were then installed between the supports and the load saddles. The shear clamps were tightened down to provide additional shear reinforcement for the pole to help insure against the poles failing in horizontal shear. The next step was to lower the load frame down and to center the rollers over the center of the saddles. Once the load frame was positioned correctly, the hydraulic ram was able to be lowered and contact the load frame in the center. When this was done the pole was in position for the test.

The following step was to set up the electronic instrumentation for the test. The electronic equipment used for data collection during the test included, 4 clip gages, 3 cylindrical potentiometers, a 100 kip load cell, an IBM PC Portable computer, a 10 channel Vishay signal conditioner, and a HP Harrison power supply. (See Figure 16)

Figure 16 Picture of Testing Equipment

The 100 kip electronic load cell was located between the hydraulic ram and the flat surface of the load frame and was used to measure the load applied to the pole. The load cell was fabricated by the civil engineering shop and calibrated in a beam-balance testing machine. The load acting through the cell was measured by the use of a four-arm arrangement of electronic resistance strain gages. The gages were attached to the inside walls of the cylindrical vessel so as to measure only axial strain and cancel out any effects due to bending.

The other data that was collected using electronic instrumentation was the mid-span deflection, the horizontal movement of the ends and the strain diagram for the pole. The mid-span deflection and the horizontal movement of the end supports was measured by attaching a strand of nylon string and a weight to the pole and wrapping the string around the shaft of cylindrical potentiometers. The potentiometers were fixed against translational movement, but the shaft would rotate causing a linear change in resistance, which was measured and converted to deflection.

The rotation frames attached to the pole near the center were used to plot the strain diagram for an eight-inch section at the center. (See Figure 13) The frames measured axial deflections in the pole caused by bending. The deflections were measured using clip gages and slider arms. The deflections were measured on both sides of the pole and at two levels. Each level was symmetrical about the center of the pole and on opposite sides of the neutral axis. Knowing the gage length and using the corresponding values for deflection, the strain profile for the cross section was plotted. Symmetrical bending should form a plane using the four measured points of strain.

The clip gages used in the rotation frame were calibrated using a micrometer so that a change of 0.1 inch produced a measurable change in voltage of 10 millivolts. A total deflection of 0.2 inch could be measured by each gage. Before each pole test, the calibration was checked on each gage and then the gages were inserted into the rotation frame.

2.5 Discussion of Data Acquisition and Storage

The Vishay signal conditioner collected eight channels of electronic signals from the test. The signal inputs were then translated, converted and stored as electronic data files on the computer using a Quick Basic computer program called Poletest. This program was written to convert the electronic readings from the electronic instrumentation via the Vishay signal conditioner into the desired measurements collected from the test.

The eight channels of data and the order in which they were measured and stored were as follows;

1. Channel 0 - Test Load
2. Channel 1 - Midspan Deflection
3. Channel 2 - East-Top Rotation Frame Deflection
4. Channel 3 - East-Bottom Rotation Frame Deflection
5. Channel 4 - West-Top Rotation Frame Deflection
6. Channel 5 - West-Bottom Rotation Frame Deflection
7. Channel 6 - South end Translation
8. Channel 7 – North end Translation

This data was stored in a text format file that was named by the user. An additional text format file was generated and stored by the program that contained the following data;

1. Pole number
2. Date and time of the test
3. Eight different calibration factors
4. North span length
5. South Span length
6. Rotational Orientation of the pole
7. Location of pole fracture
8. Measured circumference at the fracture location
9. Calculated diameter of the pole at the fracture location
10. Calculated moment of inertia of the pole at the fracture location
11. Calculated maximum pole loading during the test
12. Calculated bending moment at the maximum load
13. Calculated Modulus of Rupture at Ground-line (MORGL) at the fracture location

Once the set up was complete, all pertinent test parameters had been entered and all electronic instrumentation and data collection systems had been initialized and allowed to stabilize, the test was started by setting the hydraulic load controls to start applying the load to the test specimen at a slow and steady rate. The test was then allowed to run until complete failure of the specimen was determined by observation of a drastic reduction in the measured load. To better illustrate the following information, the

complete sets of test data for Poles 40 and 42 are reproduced in the Appendix 6.1 for an example.

After the completion of the test, the data acquisition program would first store the raw test results and then calculate and store the other parameters indicated above. The diameter of the pole was calculated using the measured circumference at the failure location by assuming that the pole cross-section was circular. Again assuming a circular cross-section, the poles moment of inertia for the failure location was calculated using the calculated diameter. The program then selected the maximum measured load value from the test and added the weight of the load frames and saddles to determine the maximum load value to be used for calculating the maximum moment. The maximum moment for the failure location was calculated using the standard moment equations for a four-point loading, the maximum calculated load and the measured span distances. Lastly the MORGL was calculated using the geometric parameters for the failure location. The program then stored and printed plots of the following data, load versus deflection (mid-span), load versus deflection (each of the four inputs from the rotation frame) and load versus deflection (each of two end span).

2.6 Discussion of Failure Modes

Several different types of failure were observed during the testing of the complete data set. Pole 42 exhibited a slow and deliberate failure during testing. First buckling of the extreme fibers in the compression zone started occurring, followed by fracture of the extreme tensile fibers and the finally failure occurred. The failure location for this pole was section 4200, which is located at ground-line. (See Figure 17) Pole 40 also exhibited

a slow and deliberate failure during testing. This pole however, showed no signs of buckling of the extreme fibers in the compression zone during the test and failure was initiated and occurred by fracture of the extreme tensile fibers. The failure location for this pole was section 4003, which is located at 18 inches below ground-line. (See Figure 18) Both of these poles were top sections out of other poles and one could readily guess the probable failure location by inspecting the graphical representations of the scans. Other specimens that were top sections, had large visible knots and during testing exhibited sudden catastrophic failure. In some poles, the measured load would progressively increase until failure and then steadily decrease. Others would progressively increase until failure and the suddenly decrease with a sudden failure. And yet others would exhibit progressively increasing load and then one or more cycles of decreasing load with increased deflection and then increased load with increasing deflection until failure.

While the failure plane for a majority of the poles in the data set was confined to a well-defined area (< 6 inches), several poles exhibited very jagged failure planes where it was hard to assign a failure location. (See Figure 19) Even with the attempts that were made to prevent unsymmetrical bending, some out of plane horizontal movement was observed in several poles during the testing.

Figure 17 Picture of Failure Section (Pole 42), buckling of comp. fibers

Figure 18 Picture of Failure Section (Pole 40), tensile fiber fracture

Figure 19 Picture of Failure Section (Pole 44), jagged failure plane

2.7 Summary of Test Data

Table 2, Part (a) shows the summary of the physical test data and Table 2, Part (b) shows the summary of the measured moisture contents for the complete data set of 35 pole specimens. The bottom four specimens that are shaded in the table were tested after the completion of my research and are not included in the modeling analysis.

POLE #	DATE TESTED	POLE DIA.	ROT. ANG.	MAX. LOAD	MAX. MOM.	MORGL @ BRK. LINE	MIDSPAN DEFL.
	(MM/DD/YYYY)	(IN.)	(DEG.)	(KIPS)	(IN. x KIPS)	(KSI)	(IN.)
1	07/07/1988	10.19	57	22.30	614.53	5.92	1.58
2	06/29/1988	9.55	264	18.70	510.09	5.97	2.24
4	06/10/1988	9.31	81	4.37	119.43	1.51	0.33
5	06/07/1988	9.75	0	13.79	377.17	4.20	1.88
6	02/23/1988	8.83	105	15.62	444.46	6.57	2.18
8	06/22/1988	9.31	310	6.61	180.02	2.21	0.90
11	04/05/1988	7.96	80	10.83	277.31	5.61	1.32
14	04/05/1988	8.12	294	16.13	459.82	8.76	2.80
15	03/29/1988	7.96	167	12.40	358.57	7.25	2.47
16	03/22/1988	7.96	222	12.59	358.88	7.43	2.33
17	06/02/1988	8.80	263	16.83	462.89	7.11	2.21
18	03/10/1988	9.23	139	12.85	365.62	4.73	2.51
19	05/26/1988	8.59	186	25.86	707.00	11.19	2.67
20	03/03/1988	8.67	258	3.49	108.27	1.69	0.80
22	07/18/1988	8.59	345	15.27	418.13	6.71	1.90
23	07/20/1988	8.28	32	17.98	495.55	8.90	1.99
24	08/03/1988	9.23	307	10.02	276.24	3.58	1.27
25	08/16/1988	7.32	80	3.56	97.33	2.53	2.21
26	08/17/1988	7.32	73	9.54	236.04	6.13	2.65
27	08/30/1988	7.64	254	10.45	286.84	6.55	2.08
28	09/13/1988	8.79	0	12.08	320.90	4.82	2.28
29	09/21/1988	6.92	168	5.77	158.60	4.87	1.61
30	10/06/1988	7.00	0	7.87	216.48	6.42	1.75
31	09/27/1988	7.40	5	10.89	299.59	7.53	2.22
32	10/12/1988	7.00	293	3.22	88.51	2.63	1.67
39	11/10/1988	7.00	32	6.07	166.55	4.94	1.55
40	12/22/1988	8.12	110	7.63	200.83	3.83	2.09
41	11/02/1988	7.88	244	5.19	133.02	2.77	1.69
42	12/07/1988	7.16	0	4.23	116.70	3.24	1.61
43	11/15/1988	8.52	348	8.50	233.80	3.86	2.31
44	12/22/1988	6.92	110	6.72	183.95	5.65	2.94
38	04/21/1989	10.19	318	24.84	638.36	6.15	1.62
45	02/24/1989	11.22	283	7.17	197.74	1.43	1.55
48	04/26/1989	10.82	310	19.83	510.49	4.10	1.77
56	03/03/1989	11.46	128	26.07	716.79	4.85	1.19

Table 2, Part (a) Physical Destructive Test Data

POLE #	FAIL. SECTION	% M.C. @ 0.5"	% M.C. @ 1.5"	% M.C. @ 2.5"	% M.C. X-Sec.
		(AVG.)	(AVG.)	(AVG.)	(AVG.)
1	00	12.8	19.2	27.9	20.0
2	01	13.0	21.2	30.5	21.6
4	02	9.3	10.4	12.7	10.8
5	01	11.7	23.7	36.8	24.1
6	12	37.0	41.4	40.2	39.5
8	02	9.7	15.9	22.6	16.1
11	12	10.1	14.1	17.4	13.9
14	00	17.5	23.0	23.0	21.2
15	11	27.6	43.5	43.5	38.2
16	00	15.0	17.9	17.9	16.9
17	01	9.8	13.5	16.1	13.1
18	11	26.0	41.2	41.2	36.1
19	02	11.4	15.4	17.1	14.6
20	02	20.1	26.6	26.6	24.4
22	00	16.1	26.7	35.0	25.9
23	11	12.3	15.0	17.0	14.8
24	01	N.A.	N.A.	N.A.	N.A.
25	12	21.3	30.4	42.2	31.3
26	13	13.3	16.0	17.9	15.7
27	12	13.8	16.3	17.7	15.9
28	11	16.3	24.5	34.0	24.9
29	12	9.6	13.9	17.2	13.6
30	12	11.4	13.8	14.9	13.4
31	01	11.3	13.7	15.7	13.6
32	02	12.3	20.4	32.5	21.7
39	01	12.4	16.4	27.8	18.9
40	03	15.4	26.8	35.1	25.8
41	13	10.1	16.4	21.0	15.8
42	00	13.2	27.2	39.9	26.8
43	02	12.8	28.3	40.7	27.3
44	00	12.1	18.5	25.7	18.8
38	01	N.A.	N.A.	N.A.	N.A.
45	00	N.A.	N.A.	N.A.	N.A.
48	00	N.A.	N.A.	N.A.	N.A.
56	03	N.A.	N.A.	N.A.	N.A.

Table 2, Part (b) Measured Moisture Contents

CHAPTER 3 – DEVELOPMENT OF PREDICTIVE MODEL

3.1 Introduction

As stated previously, the goal of this research was to develop a computer program that could develop a statistically accurate prediction for a poles ultimate bending strength using the scan image produced by the prototype CAT scanner. To develop this model, basic laws of equilibrium and material behavior are used. Since the objective of the model is to predict the poles ultimate bending strength, the model must assume a relationship between stress and strain for the poles cross section. The scan image is a measure of the relative density across the cross section. Therefore, to be able to predict the ultimate bending strength of a pole, the model must assume a relationship between the relative density and the stress in the wood.

Other factors that need to be accounted for in the model are how the moisture content of the wood affects the relative density measurements of the scan images and how to account for knots and other discontinuities in the predictive model. Moisture content in the wood will cause the relative density for lower wood density areas to read higher because the lower wood density areas have more void space to hold moisture. The wood species used for the test specimens have a lower density than water. Discontinuities such as knots often have higher wood densities than surrounding wood, however the discontinuity in the longitudinal structure of the wood fibers lowers the poles bending strength because the area of the discontinuity has little strength in tension.

3.2 Stress Versus Strain Diagrams

Wood has a different stress versus strain relationship in tension versus compression. The ultimate compressive strength of wood parallel to the grain is significantly less than the ultimate tensile strength. In compression, the microscopic cell walls buckle and fail at a lower stress than they can handle in tension. This is illustrated in the typical stress versus strain diagram shown in Figure 20. In bending, wood beams typically exhibit initial localized compression failures in the compression zone. These localized compression failures are exhibited by small wrinkles in the outer compression zone. As more load is applied to the beam, the compression zone expands and the beam then finally fails in tension.

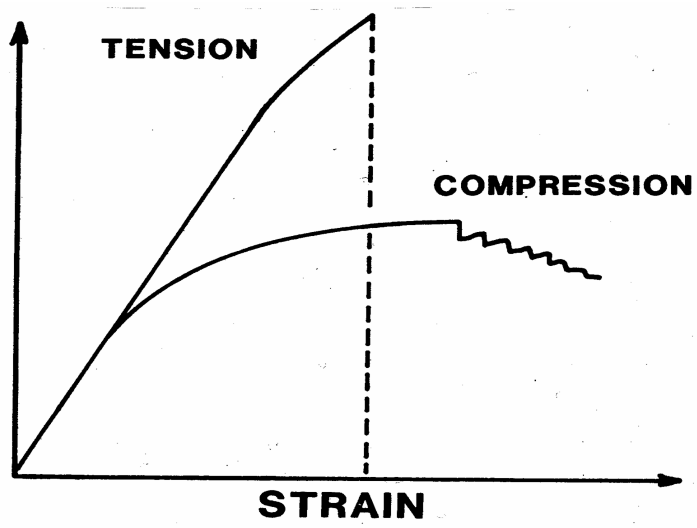

Figure 20 Comparison of Typical Stress vs. Strain Diagrams for Wood in Tension and Compression

3.2.1 Fully Plastic

In the fully plastic model, it is assumed that the stress across the cross section does not vary with the strain or the distance from the neutral axis but that the stress is only a linear function of density. The model assumes that the stresses in both compression and tension are a direct function of the relative density and that different constants control this relationship in tension and compression. Since the model is trying to predict the ultimate bending strength of the pole, the application of the fully plastic model is more applicable than if the model was trying to predict an allowable bending strength. However, there is most assuredly some variation in the stresses that is a function of the distance from the neutral axis. The following is a summary of the analysis that was used to develop the fully plastic model.

Assume a fully plastic Stress vs. Strain Diagram as shown below in Figure 21.

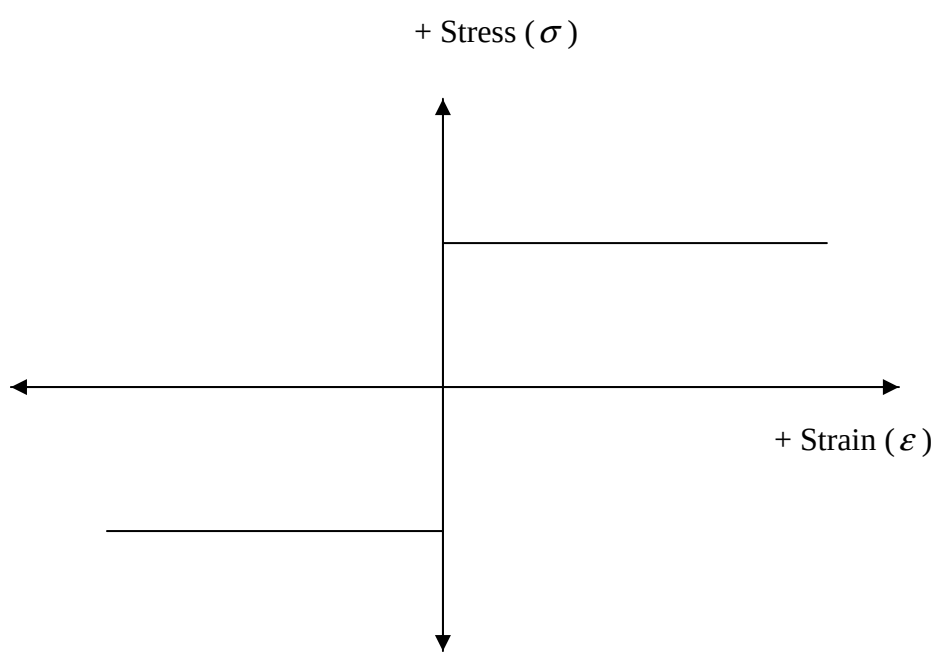

Figure 21 Fully Plastic Stress vs. Strain Diagram

Also assume that stress is linearly related to density, where

$\sigma_i =$ Stress for the ith element

D_i= Density for the ith element

n = number of elements (441, in a 21 x 21 sq. matrix)

so,

$$\sigma_i = +(k_T)D_i \text{ for } \varepsilon \rangle 0 \text{ (Tension) } (1)$$

and

$$\sigma_i = -(k_C)D_i \text{ for } \varepsilon \langle 0 \text{ (Comp.) } (2)$$

Figure 22 shows the coordinate system that was used.

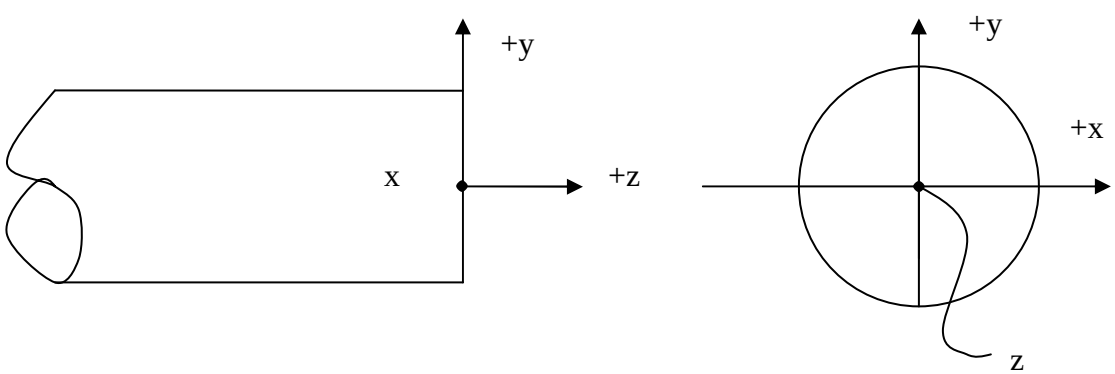

Figure 22 Assumed Coordinate System

Summing the forces in the z-direction over the cross-section produces the following equation, where F_z= the axial force on the cross-section.

$$\int_{y>0}^{A} -(k_c)D_i dA + \int_{y<0}^{A} (k_T)D_i dA = F_z \quad (3)$$

The scan image for the poles is divided into 441 equal size elements that form a 21 x 21 square matrix of elements. Each of these elements represents the incremental area dA and will be called ΔA. The dimension of each incremental square area ΔA is equal to the pole diameter divided by 20. Therefore equation (3) can be rewritten in the following form assuming positive bending.

$$\left[\sum_{y>0}^{i} -(k_c)D_i \Delta A + \sum_{y<0}^{i} +(k_T)D_i \Delta A\right] = F_z \quad (4)$$

factoring out the constants, produces the following equation

$$\left[(k_T)\Delta A\left(\sum_{y>0}^{i} -D_i(k_c/k_T) + \sum_{y<0}^{i} D_i\right)\right] = F_z \quad (5)$$

For the analysis of the poles that have been tested F_z=0, since there are no external axial loads applied to the poles. Since this is true, the term

$$\left(\sum_{y>0}^{i} -D_i(k_c/k_T) + \sum_{y<0}^{i} D_i\right) \quad (6)$$

must be equal to 0 for equilibrium. Therefore by forcing this term to 0, the neutral axis for the cross-section is located.

Summing the moments about the neutral axis of the cross-section, the following equation can be written.

$$-\left[\int_A + y_{i_{y>0}}(-k_c)(D_i)\Delta A + \int_A y_{i_{y<0}}(k_T)(D_i)\Delta A\right] = M_x \quad (7)$$

M_x is the moment on the cross-section due to the transverse loading. Factoring out the constants and expressing the integrals as summations results in the following equation,

$$M_x = \left[+k_T \Delta A(\sum_{i=1}^{n} y_{i_{y>0}} D_i (k_c / k_T) + \sum_{i=1}^{n} - y_{i_{y<0}} D_i)\right] \quad (8)$$

This is the equation that was used to calculate the predicted moment assuming the fully plastic stress vs. strain diagram. Regression analysis was used assuming different values for the constants k_c and k_T to develop the best fit model for this set of equations.

3.2.2 Linear

In the linear model, it is assumed that the stress across the cross section varies as a linear function with the strain or the distance from the neutral axis and that the modulus of elasticity or the slope of this linear relationship is a linear function of the density. With this model the equation used to calculate stress is assumed to be the same for the tension and compression zones at equal distances from the neutral axis. This assumption and the linear relationship of stress versus strain does not match what we know about wood's behavior in bending above the proportional limits (increasingly larger increases

in strain for incremental increases in stress and ultimate compressive stresses that are between 40-60% smaller than ultimate tensile stresses), however it should be an improvement over the fully plastic model. The following is a summary of the analysis that was used to develop the linear model.

Assume a linear Stress vs. Strain diagram as shown in Figure 23 and that the modulus or slope of the diagram has a direct relationship with density. The diagram is limited by the strains ε_{mc} in compression and ε_{mT} in Tension.

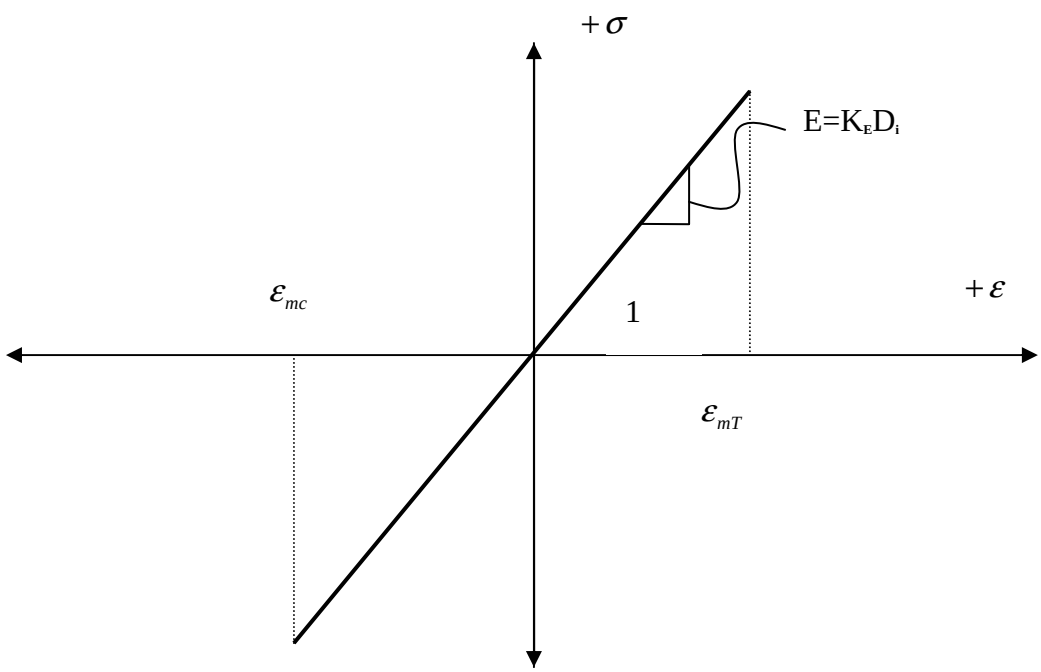

Figure 23 Linear Stress vs. Strain Diagram

The stress on each element can be expressed by the following equations.

$$\sigma_i = E_i \varepsilon_i \quad (9)$$

Substituting for E, the equation transforms to,

$$\sigma_i = k_E D_i \varepsilon_i \quad (10)$$

Summing the forces in the z-direction produces the following equation,

$$F_z = \sum_{i=1}^{n} (\sigma_i \Delta A) = \sum_{i=1}^{n} (k_E D_i \varepsilon_i) \Delta A \quad (11)$$

Factoring out the constants gives the following equation,

$$F_z = \Delta A (k_E) \sum_{i=1}^{n} (D_i \varepsilon_i) \quad (12)$$

The strain distribution on the cross-section is linear so,

$$\varepsilon_i = -(y_i / c) \varepsilon_c \quad (13)$$

where

c = the distance to the furthermost fiber from the neutral axis (NA)

and

ε_c = the strain at location c

Substituting for ε_i into equation (12) using equation (13) gives the following equation,

$$F_z = \Delta A(k_E)\sum_{i=1}^{n}(D_i)(-y_i / c)(\varepsilon_c) \quad (14)$$

Assuming that ε_{mT} is reached first then, $\varepsilon_c = \varepsilon_{mT}$ and c = c_b or the distance from the NA to the bottom fiber of the pole. Making these substitutions into equation (14) gives the following equation,

$$F_z = \Delta A(k_E)\sum_{i=1}^{n}(D_i)(-y_i / c_b)(\varepsilon_{mT}) \quad (15)$$

Factoring out the constants results in the following equation,

$$F_z = -\Delta A(k_E)(\varepsilon_{mT} / c_b)\sum_{i=1}^{n}(D_i)(-y_i) \quad (16)$$

Since there are no external axial loads on the cross-section, F_z=0. Since this is true, the term

$$\sum_{i=1}^{n}(D_i)(y_i) \quad (17)$$

must be equal to 0 for equilibrium. Therefore by forcing this term to 0, the neutral axis for the cross-section is located. Please note that if it is assumed that ε_{mc} is reached first and c = c_T, the same result is obtained. Once the NA has been located, it is possible to determine which strain is reached first by looking at the strain diagram. (See Figure 24)

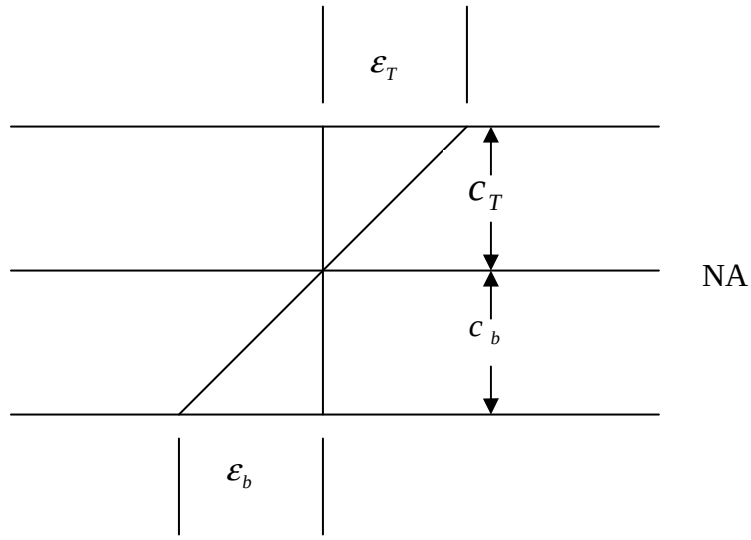

Figure 24 Strain Diagram

By similar triangles,

$$\varepsilon_b / c_b = \varepsilon_T / c_T \text{ so } c_T / c_b = \varepsilon_T / \varepsilon_b$$

so if

$\varepsilon_{mc} / \varepsilon_{mT} < c_T / c_b$, then ε_{mc} controls and if

$\varepsilon_{mc} / \varepsilon_{mT} > c_T / c_b$, then ε_{mT} controls.

Summing the moments about the neutral axis of the cross-section, the following equation can be written.

$$M_x = \sum_{i=1}^{n} -\sigma_i \Delta A(y_i) \quad (18)$$

Substituting equations (10) into equation (18) produces,

$$M_x = \sum_{i=1}^{n} \left(-(k_E D_i \varepsilon_i)(\Delta A) y_{i_{y<0}} + (k_E D_i \varepsilon_i)(\Delta A) y_{i_{y>0}} \right) \quad (19)$$

Substituting equation (13) into equation (19) produces,

$$M_x = \sum_{i=1}^{n} \left(-(k_E D_i)(y_{i_{y<0}})(\varepsilon_c / c)(\Delta A)(y_{i_{y<0}}) + (k_E D_i)(y_{i_{y>0}})(\varepsilon_c / c)(\Delta A)(y_{i_{y>0}}) \right) \quad (20)$$

Knowing that if,

$\varepsilon_{mc} / \varepsilon_{mT} < c_T / c_b$, then ε_{mc} controls and if

$\varepsilon_{mc} / \varepsilon_{mT} > c_T / c_b$, then ε_{mT} controls.

Factoring the constants out of equation (20) produces,

$$M_x = k_E \Delta A (\varepsilon_c / c) \sum_{i=1}^{n} \left(D_i (y_i)^2 + D_i (y_i)^2 \right) \quad (21)$$

or

$$M_x = 2k_E \Delta A (\varepsilon_c / c) \sum_{i=1}^{n} \left(D_i (y_i)^2 \right) \quad (22)$$

Assuming ε_{mT} controls then,

$$M_x = 2k_E \Delta A (\varepsilon_{mT} / c_b) \sum_{i=1}^{n} \left(D_i (y_i)^2 \right) \quad (23)$$

Assuming ε_{mc} controls then,

$$M_x = 2k_E \Delta A (\varepsilon_{mc} / c_T) \sum_{i=1}^{n} \left(D_i (y_i)^2 \right) \quad (24)$$

This equation can be rewritten in the following form,

$$M_x = 2k_E \Delta A(\varepsilon_{mT} / c_T)(\varepsilon_{mc} / \varepsilon_{mT}) \sum_{i=1}^{n} \left(D_i (y_i)^2 \right) \quad (25)$$

These equations were used to calculate the predicted moment assuming the linear stress vs. strain diagram. Regression analysis was used assuming different values for the constant term to develop the best fit model for this set of equations.

3.2.3 Power Function

In the power function model, it is assumed that the stress across the cross section varies as some power function with the strain or the distance from the neutral axis and that the slope of this relationship is a linear function of the density. With this model the equation used to calculate stress is assumed to be the same for the tension and compression zones at equal distances from the neutral axis. This assumption does not match what we know about wood's behavior in bending above the proportional limits (ultimate compressive stresses that are between 40-60% smaller than ultimate tensile stress), but it should be an improvement over the fully plastic and the linear model. The following is a summary of the analysis that was used to develop the power function model.

Assume the Stress vs. Strain diagram to be a power function of the following form, $\sigma_i = \pm C|\varepsilon|^m$, and that the constant C is a linear function of density, $C = k_p D_i$ (26). Also assume that the diagram is controlled by the two strain values, ε_{mT} and ε_{mc} as shown in Figure 25.

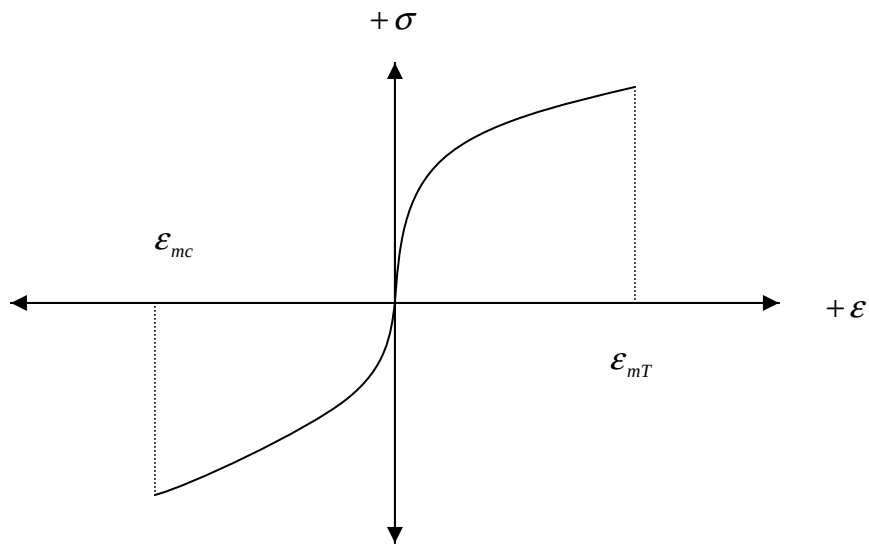

Figure 25 Power Function Stress vs. Strain Diagram

So

$$\sigma_i = +C|\varepsilon|^m \quad \text{if } \varepsilon > 0 \text{ (for y < 0) (27)}$$

and

$$\sigma_i = -C|\varepsilon|^m \quad \text{if } \varepsilon < 0 \text{ (for y > 0) (28)}$$

Summing the forces in the z-direction gives the following equation,

$$F_z = \sum_{i=1}^{n} (\sigma_i \Delta A) \quad (29)$$

Substituting in equations (27) and (28) gives the following,

$$F_z = \sum_{i=1}^{n} (\pm C|\varepsilon_i|^m)\Delta A \quad (30)$$

Substituting in equation (26) gives the following,

$$F_z = \sum_{i=1}^{n} \pm k_p D_i \left|\varepsilon_i\right|^m \Delta A \quad (31)$$

The strain distribution on the cross-section is linear so,

$$\varepsilon_i = \left(-y_i / c\right)\varepsilon_c \quad (32)$$

Substituting equation (32) into equation (31) produces the following equation,

$$F_Z = \sum_{i=1}^{n} \left(k_p D_i \left|(-y_i / c)\varepsilon_c\right|^m \Delta A - k_p D_i \left|(-y_i / c)\varepsilon_c\right|^m \Delta A\right) \quad (33)$$

Factoring out the constants produces the following equation,

$$F_Z = k_p \Delta A\left(\varepsilon_c / c_m\right)^m \sum_{i=1}^{n} \left(D_i \left|y_{i_{y<0}}\right|^m - D_i \left|y_{i_{y>0}}\right|^m \right) \quad (34)$$

Since there are no external axial loads on the cross-section, F_z=0. Since this is true, the term

$$\sum_{i=1}^{n} \left(D_i \left|y_{i_{y<0}}\right|^m - D_i \left|y_{i_{y>0}}\right|^m \right)$$

must be equal to 0 for equilibrium. Therefore by forcing this term to 0, the neutral axis for the cross-section is located. Summing the moments about the neutral axis of the cross-section, the following equation can be written.

$$M_x = \sum_{i=1}^{n} -\sigma_i \Delta A(y_i) \quad (35)$$

Substituting equations (27) and (28) into equation (35) produces,

$$M_x = \sum_{i=1}^{n}\left(-(k_p D_i \left|\varepsilon_i\right|^m \Delta A(y_{i_{y<0}}) + (k_p D_i)\left|\varepsilon_i\right|^m \Delta A(y_{i_{y>0}})\right) \quad (36)$$

Substituting equation (32) into equation (36) produces,

$$M_x = \sum_{i=1}^{n}\left(-(k_p D_i \left|(y_{i_{y<0}}/c)\varepsilon_c\right|^m \Delta A(y_{i_{y<0}}) + (k_p D_i)\left|(y_{i_{y>0}}/c)\varepsilon_c\right|^m \Delta A(y_{i_{y>0}})\right) \quad (37)$$

Knowing that if,

$\varepsilon_{mc}/\varepsilon_{mT} < c_T/c_b$, then ε_{mc} controls and if

$\varepsilon_{mc}/\varepsilon_{mT} > c_T/c_b$, then ε_{mT} controls.

Factoring the constants out of equation (37) produces,

$$M_x = k_p \Delta A(\varepsilon_c/c)^m \sum_{i=1}^{n}\left(D_i\left|y_i\right|^{m+1} + D_i\left|y_i\right|^{m+1}\right) \quad (38)$$

or

$$M_x = 2k_p \Delta A(\varepsilon_c/c)^m \sum_{i=1}^{n}\left(D_i\left|y_i\right|^{m+1}\right) \quad (39)$$

Assuming ε_{mT} controls then,

$$M_x = 2k_p \Delta A(\varepsilon_{mT}/c_b)^m \sum_{i=1}^{n}\left(D_i\left|y_i\right|^{m+1}\right) \quad (40)$$

Assuming ε_{mc} controls then,

$$M_x = 2k_p \Delta A(\varepsilon_{mc}/c_T)^m \sum_{i=1}^{n}\left(D_i\left|y_i\right|^{m+1}\right) \quad (41)$$

This equation can be rewritten in the following form,

$$M_x = 2k_p \Delta A(\varepsilon_{mT} / c_T)^m (\varepsilon_{mc} / \varepsilon_{mT})^m \sum_{i=1}^{n} \left(D_i \left| y_i \right|^{m+1} \right) \quad (42)$$

These equations were used to calculate the predicted moment assuming the power function stress vs. strain diagram. Regression analysis was used assuming different values for the power of the exponent in the equation to develop the best fit model for this set of equations.

3.3 Effect of Other Variables

Later versions of the experimental model also tried to take account the effect of decay and moisture content. A summary of the techniques used in the analysis to account for these factors follows.

3.3.1 Decay

As noted previously in Chapter 1, research indicates that small reductions in density due to decay result in much larger decreases in wood's mechanical properties. To model a loss in strength due to decay without changing the analytical models outlined above for the three different stress vs. strain relationships, it was decided to instead adjust the density for the scan images from the actual measured values to adjusted values. First the maximum density value for a scan was determined. Next, the analysis included an option where a threshold density value could be chosen. This threshold value could be a certain percentage of the maximum measured value. Then all density values above the calculated threshold value could be normalized to a common value. Density values

below the threshold value could then be reduced by a power function so that as density values got lower they were reduced by an increasing amount. The following is a summary of the analysis that was used to reduce density values by a power function to simulate strength reductions due to decay.

1. Calculate a maximum density value (Max. Den.) from the scan images.
2. Decide what percentage (N %) of Max. Den. to use for the threshold value.
3. Assume all density values above (N% x Max. Den.) to be wood without decay and set equal to Max. Den.
4. Reduce the densities below the threshold value by the following formula,

$$NDen_i = Den_i \times \left(Den_i / Max.Den.\right)^P$$

5. Regression analysis was used assuming different values for the exponent in the power function used in the equation to develop the best fit model for this method of adjustment.

3.3.2 Moisture Content

As previously noted in Chapter 2, moisture content data were also taken for each pole at each of the seven scan locations. The readings were taken in four quadrants around the circumference of the pole at depths of 0.5", 1.5", and 2.5" using a Delmhorst moisture detector. During the development of the model, it was decided that there was not enough difference in the moisture content readings for a given depth between the quadrants to justify the added trouble of maintaining and applying any corrections

separately for each quadrant. Therefore, the four values obtained for each quadrant were averaged to obtain one value for each of the specified depths an then an average was calculated using the three depth values to obtain a single average moisture content for each scan location. To adjust the density values from the scan for the moisture content, each density value was adjusted by dividing the density value from the scan by the value of (1 + % Moisture Content).

CHAPTER 4 – MODELING RESULTS

4.1 Introduction

The following is a summary of the results of the research. Each variation was explored and the predictive model was developed for a best-fit correlation between the observed/measured results of the full scale testing and the predictive analytical model using regression analysis. A statistical analysis is included for each presentation of the results.

4.2 Comparison of Methods

4.2.1 Fully Plastic without Adjustments

This predictive model is the least involved and therefore would be expected to provide the least accurate correlation. Table 3 contains the statistical analysis for a data set using this predictive model.

4.2.2 Linear without Adjustments

One would have assumed that this predictive model should have shown improved results when compared with the fully plastic model, the reasoning being that it more closely reflects the actual observed stress-strain relationship for wood; however for the initial data set of 23 poles the fully plastic model actually gave slightly better results.

4.2.3 Linear with Adjustments for Decay

When adjustments were made in the model to adjust for the effects of decay the results improved. This predictive model showed improved results over the fully plastic and the linear models without the adjustment for decay. Table 4 contains the statistical

analysis for the same data set using this predictive model. As can be observed, these results show a lower % error value and a higher correlation.

4.2.4 Power Function with Adjustments for Decay

As the data set expanded, the power function model provided the best results. However, the type of predictive model used did not affect the results nearly as much as the adjustments made for decay. Table 5 contains the statistical analysis for an expanded data set using the power function model with the most accurate adjustment found for decay. Again, the results continue to improve. This can be seen by the lower % error and the higher correlation value.

4.2.5 Power Function with Adjustments for Decay and Moisture Content

Small improvements were made to the model when adjustment was made for the average moisture content at the scan location. Table 6 contains the statistical analysis for an expanded data set using the power function model with the most accurate adjustments found for decay and moisture content. This was the most accurate model developed in the research as measured by the % error and correlation values. A graphical representation of the data contained in Table 6 is shown in Figure 26. This graph plots the poles predicted MORGL against the actual MORGL where both values have been divided by the highest predicted value. In general, this plot illustrates the trend that the predictive model over predicted the strength of the lower strength poles and under predicted the strength of the higher strength poles.

TABLE 3	FULLY PLASTIC ANALYSIS (Kc/Kt) = 1 NO DECAY			
		ACT. MOM.	PRE. MOM.	|DIFF|
	POLE #	(IN. x KIPS)	(IN. x KIPS)	(IN. x KIPS)
	1	614.53	549.23	65.30
	2	510.09	438.00	72.09
	4	119.43	313.80	194.37
	5	377.17	438.72	61.55
	6	444.46	440.99	3.47
	8	180.02	363.61	183.59
	11	277.31	263.09	14.22
	14	459.82	300.23	159.59
	15	358.57	282.74	75.83
	16	358.88	314.89	43.99
	17	462.89	428.72	34.17
	18	365.62	502.11	136.49
	19	707.00	352.65	354.35
	20	108.27	323.68	215.41
	22	418.13	399.14	18.99
	23	495.55	326.61	168.94
	24	276.24	382.17	105.93
	25	97.33	218.46	121.12
	26	236.04	203.13	32.91
	27	286.84	273.48	13.35
	28	320.90	319.32	1.58
	29	158.60	242.35	83.75
	31	299.59	256.15	43.45
# IN DATA SET =	23			
SUM =		7933.27	7933.27	2204.45
AVG. =		344.92	344.92	95.85
STAN. DEV. =		158.86	90.55	86.22
CORREL. =		57.00%		
STAN. ERROR =		133.60		
% ERROR =		27.79%		

TABLE 4 **LINEAR ANALYSIS**

DECAY A FUNCTION OF (DEN.)^2

		ACT. MOM.	PRE. MOM.	|DIFF|
	POLE #	**(IN. x KIPS)**	**(IN. x KIPS)**	**(IN. x KIPS)**
	1	614.53	533.78	80.74829836
	2	510.09	374.33	135.76
	4	119.43	260.27	140.84
	5	377.17	424.21	47.04
	6	444.46	488.17	43.72
	8	180.02	310.42	130.40
	11	277.31	249.89	27.43
	14	459.82	301.14	158.69
	15	358.57	285.17	73.41
	16	358.88	344.85	14.03
	17	462.89	473.30	10.42
	18	365.62	560.83	195.21
	19	707.00	377.64	329.37
	20	108.27	289.03	180.76
	22	418.13	434.05	15.92
	23	495.55	344.88	150.67
	24	276.24	340.83	64.60
	25	97.33	214.92	117.59
	26	236.04	191.75	44.29
	27	286.84	294.77	7.93
	28	320.90	278.41	42.49
	29	158.60	284.70	126.10
	31	299.59	275.94	23.66
# IN DATA SET =	23			
SUM =		7933.27	7933.27	2161.04
AVG. =		344.92	344.92	93.96
STAN. DEV. =		158.86	99.35	78.34
CORREL. =		62.54%		
STAN. ERROR =		126.88		
% ERROR =		27.24%		

TABLE 5 **POWER FUNCTION ANALYSIS**
DECAY A FUNCTION OF (DEN.)^m

		ACT. MOM.	PRE. MOM.	|DIFF|
	POLE #	(IN. x KIPS)	(IN. x KIPS)	(IN. x KIPS)
	1	614.53	538.64	75.88
	2	510.09	388.24	121.85
	4	119.43	269.50	150.08
	5	377.17	499.27	122.10
	6	444.46	389.12	55.34
	8	180.02	344.44	164.42
	11	277.31	283.91	6.60
	14	459.82	329.11	130.71
	15	358.57	280.50	78.08
	16	358.88	372.82	13.95
	17	462.89	424.76	38.12
	18	365.62	533.03	167.41
	19	707.00	424.77	282.23
	20	108.27	222.53	114.27
	22	418.13	441.55	23.42
	23	495.55	397.05	98.50
	24	276.24	407.30	131.06
	25	97.33	179.89	82.56
	26	236.04	210.96	25.08
	27	286.84	318.49	31.66
	28	320.90	297.51	23.39
	29	158.60	157.33	1.27
	30	216.48	155.31	61.17
	31	299.59	269.55	30.04
	32	88.51	119.05	30.54
	39	166.55	142.17	24.37
	40	200.83	184.71	16.12
	41	133.02	138.79	5.76
	42	116.70	150.91	34.21
	43	233.80	290.17	56.37
	44	183.95	111.73	72.22
# IN DATA SET =	31			
SUM =		9273.11	9273.11	2268.78
AVG. =		299.13	299.13	73.19
STAN. DEV. =		159.19	125.71	63.29
CORREL. =		78.97%		
STAN. ERROR =		99.34		
% ERROR =		24.47%		

TABLE 6 POWER FUNCTION ANALYSIS
DECAY A FUNCTION OF (DEN.)^m
WITH MOISTURE CONTENT ADJUSTMENT

		ACT. MOM.	PRE. MOM.	|DIFF|
	POLE #	(IN. x KIPS)	(IN. x KIPS)	(IN. x KIPS)
	1	614.53	512.96	101.57
	2	510.09	361.61	148.48
	4	119.43	294.13	174.70
	5	377.17	525.55	148.38
	6	444.46	325.14	119.32
	8	180.02	355.44	175.43
	11	277.31	311.08	33.77
	14	459.82	335.59	124.24
	15	358.57	246.84	111.73
	16	358.88	387.13	28.26
	17	462.89	456.42	6.46
	18	365.62	476.18	110.56
	19	707.00	467.77	239.23
	20	108.27	209.33	101.06
	22	418.13	434.77	16.64
	23	495.55	436.00	59.55
	24	276.24	404.44	128.20
	25	97.33	163.96	66.63
	26	236.04	226.18	9.86
	27	286.84	344.08	57.24
	28	320.90	283.94	36.95
	29	158.60	159.17	0.57
	30	216.48	166.63	49.85
	31	299.59	293.82	5.77
	32	88.51	114.89	26.38
	39	166.55	144.93	21.62
	40	200.83	180.70	20.13
	41	133.02	135.86	2.83
	42	116.70	138.50	21.80
	43	233.80	267.51	33.71
	44	183.95	112.56	71.39
# IN DATA SET =	31			
SUM =		9273.11	9273.11	2252.30
AVG. =		299.13	299.13	72.65
STAN. DEV. =		159.19	126.56	62.20
CORREL. =		79.50%		
STAN. ERROR =		98.21		
% ERROR =		24.29%		

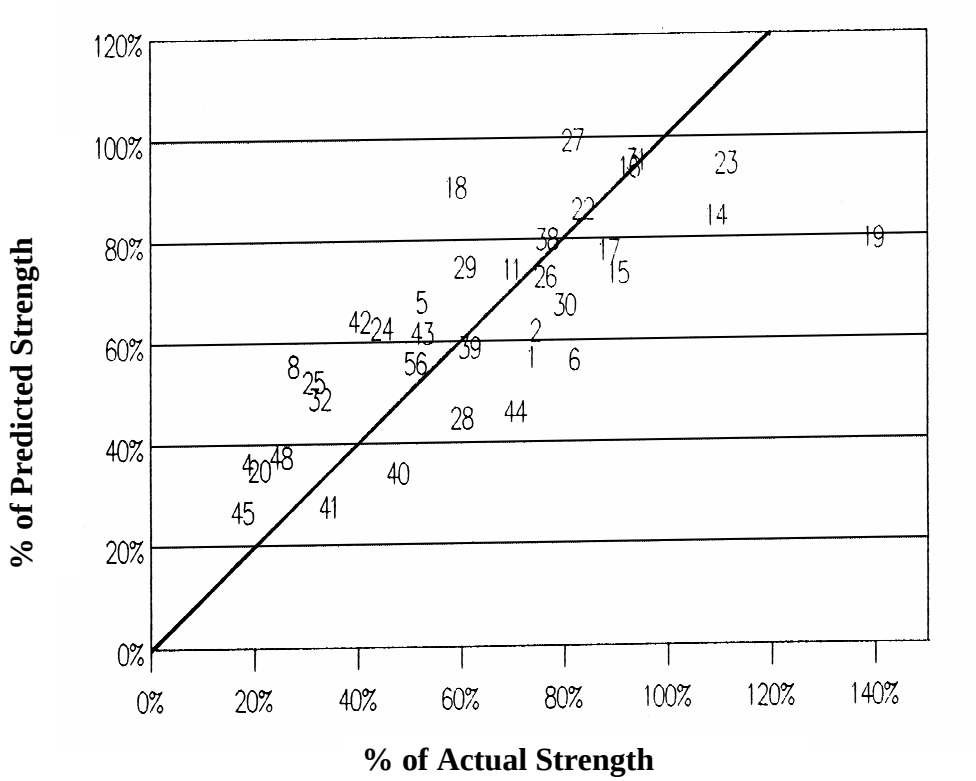

Figure 26 Actual vs. Predicted MORGL

4.3 Comparison with E.D.M. Device

The data sample for this comparison is smaller than the total data sample since an E.D.M. prediction was not obtained for all of the poles that were physically tested. Table 7 contains the statistical analysis comparing the best predictive model developed in the research with the predictions made by the Poletest EDM device. For some reason, the statistical results for this reduced data set are much better than the results for the total data set.

TABLE 7 BEST PREDICTION FROM MODEL VS. EDM PREDICTION

		ACT. MOM.	PRE. MOM.	|DIFF-PRE|	|DIFF-EDM|	EDM MOM.
	POLE #	(IN. x KIPS)	(IN. x KIPS)	(IN. x KIPS)	(IN. x KIPS)	(IN. x KIPS)
	1	614.53	512.96	101.57	274.79	339.74
	2	510.09	361.61	148.48	209.67	300.42
	4	119.43	294.13	174.70	319.35	438.78
	5	377.17	525.55	148.38	89.02	288.15
	17	462.89	456.42	6.46	59.15	403.73
	19	707.00	467.77	239.23	286.27	420.73
	22	418.13	434.77	16.64	166.32	251.81
	23	495.55	436.00	59.55	284.31	211.25
	25	97.33	163.96	66.63	59.80	157.13
	26	236.04	226.18	9.86	94.78	141.26
	27	286.84	344.08	57.24	129.95	156.89
	28	320.90	283.94	36.95	54.05	266.85
	29	158.60	159.17	0.57	20.09	138.51
	30	216.48	166.63	49.85	69.26	147.22
	31	299.59	293.82	5.77	168.47	131.13
	32	88.51	114.89	26.38	42.92	131.43
	39	166.55	144.93	21.62	44.66	211.20
	40	200.83	180.70	20.13	51.47	149.37
	41	133.02	135.86	2.83	102.15	235.17
	42	116.70	138.50	21.80	23.96	140.66
	43	233.80	267.51	33.71	46.89	186.91
	44	183.95	112.56	71.39	32.15	151.80
# IN DATA SET =	22					
SUM =		6443.92	6221.93	1319.75	2629.45	5000.13
AVG. =		292.91	282.82	59.99	119.52	227.28
STAN. DEV. =		175.84	139.46	64.29	96.54	99.67
CORREL. =			0.87			0.60
STAN. ERROR =			89.47			143.96
% ERROR =			20.48%			40.81%

CHAPTER 5 – SUMMARY

5.1 Introduction

The following is a summary of the conclusions and recommendations after a thorough analysis of the procedures used for data collection, testing and analysis for this research project.

5.2 Conclusions

5.2.1 Data Collection

The CAT scanning device that was used in this research did not adjust the density values that were recorded in the scan images for the moisture content of the wood. A large number of moisture readings (12/scan x 7 scan locations x 3 depths = 84) were taken for the pole specimens to be used by the predictive model to make this adjustment. It would have greatly simplified the research project, if the scanning device was able to automatically adjust the density values for the actual moisture content at each specific location in the poles.

5.2.2 Testing Procedures

The testing procedures used for data collection were well-grounded. At the beginning of the physical testing of the poles, several of the test specimens exhibited horizontal shear failures. In an attempt to prevent the further horizontal shear failures, compressive shear reinforcement rings were fabricated and used on subsequent tests. After this change to the testing procedure, only a small number of the remaining test

specimens exhibited any signs horizontal shear failure. It would have been helpful to the research project to have completed the physical testing earlier in the development of the predictive models. It would have also been helpful to have collected all measured variables, such as the water content data and the EDM prediction for the complete data set.

5.2.3 Analytical Models

The analytical models with adjustments that were developed were logical. Wood is an anisotropic, highly variable material. "The mechanical properties within a species tend to follow a normal distribution. For any given property, the variation is about the same regardless of the species if we express it as the "coefficient of variation," which is the standard deviation expressed as a percentage of the average value. For some properties the variability tends to be greater than others, but as an indication of the order of magnitude we can say that the coefficient of variation is about 20% [11]." The measured "coefficient of variance" for the best predictive model was calculated by dividing the standard deviation of the difference between the measured and the predicted moment values by the average measured moment value for the data set. This value for the best predictive model was approximately 21%.

Knowing that wood has a different stress versus strain relationship in tension versus compression, a more involved model could have been developed that would have tried to more closely simulate the actual known stress versus strain relationship.

The methods that were used to adjust the predictive model for decay, presented a dilemma when considering the matrix elements on the outer boundary of the member.

These partial elements had lower density values because the scanning software calculates the density of each element in the scan matrix based on the same rectangular area. Since these elements were on the outer boundary and only a portion of the element area has pole material in it, the scan density for the element was lower than an interior element where the whole of the element area was filled with pole material. When a straight linear relationship was used between density and strength, this anomaly did not affect the analysis because the lower element density was directly related to less pole area in that element. However, when the element densities were reduced by a power function to simulate the increased losses in strength for incremental losses in density due to decay, these elements probably should not have received the increased reduction. Because a significant number of the outer boundary elements are at some of the larger distances from the NA, these elements have a very significant effect on the pole strength. Because of the increased significance of these elements compared with other elements that are closer to the NA, the any adjustment that is applied to these elements needs to be as accurate as possible.

The method used in the predictive model to account for moisture content based on an average value at the scan location was crude. Given more time a more refined method would have been to use the measured values at different depths and possibly at the different quadrants.

5.3 Recommendations

1. Change analytical model to account for ultimate compressive stresses being lower than ultimate tensile stresses and the different shape for the stress vs. strain relationship in the tension and compression regions.
2. Change method of adjustment to account for reduced densities to prevent applying the increased reduction to the boundary elements. One method to prevent applying the reduction would be to filter out any elements that have an adjacent element with a zero density value. This method would not work if there were interior voids within the cross section. A further test should be applied to make sure that the position of the element was on the outer boundary and was not a void within the pole cross section.
3. If practical, use the scan technology that automatically adjusts the measured scan image for moisture content.
4. Perform a study to compare scan images taken in the field with laboratory scan readings for future studies.

CHAPTER 6 – APPENDICES

6.1 Physical destructive Test Data

6.1.1 Pole 40

```
SPECIMEN TESTED IS pole40     12-22-1988  11:55:21
CALIBRATION FACTORS
 10  1.671  .01  .01  .01  .01  .89  .865
NORTH END SPAN LENGTH IS  67.625  INCHES.
SOUTH END SPAN LENGTH IS  67.625  INCHES.
ROTATIONAL ORIENTATION IN DEGREES =  110
THE POLE BROKE -15 INCHES FROM GROUNDLINE.
THE APPROXIMATE CIRCUMFERENCE AT BREAKLINE IS  25.5  IN.
THE DIAMETER AT BREAKLINE IS  8.116909  IN.
THE MOMENT OF INERTIA IS  213.075 IN.^4
THE MAXIMUM LOAD IS  7.632617  KIP
THE MOMENT AT MAXIMUM LOAD IS  200.8332  IN.-KIP
THE MORGL AT BREAKLINE IS  3.825284 KSI.
```

The failure of the pole was slow and deliberate. The pole failed at the section that would seem to be predicted by the scan images. The pole is a top cut of another pole and therefore had no established groundline before the test. There were no knots at the section of failure. There was no apparent problems with the test.

SPECIMEN TESTED IS pole40 12-22-1988 11:55:35

LOAD(kips)	DEFLECTIONS(inches)						
CH.0	CH.1 MDSPAN	CH.2 ETROT	CH.3 EBROT	CH.4 WTROT	CH.5 WBROT	CH.6 SEND	CH.7 NEND
-0.02	+16.601	+.09904	+.09858	+.09874	+.09824	+2.618	+3.998
0.08	+16.602	+.09885	+.09824	+.09843	+.09787	+4.240	+3.996
0.20	+16.589	+.09837	+.09773	+.09786	+.09737	+4.210	+3.996
0.30	+16.579	+.09792	+.09731	+.09745	+.09690	+4.182	+3.991
0.41	+16.570	+.09745	+.09687	+.09693	+.09646	+4.142	+3.991
0.52	+16.547	+.09702	+.09647	+.09652	+.09605	+4.110	+3.991
0.63	+16.526	+.09649	+.09592	+.09601	+.09546	+4.066	+3.987
0.73	+16.514	+.09607	+.09550	+.09553	+.09506	+4.034	+3.985
0.83	+16.499	+.09565	+.09510	+.09512	+.09463	+3.998	+3.979
0.93	+16.486	+.09524	+.09467	+.09468	+.09418	+3.962	+3.979
1.05	+16.461	+.09480	+.09425	+.09422	+.09375	+3.927	+3.969
1.15	+16.449	+.09423	+.09375	+.09375	+.09320	+3.880	+3.966
1.25	+16.430	+.09390	+.09336	+.09335	+.09283	+3.854	+3.966
1.36	+16.410	+.09345	+.09293	+.09289	+.09236	+3.813	+3.946
1.46	+16.384	+.09307	+.09252	+.09248	+.09198	+3.783	+3.945
1.57	+16.375	+.09260	+.09213	+.09202	+.09156	+3.746	+3.941
1.67	+16.351	+.09219	+.09172	+.09158	+.09115	+3.712	+3.942
1.78	+16.331	+.09172	+.09125	+.09114	+.09066	+3.675	+3.932
1.89	+16.316	+.09135	+.09085	+.09075	+.09028	+3.644	+3.932
2.00	+16.303	+.09085	+.09041	+.09027	+.08984	+3.605	+3.915
2.10	+16.286	+.09048	+.09002	+.08987	+.08942	+3.576	+3.910
2.21	+16.262	+.08999	+.08958	+.08942	+.08899	+3.536	+3.907
2.31	+16.253	+.08953	+.08915	+.08901	+.08857	+3.505	+3.898
2.42	+16.236	+.08911	+.08871	+.08856	+.08811	+3.464	+3.898
2.53	+16.212	+.08867	+.08827	+.08809	+.08767	+3.430	+3.888
2.64	+16.188	+.08823	+.08788	+.08768	+.08729	+3.394	+3.886
2.74	+16.180	+.08782	+.08750	+.08730	+.08688	+3.359	+3.886
2.86	+16.155	+.08742	+.08708	+.08688	+.08649	+3.327	+3.882
2.95	+16.140	+.08689	+.08663	+.08645	+.08601	+3.290	+3.873
3.06	+16.119	+.08652	+.08625	+.08608	+.08565	+3.262	+3.879
3.17	+16.091	+.08599	+.08576	+.08561	+.08514	+3.218	+3.880
3.28	+16.076	+.08557	+.08534	+.08519	+.08472	+3.186	+3.865
3.38	+16.057	+.08511	+.08493	+.08482	+.08428	+3.149	+3.865
3.49	+16.042	+.08472	+.08452	+.08446	+.08382	+3.112	+3.866
3.60	+16.016	+.08419	+.08407	+.08412	+.08326	+3.069	+3.852
3.71	+15.992	+.08379	+.08370	+.08375	+.08281	+3.036	+3.852
3.81	+15.981	+.08339	+.08324	+.08351	+.08241	+2.982	+3.852
3.94	+15.950	+.08295	+.08268	+.08301	+.08194	+2.948	+3.844
4.04	+15.922	+.08246	+.08223	+.08275	+.08131	+2.908	+3.835
4.14	+15.907	+.08206	+.08184	+.08243	+.08085	+2.868	+3.818
4.25	+15.883	+.08158	+.08136	+.08202	+.08034	+2.827	+3.797
4.37	+15.860	+.08111	+.08091	+.08172	+.07981	+2.784	+3.794
4.47	+15.842	+.08067	+.08050	+.08142	+.07930	+2.750	+3.789
4.58	+15.821	+.08024	+.08008	+.08118	+.07879	+2.708	+3.789
4.69	+15.799	+.07976	+.07966	+.08085	+.07825	+2.663	+3.772
4.79	+15.780	+.07935	+.07924	+.08062	+.07770	+2.620	+3.764
4.89	+15.764	+.07891	+.07878	+.08034	+.07714	+2.574	+3.763
5.00	+15.739	+.07856	+.07840	+.08009	+.07670	+2.539	+3.762
5.11	+15.719	+.07812	+.07794	+.07988	+.07604	+2.487	+3.754
5.22	+15.698	+.07770	+.07750	+.07962	+.07553	+2.445	+3.751

LOAD(kips)	----------DEFLECTIONS(inches)----------						
CH.0	CH.1 MDSPAN	CH.2 ETROT	CH.3 EBROT	CH.4 WTROT	CH.5 WBROT	CH.6 SEND	CH.7 NEND
5.32	+15.674	+.07728	+.07708	+.07932	+.07500	+2.404	+3.751
5.43	+15.662	+.07684	+.07662	+.07904	+.07447	+2.357	+3.751
5.53	+15.633	+.07646	+.07617	+.07871	+.07402	+2.315	+3.717
5.65	+15.606	+.07599	+.07569	+.07845	+.07344	+2.274	+3.717
5.75	+15.592	+.07562	+.07523	+.07808	+.07307	+2.236	+3.717
5.87	+15.560	+.07520	+.07475	+.07762	+.07268	+2.204	+3.705
5.98	+15.543	+.07480	+.07422	+.07714	+.07232	+2.172	+3.704
6.08	+15.524	+.07438	+.07375	+.07664	+.07199	+2.142	+3.704
6.19	+15.480	+.07401	+.07325	+.07618	+.07164	+2.118	+3.705
6.30	+15.461	+.07358	+.07270	+.07557	+.07131	+2.086	+3.704
6.40	+15.438	+.07321	+.07218	+.07500	+.07107	+2.062	+3.691
6.53	+15.405	+.07269	+.07158	+.07438	+.07066	+2.032	+3.691
6.64	+15.387	+.07227	+.07103	+.07363	+.07063	+2.019	+3.691
6.73	+15.336	+.07325	+.06955	+.07281	+.07129	+2.055	+3.672
6.84	+15.307	+.07270	+.06903	+.07221	+.07101	+2.051	+3.670
6.53	+15.307	+.07585	+.06789	+.07292	+.07342	+2.066	+3.672
5.33	+15.241	+.07419	+.07666	+.05917	+.07713	+2.372	+3.671
5.21	+15.236	+.07900	+.07691	+.05960	+.07668	+2.380	+3.671
5.31	+15.217	+.07884	+.07708	+.05938	+.07641	+2.433	+3.671
5.42	+15.195	+.07853	+.07700	+.05894	+.07615	+2.448	+3.672
5.53	+15.168	+.07833	+.07725	+.05838	+.07596	+2.444	+3.671
5.63	+15.143	+.07811	+.07804	+.05784	+.07577	+2.435	+3.671
5.74	+15.111	+.07768	+.07837	+.05728	+.07555	+2.421	+3.671
5.84	+15.086	+.07761	+.07862	+.05682	+.07555	+2.412	+3.672
5.95	+15.046	+.07729	+.07894	+.05610	+.07533	+2.403	+3.671
6.05	+15.021	+.07711	+.07932	+.05559	+.07521	+2.388	+3.672
6.16	+14.980	+.07702	+.07972	+.05514	+.07511	+2.381	+3.672
6.26	+14.948	+.07712	+.08012	+.05451	+.07480	+2.358	+3.671
6.37	+14.906	+.07767	+.08031	+.05408	+.07480	+2.346	+3.671
6.48	+14.862	+.07916	+.07238	+.05341	+.07467	+2.335	+3.672
6.58	+14.808	+.07969	+.07014	+.05252	+.07499	+2.354	+3.672
6.68	+14.777	+.07994	+.06832	+.05182	+.07509	+2.368	+3.670
6.79	+14.744	+.08027	+.06680	+.05090	+.07517	+2.377	+3.671
6.89	+14.697	+.08048	+.06548	+.04998	+.07557	+2.405	+3.672
7.01	+14.646	+.08107	+.06353	+.04780	+.07717	+2.501	+3.672
6.94	+14.589	+.08176	+.05116	+.04410	+.08167	+2.789	+3.672
7.06	+14.554	+.08196	+.04896	+.04276	+.08257	+2.956	+3.654
7.16	+14.514	+.08205	+.04775	+.04183	+.08283	+2.991	+3.653
6.89	+14.488	+.07449	+.04033	+.03823	+.08738	+3.037	+3.640
2.73	+14.377	+.02645	+.02333	+.04501	-.03717	+2.468	+3.626
3.00	+14.350	+.00856	+.02325	+.02420	-.03842	+1.655	+3.414
3.13	+14.328	-.02129	+.02292	+.02384	-.03883	-3.294	+3.413
3.23	+14.325	-.02173	+.02272	+.02359	-.03921	-5.102	+3.413
3.34	+14.303	-.02226	+.02240	+.02332	-.03979	-6.079	+3.413
3.45	+14.262	-.02303	+.02174	+.02346	-.04062	-6.559	+3.413
3.55	+14.239	-.02351	+.02101	+.02377	-.04145	-6.706	+3.413
3.66	+14.197	-.02473	+.01885	+.02447	-.04250	-6.811	+3.413
3.71	+14.144	-.02777	+.01478	+.02590	-.04461	-6.971	+3.409
3.82	+14.124	-.02827	+.01462	+.02648	-.04516	-7.019	+3.409
3.71	+14.115	-.02948	+.01241	+.02833	-.04569	-7.014	+3.410

LOAD(kips)	----------DEFLECTIONS(inches)----------						
CH.0	CH.1 MDSPAN	CH.2 ETROT	CH.3 EBROT	CH.4 WTROT	CH.5 WBROT	CH.6 SEND	CH.7 NEND
3.82	+14.099	-.02971	+.01234	+.02768	-.04592	-7.067	+3.392
3.88	+14.047	-.03131	+.01041	+.02800	-.04741	-7.190	+3.381
3.87	+13.994	-.03350	+.00689	+.03019	-.04973	-7.312	+3.373
3.94	+13.941	-.03522	+.00513	+.03021	-.05077	-7.434	+3.363
4.05	+13.897	-.03726	+.00313	+.03051	-.05223	-7.547	+3.355
3.99	+13.846	-.03604	-.00111	+.03368	-.05466	-7.667	+3.354
4.09	+13.827	-.03610	-.00113	+.03229	-.05510	-7.734	+3.354
3.98	+13.817	-.03310	-.00341	+.03571	-.05755	-7.793	+3.332
4.10	+13.795	-.03355	-.00344	+.03493	-.05822	-7.925	+3.328
3.90	+13.772	-.03108	-.00741	+.04527	-.06952	-8.019	+3.324
3.58	+13.732	+.00175	-.01576	+.05775	-.08785	-8.176	+3.324
3.67	+13.680	-.00269	-.01844	+.06208	-.08848	-8.900	+3.324
3.69	+13.622	-.00389	-.02463	+.06833	-.08856	-8.900	+3.320
3.79	+13.577	-.01430	-.02767	+.07058	-.08869	-8.900	+3.290
3.66	+13.571	-.01748	-.03054	+.07363	-.08849	-8.900	+3.290
3.77	+13.544	-.01792	-.03054	+.07303	-.08867	-8.900	+3.290
3.85	+13.491	-.02201	-.03336	+.07500	-.08857	-8.900	+3.272
3.71	+13.490	-.02456	-.03581	+.07781	-.08858	-8.900	+3.270
3.82	+13.475	-.02505	-.03585	+.07725	-.08833	-8.900	+3.270
3.87	+13.422	-.02867	-.03832	+.07939	-.08848	-8.900	+3.252
3.76	+13.414	-.03088	-.04042	+.08203	-.08849	-8.900	+3.248
3.87	+13.390	-.03141	-.04043	+.08162	-.08853	-8.900	+3.248
0.02	+13.306	-.01650	-.02057	+.07424	-.08857	-8.900	+3.134
0.13	+13.304	-.01582	-.01914	+.05774	-.08857	-8.900	+2.940
0.23	+13.303	-.01643	-.01938	+.05772	-.08859	-8.900	+2.940
0.34	+13.284	-.01677	-.01962	+.05785	-.08862	-8.900	+2.940
0.35	+13.227	-.01869	-.01855	+.04330	-.08866	-8.900	+2.923
0.40	+13.175	-.01890	-.01855	+.04928	-.08867	-8.900	+2.907
0.43	+13.122	-.01894	-.01856	+.05032	-.08870	-8.900	+2.881
0.42	+13.063	-.01918	-.01846	+.05136	-.08872	-8.900	+2.848
0.06	+13.003	-.02079	-.01629	+.07250	-.08876	-8.900	+2.813
0.14	+12.949	-.02125	-.01619	+.08115	-.08877	-8.900	+2.761
0.16	+12.892	-.02157	-.01602	+.08653	-.08879	-8.900	+2.720
0.17	+12.829	-.02211	-.01549	+.09995	-.08881	-8.900	+2.639
0.15	+12.775	-.02255	-.01500	+.09995	-.08882	-8.900	+2.666
0.15	+12.724	-.02298	-.01460	+.09995	-.08882	-8.900	+2.666

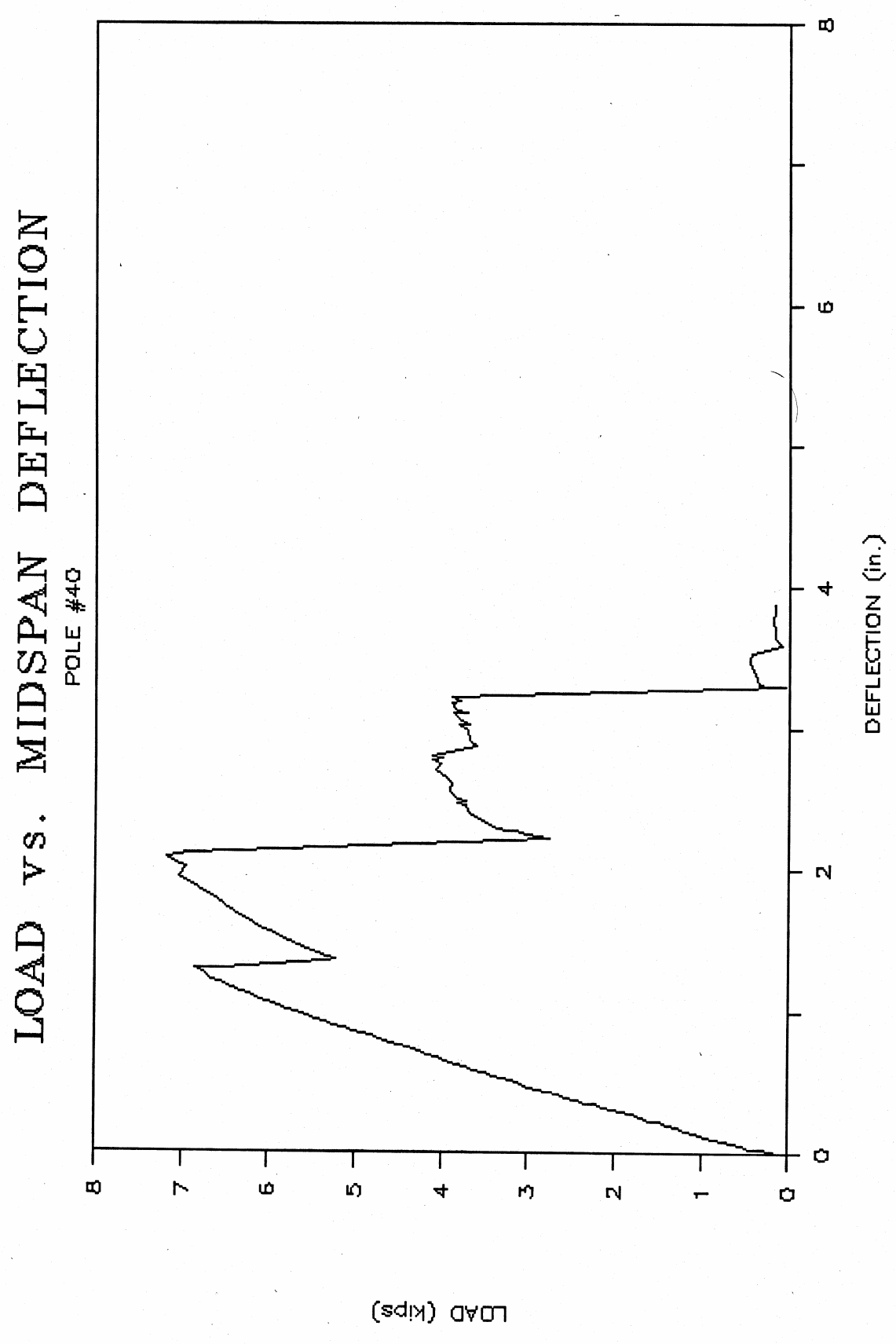
LOAD VS. MIDSPAN DEFLECTION
POLE #40
LOAD (kips)
DEFLECTION (in.)
0
1
2
3
4
5
6
7
8
0
2
4
6
8

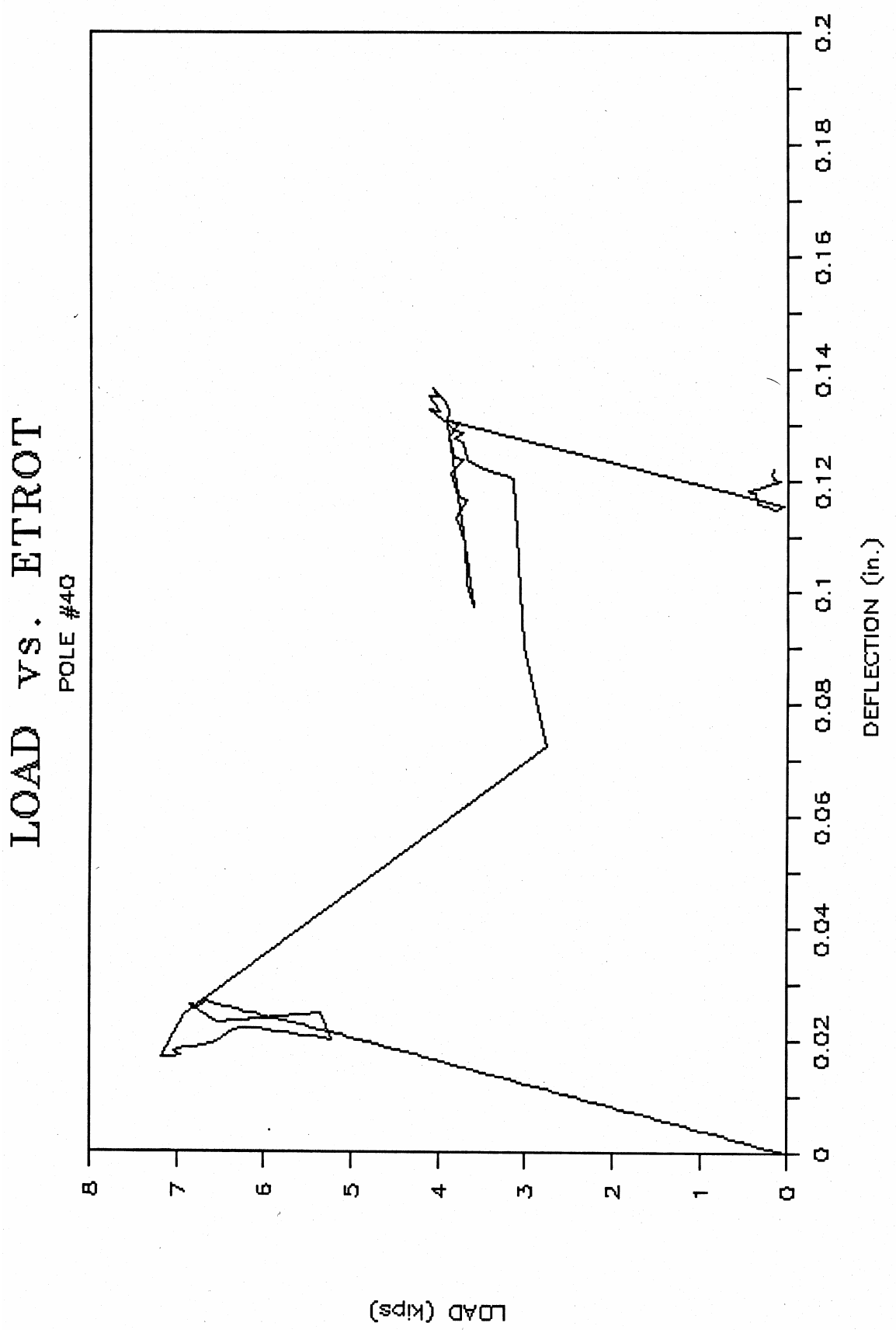
LOAD VS. ETROT
POLE #40
LOAD (kips)
DEFLECTION (in.)
0
1
2
3
4
5
6
7
8
0
0.02
0.04
0.06
0.08
0.1
0.12
0.14
0.16
0.18
0.2

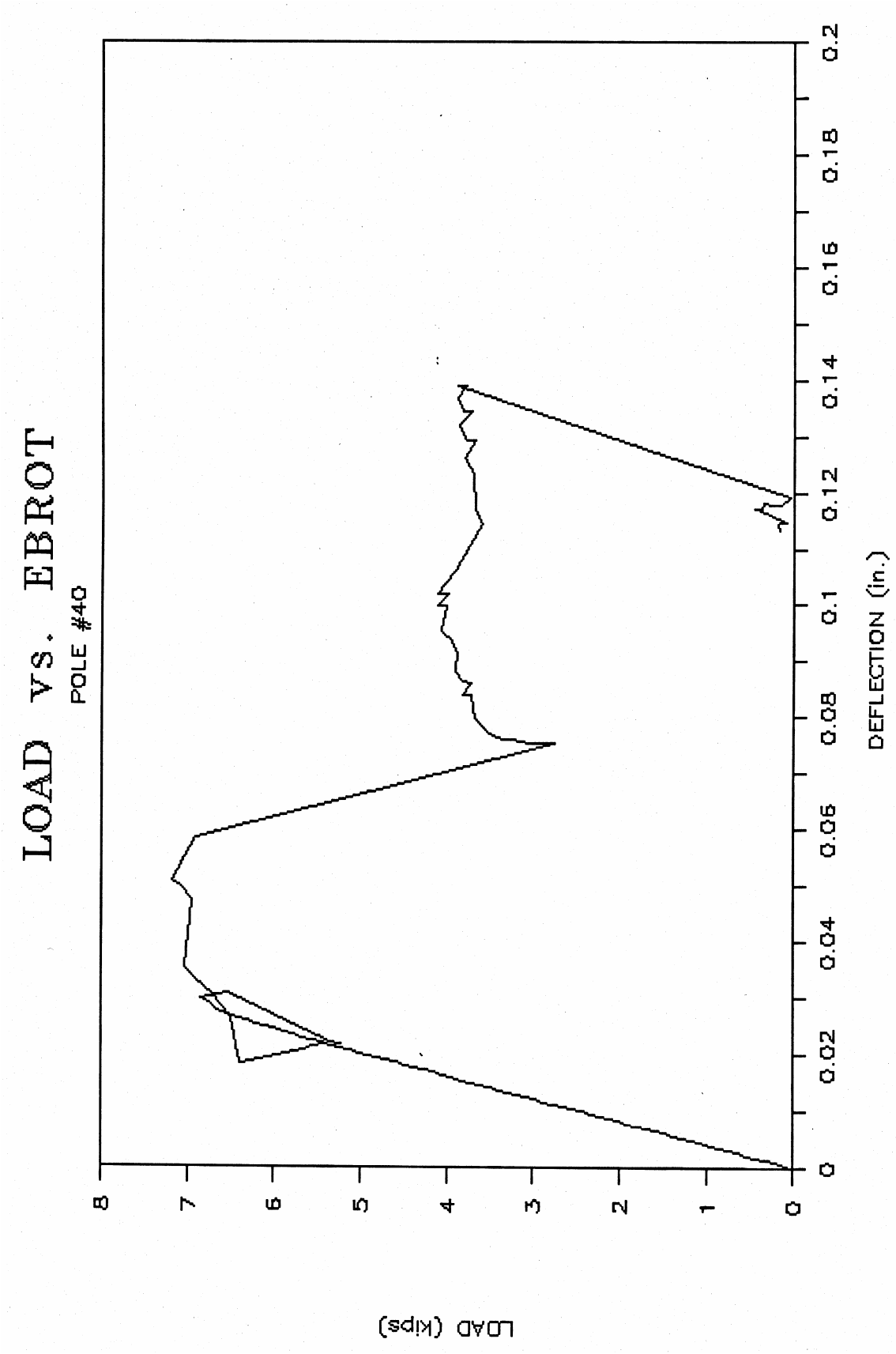
LOAD VS. EBROT
POLE #40
LOAD (kips)
DEFLECTION (in.)
0
1
2
3
4
5
6
7
8
0
0.02
0.04
0.06
0.08
0.1
0.12
0.14
0.16
0.18
0.2

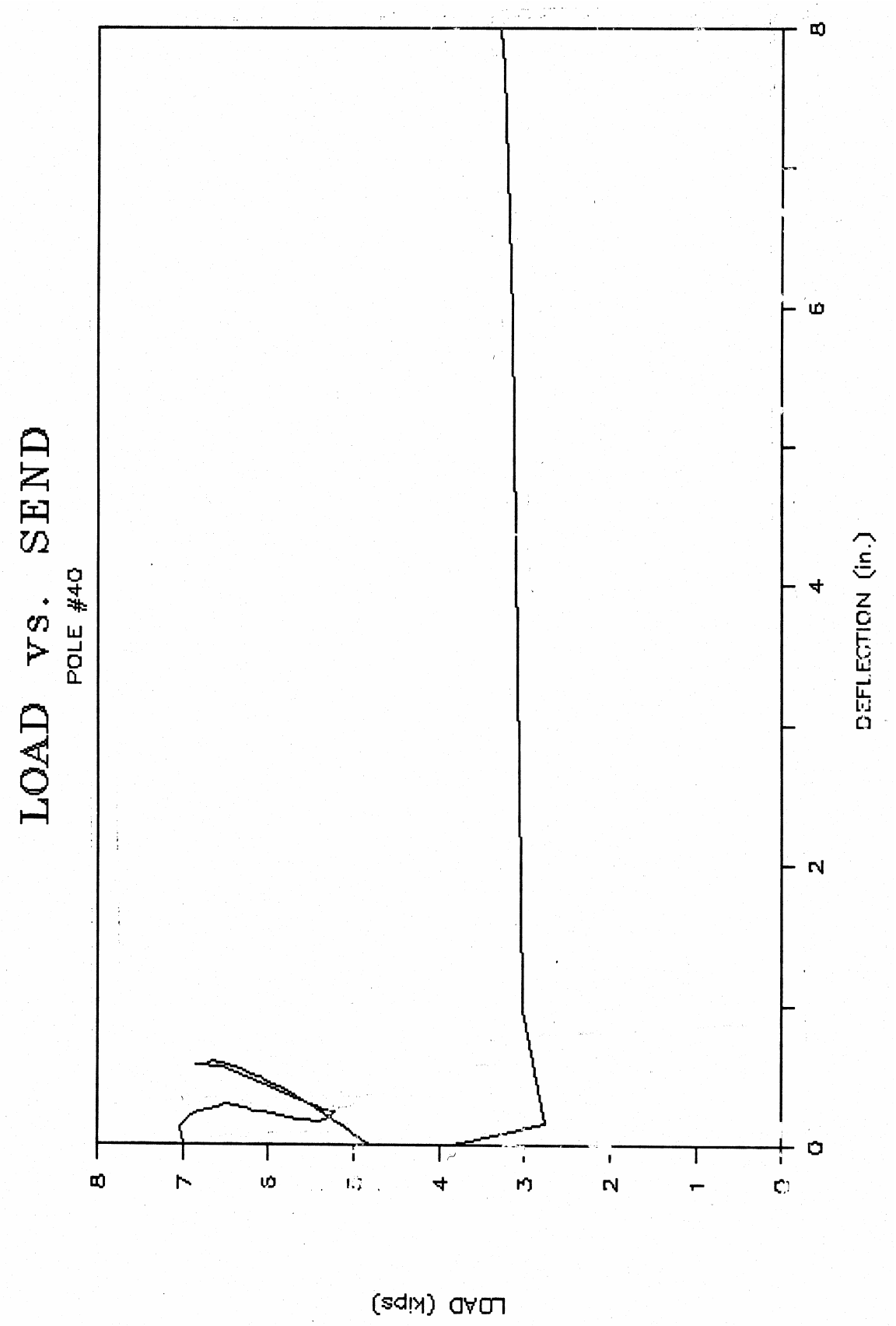
LOAD VS. SEND
POLE #40
LOAD (kips)
DEFLECTION (in.)
0
1
2
3
4
5
6
7
8
0
2
4
6
8

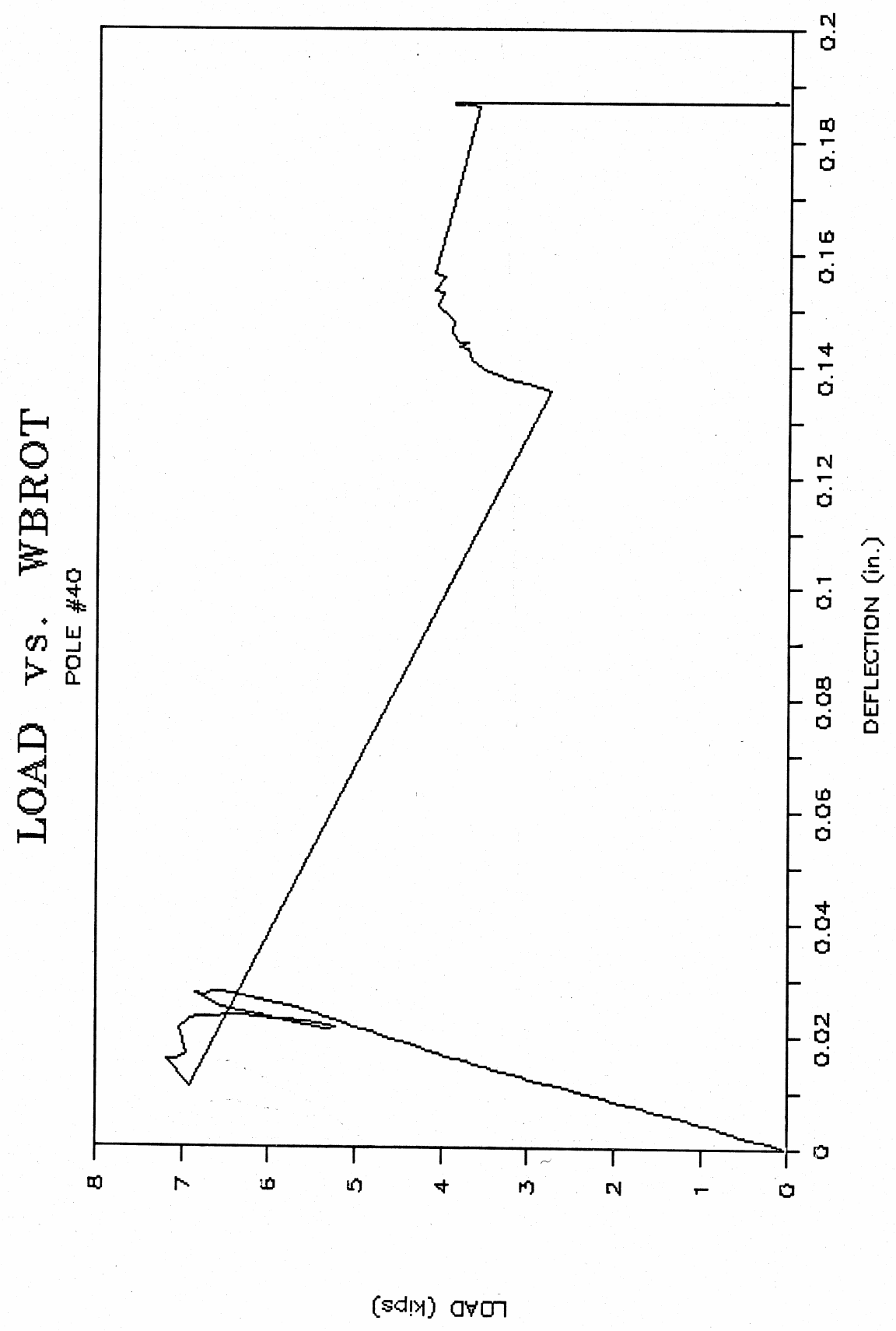
LOAD VS. WBROT
POLE #40
LOAD (kips)
DEFLECTION (in.)
0
1
2
3
4
5
6
7
8
0
0.02
0.04
0.06
0.08
0.1
0.12
0.14
0.16
0.18
0.2

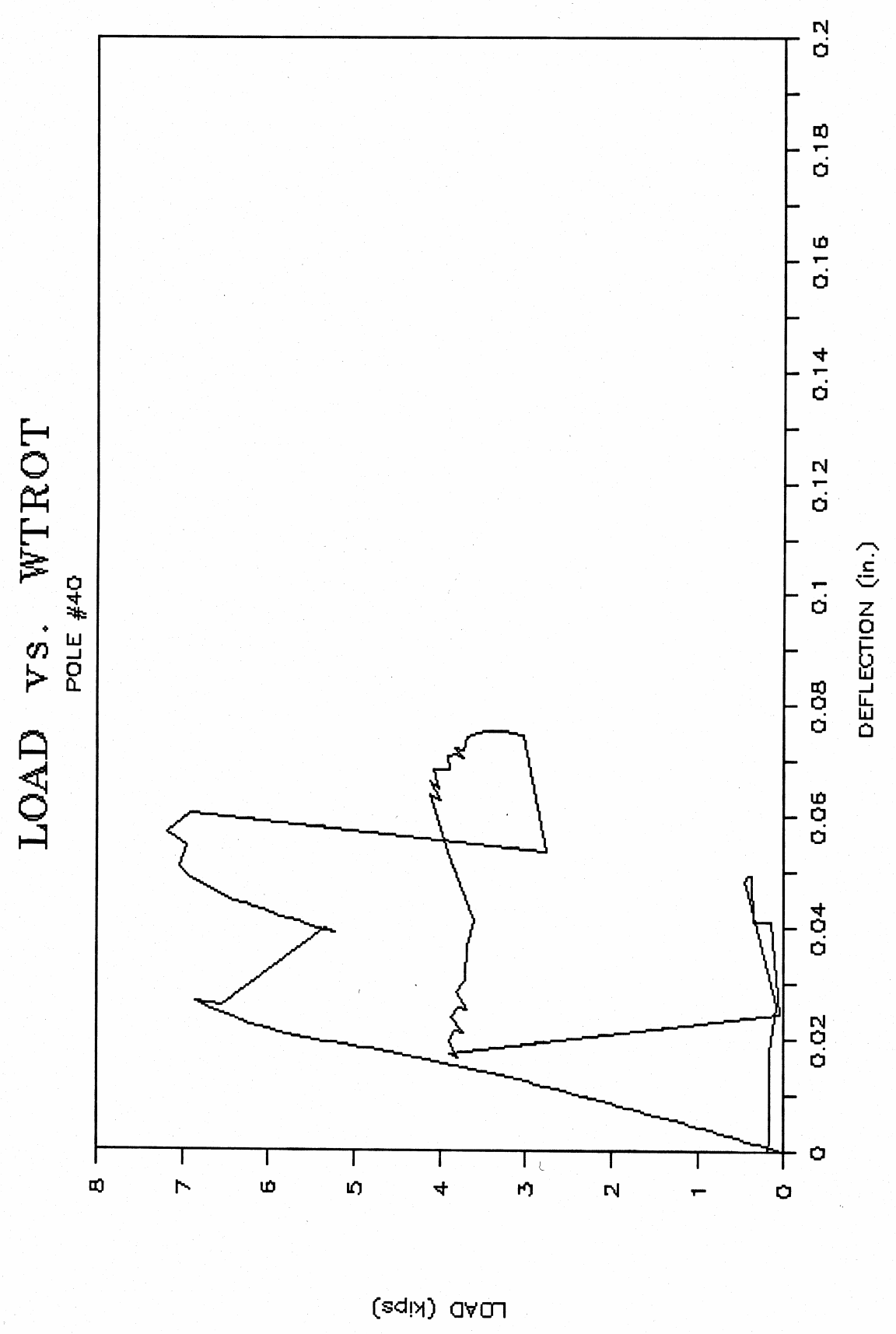
LOAD vs. WTROT
POLE #40
LOAD (kips)
DEFLECTION (in.)
0
1
2
3
4
5
6
7
8
0
0.02
0.04
0.06
0.08
0.1
0.12
0.14
0.16
0.18
0.2

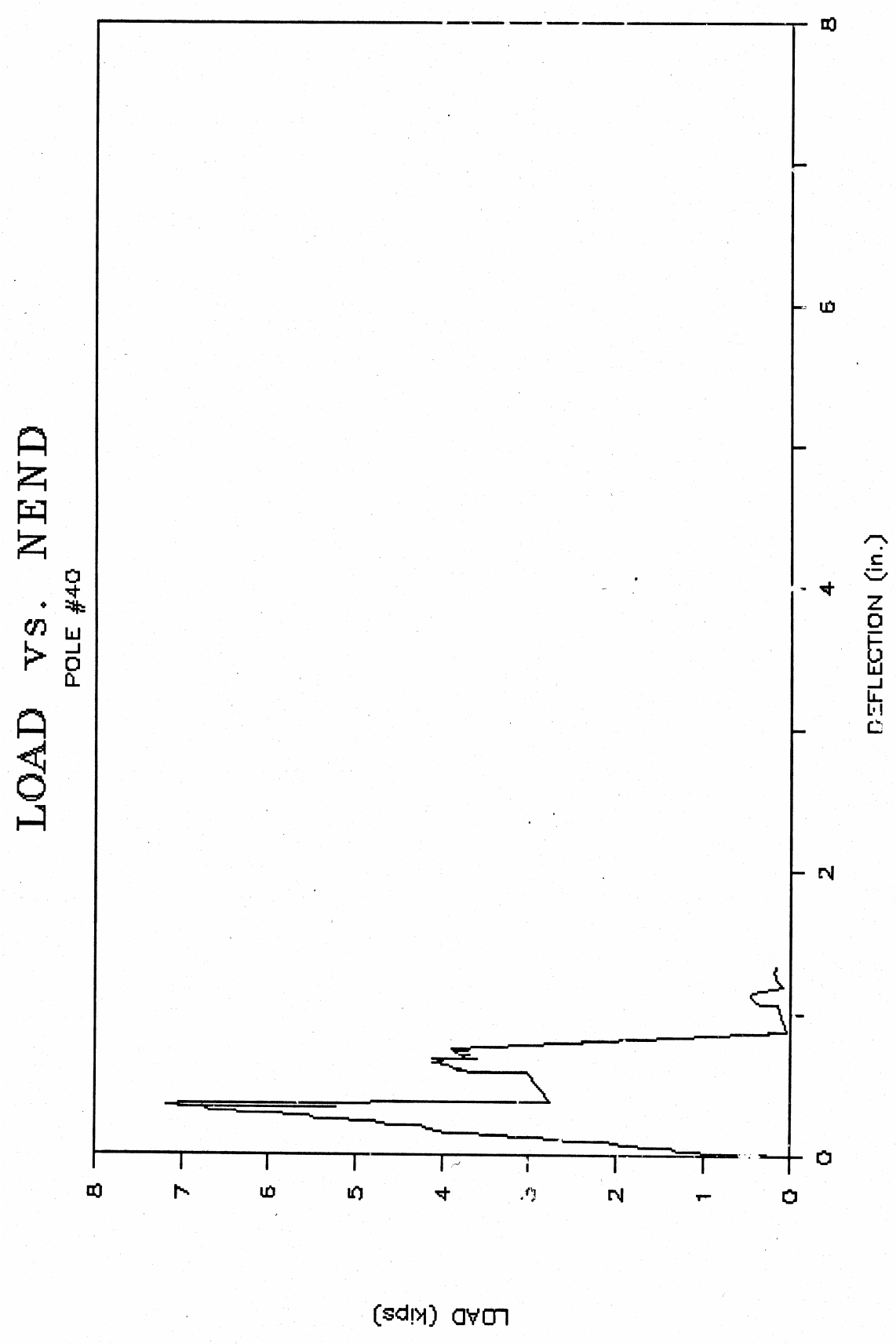
LOAD VS. NEND
POLE #40
LOAD (kips)
DEFLECTION (in.)
0
1
2
3
4
5
6
7
8
0
2
4
6
8

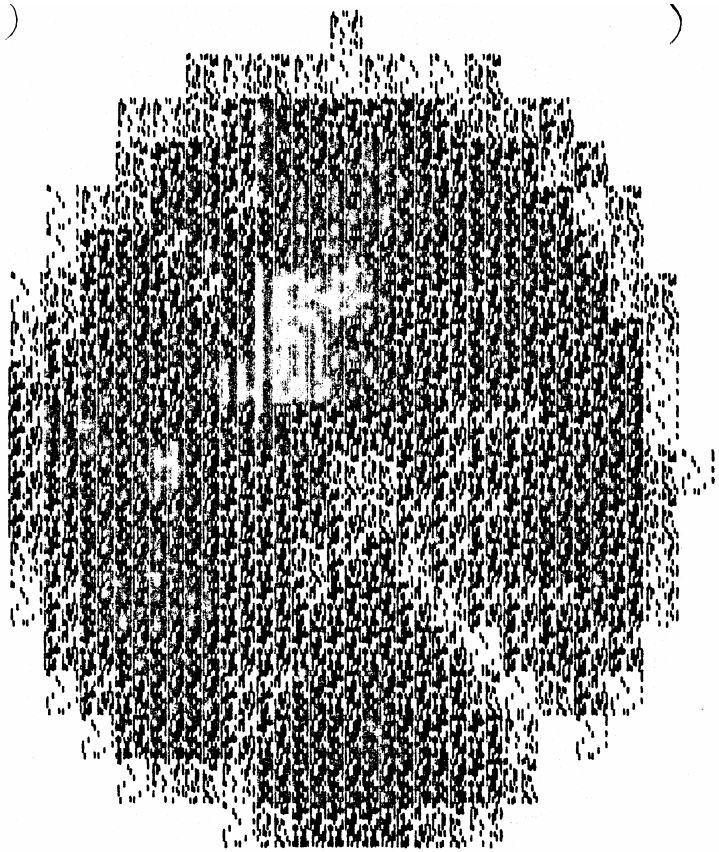

POLE IDENTIFICATION # 4013
IMAGED ON 12-01-1988
CIRCUMFERENCE (IN.) 23.5

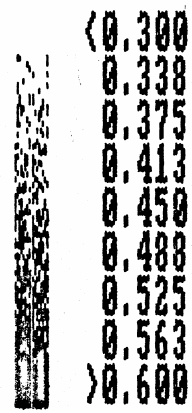

SOURCE POSITION ERROR = -.0012
DETECTOR POSITION ERROR = +.0023

MIN+ MIN- MAX+ MAX- STRENGTH QUIT

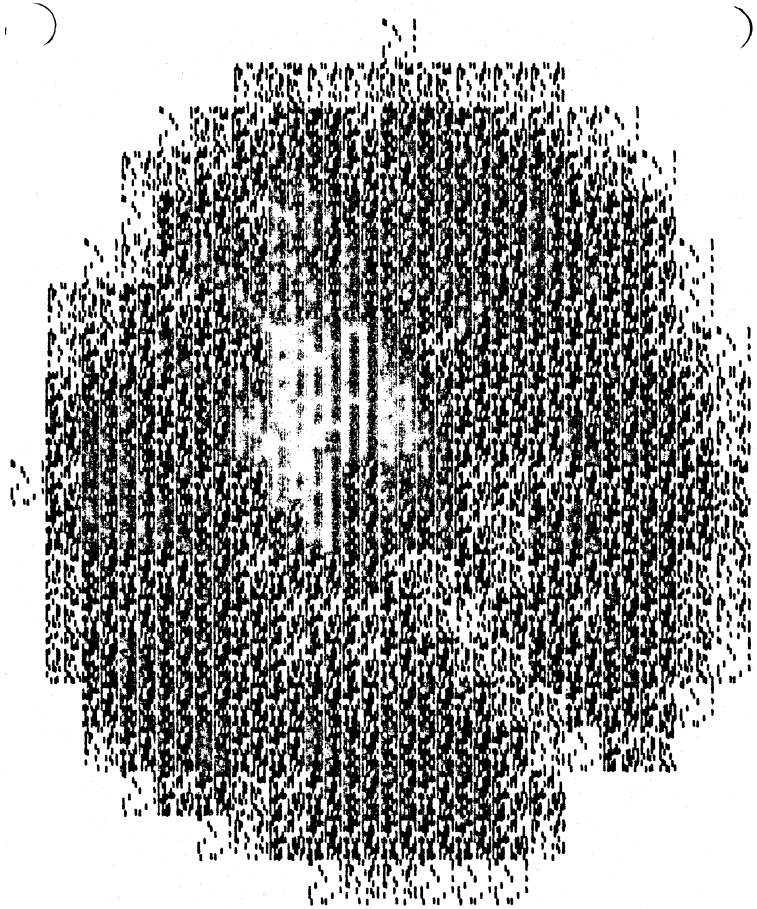

POLE IDENTIFICATION # 4012
IMAGED ON 12-01-1988
CIRCUMFERENCE (IN.) 23.75

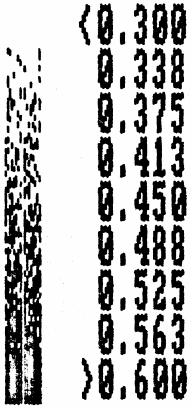

SOURCE POSITION ERROR = +.0001
DETECTOR POSITION ERROR = +.0010

MIN+ MIN- MAX+ MAX- STRENGTH QUIT

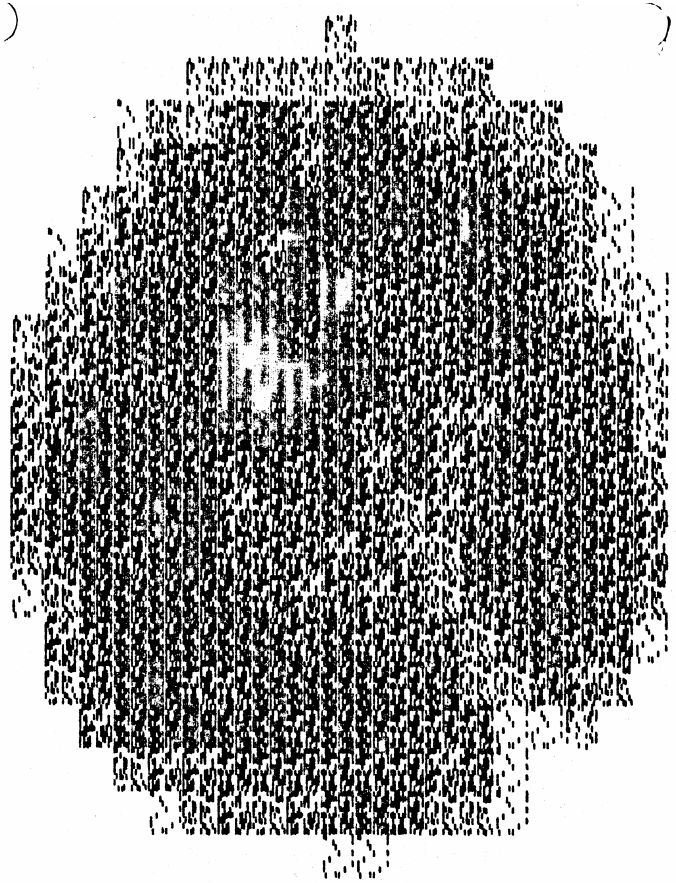

POLE IDENTIFICATION # 4011
IMAGED ON 12-01-1988
CIRCUMFERENCE (IN.) 24

<0.300
0.338
0.375
0.413
0.450
0.488
0.525
0.563
>0.600

SOURCE POSITION ERROR = -.0009
DETECTOR POSITION ERROR = -.0001

MIN+ MIN- MAX+ MAX- STRENGTH QUIT

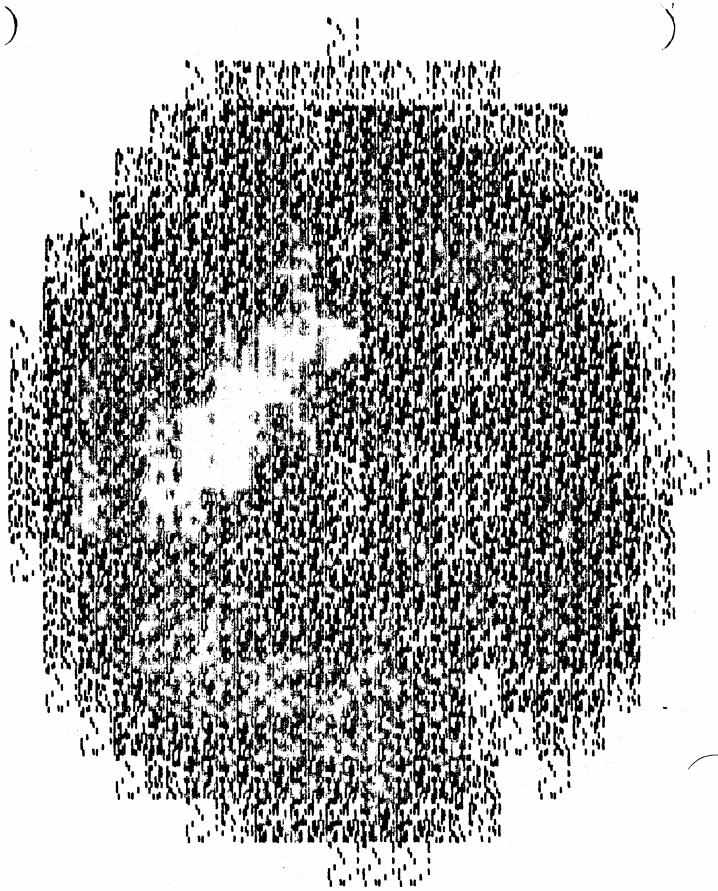

POLE IDENTIFICATION # 4000
IMAGED ON 12-01-1988
CIRCUMFERENCE (IN.) 24.25

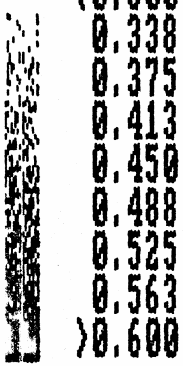

SOURCE POSITION ERROR = -.0008
DETECTOR POSITION ERROR = +.0018

MIN+ MIN- MAX+ MAX- STRENGTH QUIT

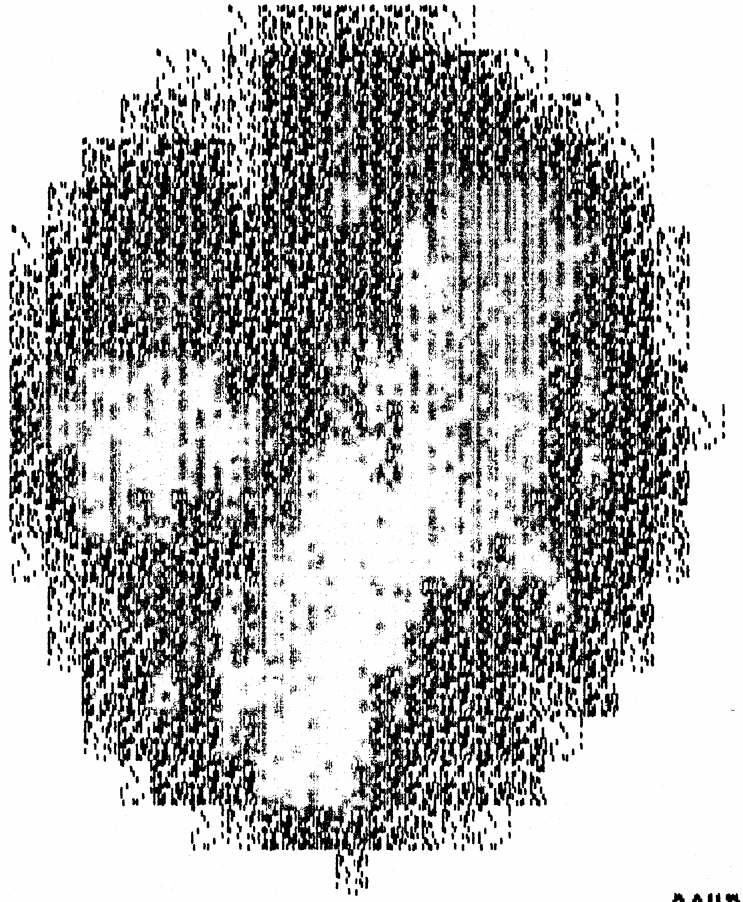

POLE IDENTIFICATION # 4001
IMAGED ON 12-01-1988
CIRCUMFERENCE (IN.) 24.5

<0.300
0.338
0.375
0.413
0.450
0.488
0.525
0.563
>0.600

SOURCE POSITION ERROR = +.0012
DETECTOR POSITION ERROR = +.0007

MIN+ MIN- MAX+ MAX- STRENGTH QUIT

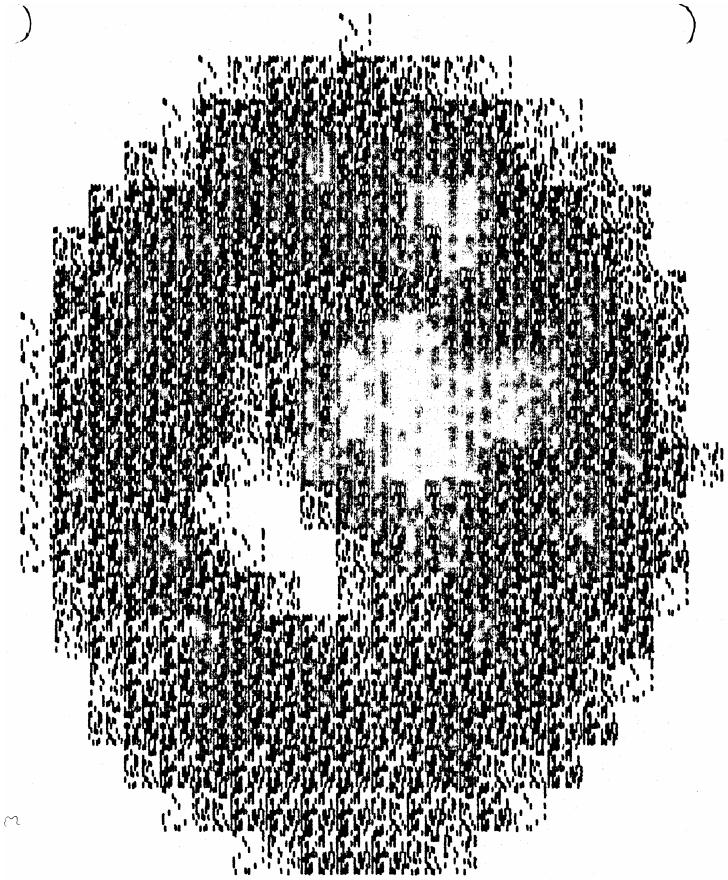

POLE IDENTIFICATION # 4002
IMAGED ON 12-01-1988
CIRCUMFERENCE (IN.) 25

<0.300
0.338
0.375
0.413
0.450
0.488
0.525
0.563
>0.600

SOURCE POSITION ERROR = +.0020
DETECTOR POSITION ERROR = +.0002

MIN+ MIN- MAX+ MAX- STRENGTH QUIT

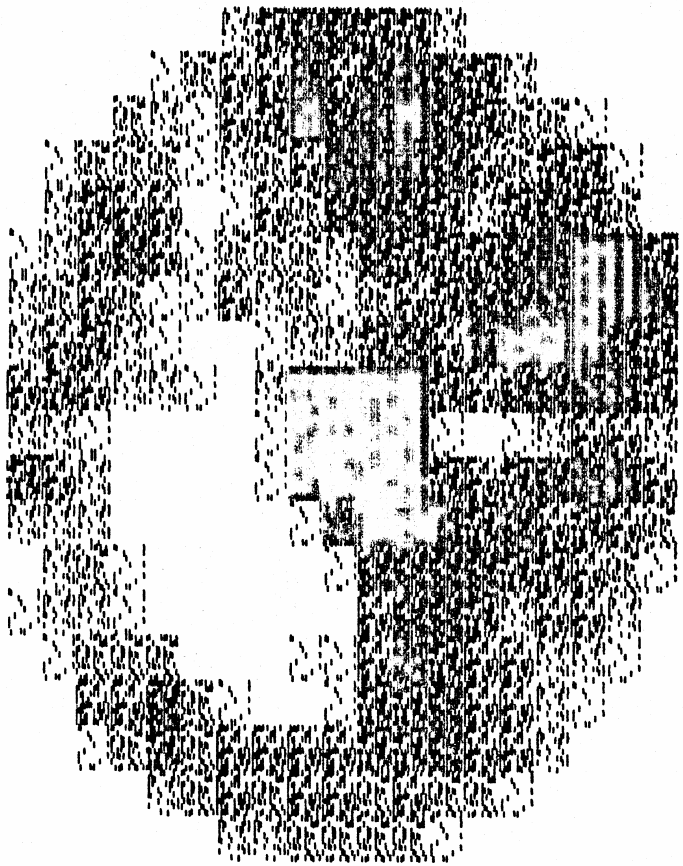

POLE IDENTIFICATION # 4003
IMAGED ON 12-01-1988
CIRCUMFERENCE (IN.) 25.5

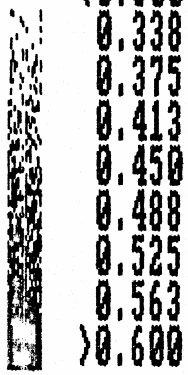

SOURCE POSITION ERROR = -.0004
DETECTOR POSITION ERROR = +.0008

MIN+ MIN- MAX+ MAX- STRENGTH QUIT

6.2 Physical destructive Test Data (Continued)

6.2.1 Pole 42

```
SPECIMEN TESTED IS pole42     12-07-1988  13:07:38
CALIBRATION FACTORS
_10  1.671  .01  .01  .01  .01  .89  .865
  RTH END SPAN LENGTH IS  67.625  INCHES.
__UTH END SPAN LENGTH IS  67.625  INCHES.
ROTATIONAL ORIENTATION IN DEGREES =  0
THE POLE BROKE  0 INCHES FROM GROUNDLINE.
THE APPROXIMATE CIRCUMFERENCE AT BREAKLINE IS  22.5  IN.
THE DIAMETER AT BREAKLINE IS  7.161978  IN.
THE MOMENT OF INERTIA IS  129.1522 IN.^4
THE MAXIMUM LOAD IS  4.23418  KIP
THE MOMENT AT MAXIMUM LOAD IS  116.7046  IN.-KIP
THE MORGL AT BREAKLINE IS  3.235854 KSI.

The pole is a top cut of another pole therefore there was
no previously established groundline.  The failure was slow
and deliberate.  There is a knot in the pole close to the
breakline but I do not think that it affected the failure of
the pole.  The knot can not be found in the scan images.
```

SPECIMEN TESTED IS pole42 12-07-1988 13:07:51

LOAD(kips)	DEFLECTIONS(inches)						
CH.0	CH.1 MDSPAN	CH.2 ETROT	CH.3 EBROT	CH.4 WTROT	CH.5 WBROT	CH.6 SEND	CH.7 NEND
-0.05	+16.432	+.09812	+.09943	+.09830	+.09935	+2.707	+4.257
0.05	+16.431	+.09810	+.09897	+.09719	+.09877	+4.330	+4.257
0.16	+16.422	+.09724	+.09795	+.09566	+.09786	+4.272	+4.258
0.26	+16.415	+.09643	+.09702	+.09433	+.09705	+4.220	+4.259
0.37	+16.384	+.09532	+.09589	+.09253	+.09607	+4.144	+4.258
0.48	+16.367	+.09440	+.09479	+.09083	+.09512	+4.071	+4.258
0.62	+16.318	+.09327	+.09347	+.08865	+.09395	+3.968	+4.260
0.72	+16.301	+.09208	+.09250	+.08701	+.09314	+3.908	+4.257
0.82	+16.263	+.09135	+.09117	+.08492	+.09180	+3.810	+4.258
0.92	+16.244	+.09057	+.09015	+.08336	+.09079	+3.734	+4.258
1.03	+16.217	+.08999	+.08855	+.08140	+.08960	+3.641	+4.254
1.13	+16.188	+.08943	+.08708	+.07957	+.08835	+3.541	+4.254
1.24	+16.159	+.08858	+.08574	+.07774	+.08704	+3.450	+4.249
1.34	+16.124	+.08792	+.08450	+.07574	+.08556	+3.338	+4.246
1.45	+16.105	+.08767	+.08369	+.07438	+.08466	+3.254	+4.246
1.55	+16.057	+.08692	+.08229	+.07215	+.08314	+3.129	+4.241
1.65	+16.041	+.08634	+.08126	+.07052	+.08200	+3.040	+4.235
1.75	+15.994	+.08561	+.08000	+.06865	+.08069	+2.935	+4.224
1.86	+15.959	+.08496	+.07885	+.06686	+.07942	+2.831	+4.220
1.96	+15.927	+.08450	+.07717	+.06500	+.07792	+2.715	+4.212
2.07	+15.883	+.08385	+.07602	+.06321	+.07638	+2.595	+4.203
2.17	+15.853	+.08274	+.07496	+.06139	+.07493	+2.487	+4.194
2.28	+15.808	+.08210	+.07390	+.05982	+.07357	+2.374	+4.190
2.38	+15.764	+.08106	+.07242	+.05749	+.07143	+2.213	+4.178
2.49	+15.731	+.08062	+.07165	+.05619	+.07029	+2.115	+4.173
2.59	+15.688	+.07974	+.07017	+.05391	+.06835	+1.958	+4.160
2.70	+15.635	+.07886	+.06913	+.05216	+.06654	+1.819	+4.156
2.80	+15.600	+.07813	+.06820	+.05058	+.06498	+1.695	+4.148
2.89	+15.547	+.07280	+.06325	+.04778	+.06235	+1.511	+4.135
3.00	+15.503	+.07221	+.06108	+.04585	+.06057	+1.346	+4.130
3.07	+15.453	+.07064	+.05545	+.04368	+.05846	+1.178	+4.124
3.17	+15.413	+.06921	+.05199	+.04154	+.05691	+1.033	+4.116
3.27	+15.360	+.06637	+.04818	+.03899	+.05408	+0.860	+4.106
3.30	+15.308	+.06310	+.04392	+.03604	+.05266	+0.675	+4.093
3.40	+15.263	+.06174	+.04013	+.03310	+.05064	+0.518	+4.089
3.49	+15.210	+.05980	+.03724	+.03052	+.04889	+0.379	+4.088
3.37	+15.198	+.05478	+.03460	+.02982	+.04715	+0.336	+4.079
3.38	+15.144	+.05459	+.03308	+.02824	+.04547	+0.181	+4.055
3.49	+15.111	+.05240	+.03040	+.02601	+.04375	-0.006	+4.055
3.38	+15.065	+.04455	+.02753	+.03147	+.04125	-0.187	+4.046
3.44	+15.013	+.04130	+.02480	+.02963	+.03867	-0.423	+4.042
3.54	+14.979	+.03902	+.02254	+.02766	+.03714	-0.574	+4.034
3.61	+14.928	+.03705	+.02047	+.02571	+.03583	-0.687	+4.033
3.70	+14.874	+.03450	+.01802	+.02311	+.03451	-0.815	+4.025
3.74	+14.824	+.03188	+.01321	+.01895	+.03359	-0.920	+4.017
3.66	+14.762	+.02292	+.00425	+.00978	+.03024	-1.067	+3.999
3.55	+14.740	+.01200	-.00213	+.00470	+.02891	-1.159	+3.984
3.42	+14.718	+.00481	-.00501	+.00531	+.02694	-1.181	+3.970
3.29	+14.687	-.01180	-.01442	-.00066	+.02486	-1.495	+3.954
3.29	+14.629	-.01864	-.01506	-.00347	+.02154	-1.747	+3.946

LOAD(kips)	----------DEFLECTIONS(inches)----------						
CH.0	CH.1 MDSPAN	CH.2 ETROT	CH.3 EBROT	CH.4 WTROT	CH.5 WBROT	CH.6 SEND	CH.7 NEND
3.33	+14.578	-.02646	-.01768	-.00698	+.01640	-2.167	+3.928
3.34	+14.527	-.03125	-.01956	-.01041	+.01801	-2.149	+3.920
3.36	+14.473	-.03646	-.02140	-.01467	+.01736	-2.280	+3.907
3.39	+14.418	-.04143	-.02284	-.01771	+.01617	-2.289	+3.890
3.41	+14.361	-.04672	-.02451	-.02292	+.01340	-2.476	+3.882
3.45	+14.301	-.05127	-.02586	-.02768	+.01072	-2.669	+3.866
3.45	+14.239	-.06068	-.02675	-.03400	+.00642	-2.986	+3.850
3.46	+14.188	-.06784	-.02831	-.03952	+.00221	-3.298	+3.840
3.46	+14.137	-.07518	-.02732	-.04647	-.00099	-3.554	+3.831
3.46	+14.084	-.07797	-.02930	-.05305	-.00394	-3.802	+3.814
3.47	+14.033	-.07842	-.03066	-.05897	-.00617	-3.989	+3.801
3.46	+13.979	-.07847	-.03103	-.06496	-.00861	-4.161	+3.789
3.49	+13.924	-.07848	-.03287	-.07153	-.01224	-4.431	+3.784
3.31	+13.894	-.07688	-.03037	-.06654	-.02111	-4.491	+3.776
3.17	+13.860	-.07834	-.04207	-.07286	-.02226	-5.016	+3.763
3.13	+13.806	-.07821	-.04538	-.07869	-.02600	-5.338	+3.755
3.10	+13.743	-.07861	-.04644	-.08537	-.03133	-5.808	+3.742
3.09	+13.685	-.07864	-.04839	-.09087	-.03583	-6.168	+3.729
3.12	+13.634	-.07863	-.05070	-.09423	-.03995	-6.481	+3.717
1.30	+13.538	-.07858	-.10000	-.07022	-.08801	-7.032	+3.686
1.36	+13.480	-.07897	-.10000	-.09430	-.08843	-8.644	+3.629
1.40	+13.429	-.07896	-.10000	-.09237	-.08860	-8.900	+3.628
1.43	+13.379	-.07896	-.10000	-.08907	-.08867	-8.900	+3.629
1.48	+13.325	-.07896	-.10000	-.08511	-.08873	-8.900	+3.625
1.48	+13.264	-.07895	-.10000	-.08185	-.08877	-8.900	+3.615
1.51	+13.211	-.07896	-.10000	-.07827	-.08881	-8.900	+3.607
1.53	+13.153	-.07896	-.10000	-.07580	-.08882	-8.900	+3.604
1.55	+13.102	-.07897	-.10000	-.07274	-.08886	-8.900	+3.594
1.56	+13.036	-.07897	-.10000	-.07106	-.08886	-8.900	+3.586
1.55	+12.985	-.07893	-.10000	-.06654	-.08887	-8.900	+3.577
1.49	+12.933	-.07899	-.10000	-.05490	-.08887	-8.900	+3.565
1.51	+12.882	-.07897	-.10000	-.05021	-.08891	-8.900	+3.556
1.50	+12.831	-.07898	-.10000	-.04846	-.08892	-8.900	+3.550
1.50	+12.772	-.07898	-.10000	-.04576	-.08895	-8.900	+3.531
1.50	+12.719	-.07898	-.10000	-.04313	-.08896	-8.900	+3.521
1.51	+12.663	-.07901	-.10000	-.04143	-.08896	-8.900	+3.512
1.51	+12.609	-.07899	-.10000	-.04025	-.08896	-8.900	+3.505
1.52	+12.541	-.07901	-.10000	-.03871	-.08897	-8.900	+3.497
1.52	+12.488	-.07899	-.10000	-.03706	-.08900	-8.900	+3.480
1.51	+12.435	-.07901	-.10000	-.03594	-.08901	-8.900	+3.469
1.51	+12.382	-.07902	-.10000	-.03555	-.08902	-8.900	+3.459
1.52	+12.329	-.07903	-.10000	-.03490	-.08902	-8.900	+3.455
1.52	+12.277	-.07902	-.10000	-.03438	-.08903	-8.900	+3.446
1.54	+12.216	-.07903	-.10000	-.03348	-.08905	-8.900	+3.439
1.53	+12.165	-.07901	-.10000	-.03271	-.08908	-8.900	+3.430
1.53	+12.115	-.07905	-.10000	-.03027	-.08908	-8.900	+3.417
1.52	+12.054	-.07905	-.10000	-.02508	-.08908	-8.900	+3.406
1.53	+12.002	-.07904	-.10000	-.02510	-.08909	-8.900	+3.396
1.52	+11.948	-.07904	-.10000	-.02493	-.08910	-8.900	+3.385
1.53	+11.891	-.07905	-.10000	-.02544	-.08911	-8.900	+3.374

LOAD(kips)	----------DEFLECTIONS(inches)----------						
CH.0	CH.1 MDSPAN	CH.2 ETROT	CH.3 EBROT	CH.4 WTROT	CH.5 WBROT	CH.6 SEND	CH.7 NEND
1.51	+11.830	-.07905	-.10000	-.02899	-.08911	-8.900	+3.363
1.51	+11.775	-.07904	-.10000	-.02988	-.08913	-8.900	+3.350
1.45	+11.720	-.07909	-.10000	-.02423	-.08913	-8.900	+3.341
1.45	+11.668	-.07908	-.10000	-.02448	-.08913	-8.900	+3.328
1.35	+11.628	-.07908	-.10000	-.02700	-.08913	-8.900	+3.320
1.29	+11.576	-.07909	-.10000	-.02723	-.08912	-8.900	+3.299
1.21	+11.522	-.07906	-.10000	-.02767	-.08916	-8.900	+3.286
1.15	+11.471	-.07912	-.10000	-.02964	-.08915	-8.900	+3.275
1.10	+11.413	-.07909	-.10000	-.03083	-.08916	-8.900	+3.262
1.04	+11.358	-.07910	-.10000	-.03186	-.08918	-8.900	+3.251
1.04	+11.300	-.07912	-.10000	-.03213	-.08918	-8.900	+3.238
1.07	+11.249	-.07912	-.10000	-.03271	-.08919	-8.900	+3.232
1.09	+11.197	-.07911	-.10000	-.03328	-.08920	-8.900	+3.224
1.07	+11.144	-.07912	-.10000	-.03479	-.08920	-8.900	+3.214
1.07	+11.092	-.07913	-.10000	-.03436	-.08920	-8.900	+3.206
1.07	+11.033	-.07911	-.10000	-.03558	-.08921	-8.900	+3.199
1.08	+10.975	-.07914	-.10000	-.03712	-.08921	-8.900	+3.189
1.08	+10.924	-.07914	-.10000	-.03874	-.08921	-8.900	+3.183
1.09	+10.868	-.07914	-.10000	-.04070	-.08922	-8.900	+3.176
1.09	+10.815	-.07913	-.10000	-.04285	-.08923	-8.900	+3.170
1.09	+10.764	-.07913	-.10000	-.04519	-.08923	-8.900	+3.165
1.07	+10.713	-.07914	-.10000	-.04638	-.08923	-8.900	+3.142
1.06	+10.662	-.07913	-.10000	-.04904	-.08923	-8.900	+3.136
1.07	+10.607	-.07915	-.10000	-.05104	-.08924	-8.900	+3.130
1.06	+10.554	-.07915	-.10000	-.05334	-.08926	-8.900	+3.118
1.07	+10.503	-.07915	-.10000	-.05563	-.08925	-8.900	+3.113
0.71	+10.434	-.07907	-.10000	-.06429	-.08925	-8.900	+3.092
0.63	+10.382	-.07915	-.10000	-.06451	-.08926	-8.900	+3.087
0.63	+10.322	-.07915	-.10000	-.06610	-.08928	-8.900	+3.079
0.53	+10.279	-.07915	-.10000	-.07144	-.08932	-8.900	+3.071

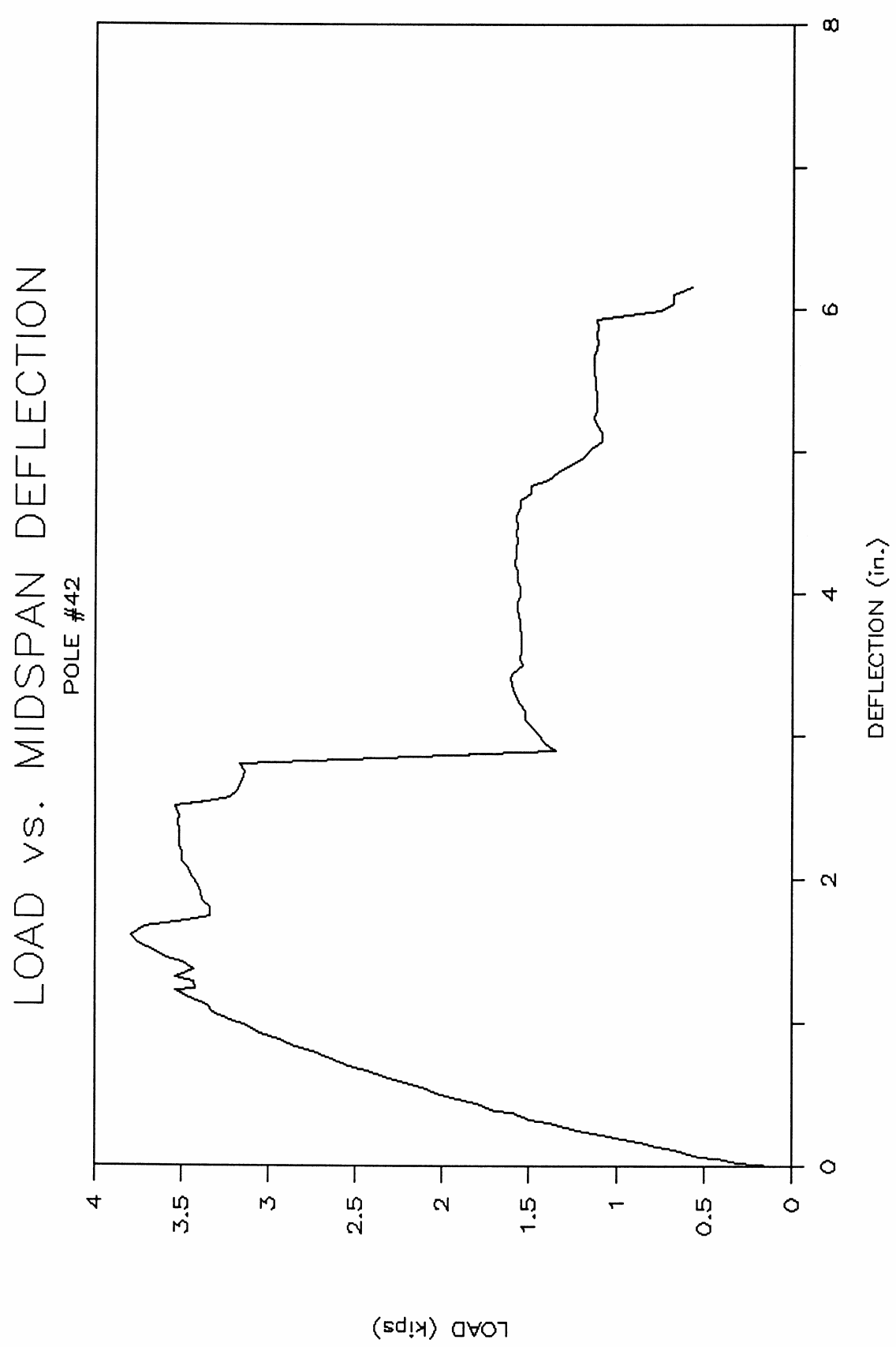
LOAD vs. MIDSPAN DEFLECTION
POLE #42
LOAD (kips)
4
3.5
3
2.5
2
1.5
1
0.5
0
0
2
4
6
8
DEFLECTION (in.)

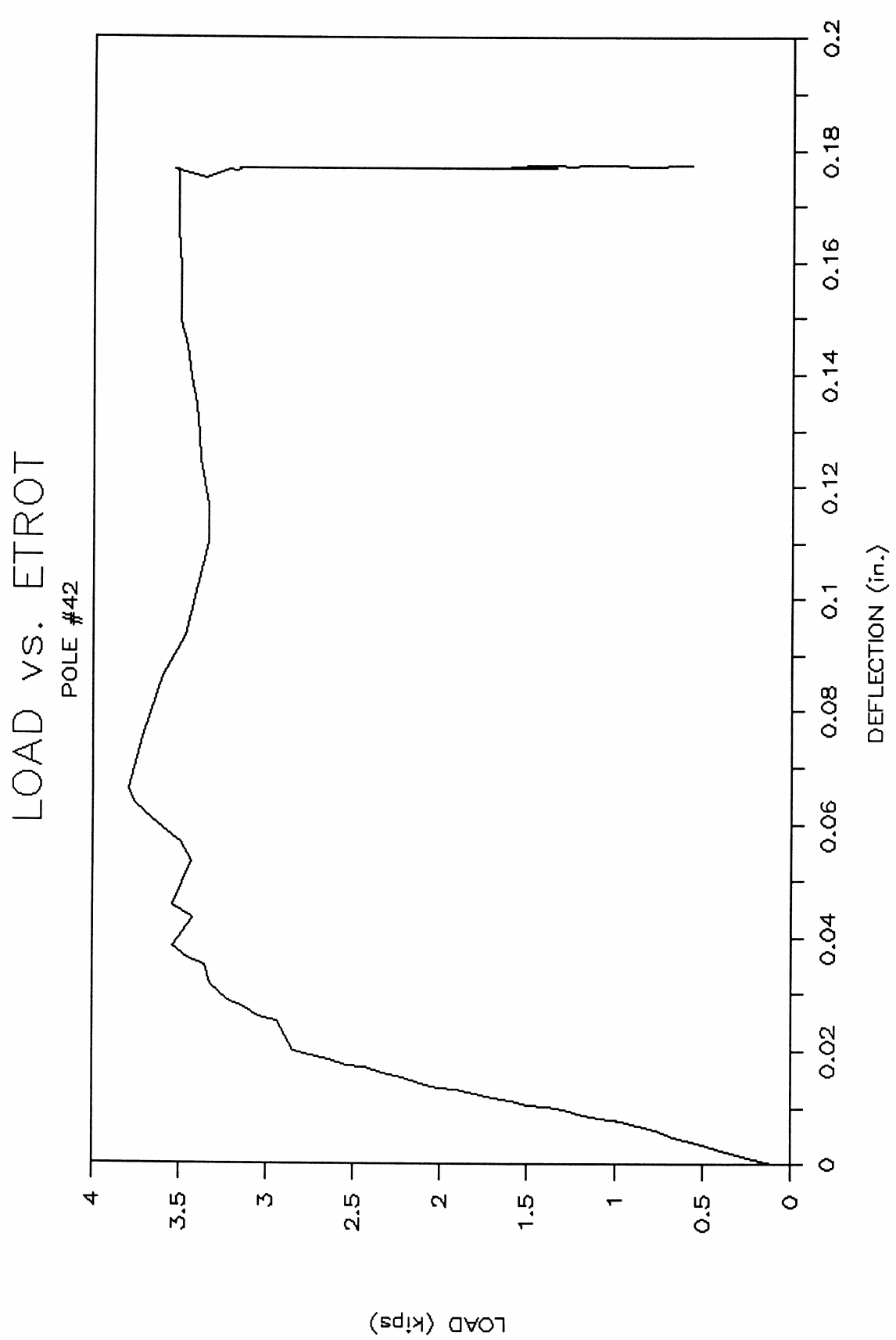
LOAD VS. ETROT
POLE #42
LOAD (kips)
DEFLECTION (in.)
0
0.5
1
1.5
2
2.5
3
3.5
4
0
0.02
0.04
0.06
0.08
0.1
0.12
0.14
0.16
0.18
0.2

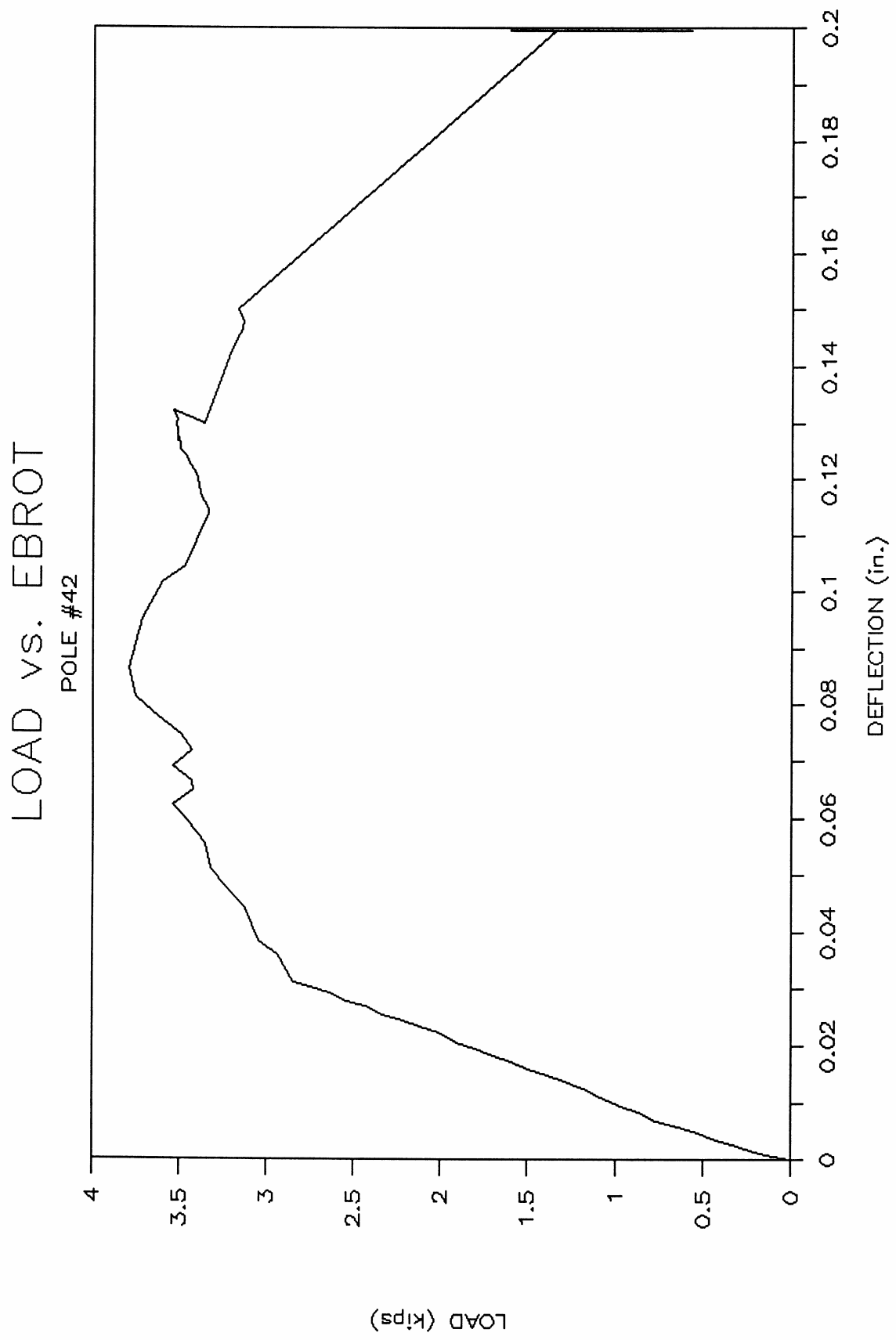
LOAD vs. EBROT
POLE #42
LOAD (kips)
4
3.5
3
2.5
2
1.5
1
0.5
0
0
0.02
0.04
0.06
0.08
0.1
0.12
0.14
0.16
0.18
0.2
DEFLECTION (in.)

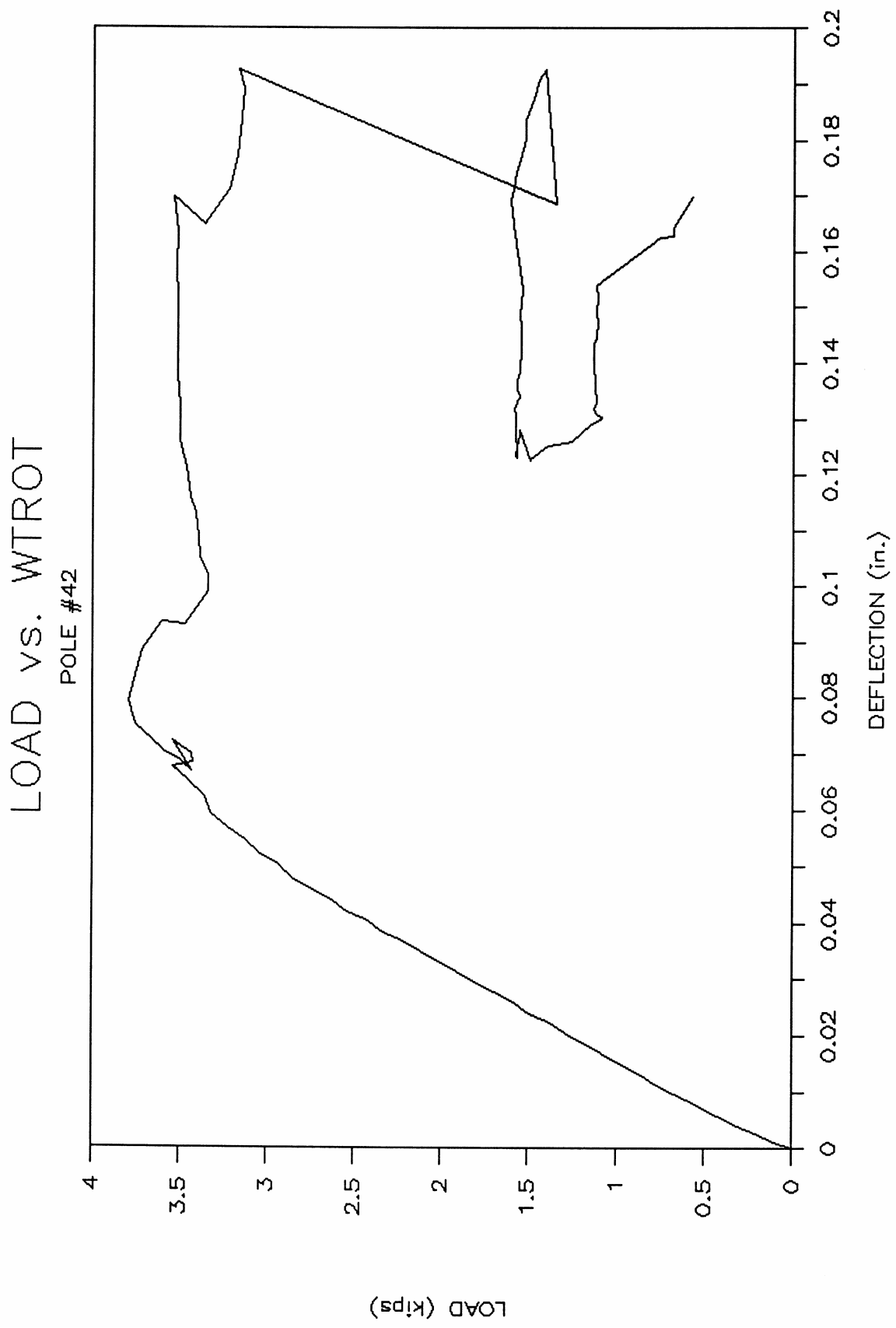
LOAD vs. WTROT
POLE #42
LOAD (kips)
4
3.5
3
2.5
2
1.5
1
0.5
0
0
0.02
0.04
0.06
0.08
0.1
0.12
0.14
0.16
0.18
0.2
DEFLECTION (in.)

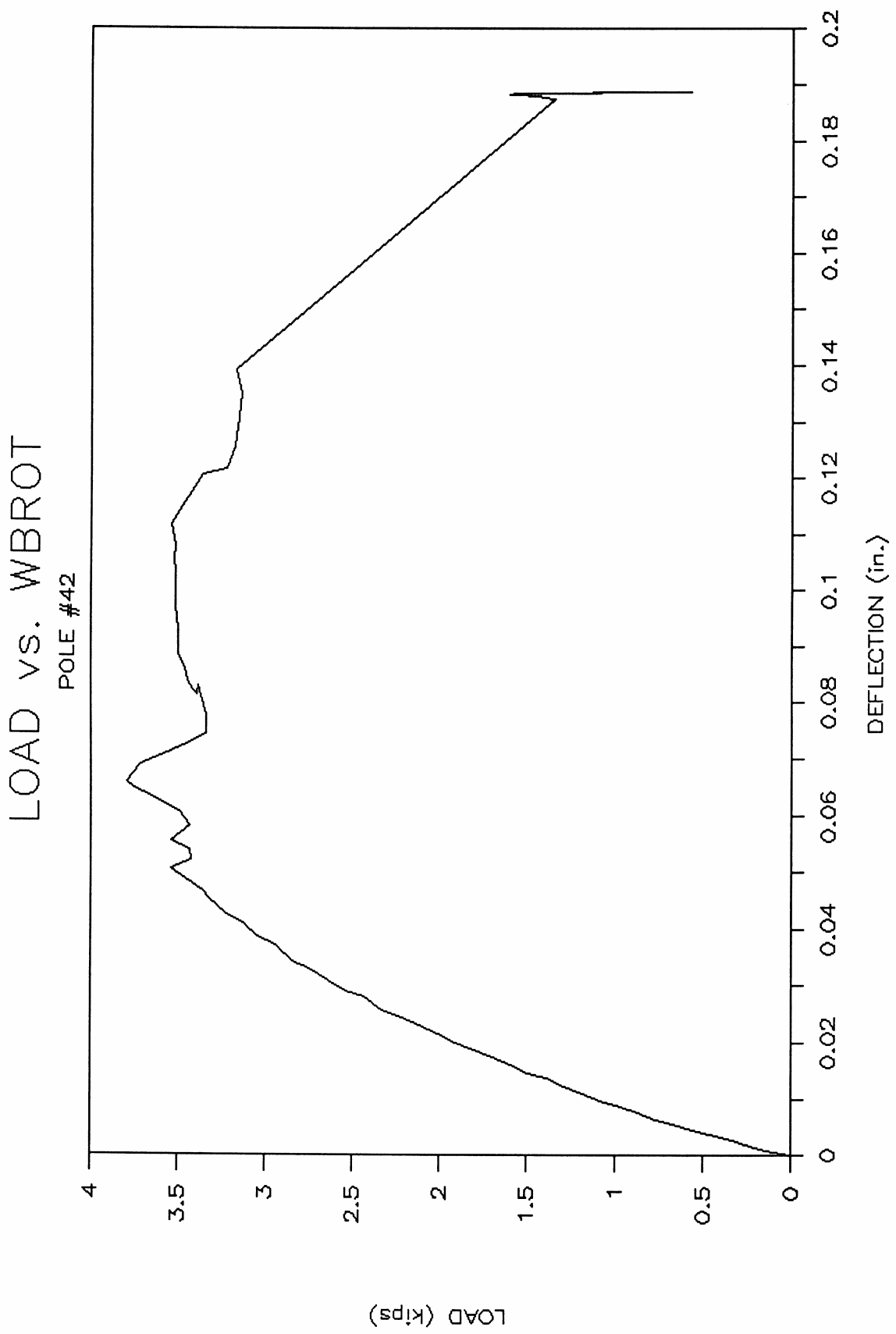
LOAD vs. WBROT
POLE #42
LOAD (kips)
4
3.5
3
2.5
2
1.5
1
0.5
0
0
0.02
0.04
0.06
0.08
0.1
0.12
0.14
0.16
0.18
0.2
DEFLECTION (in.)

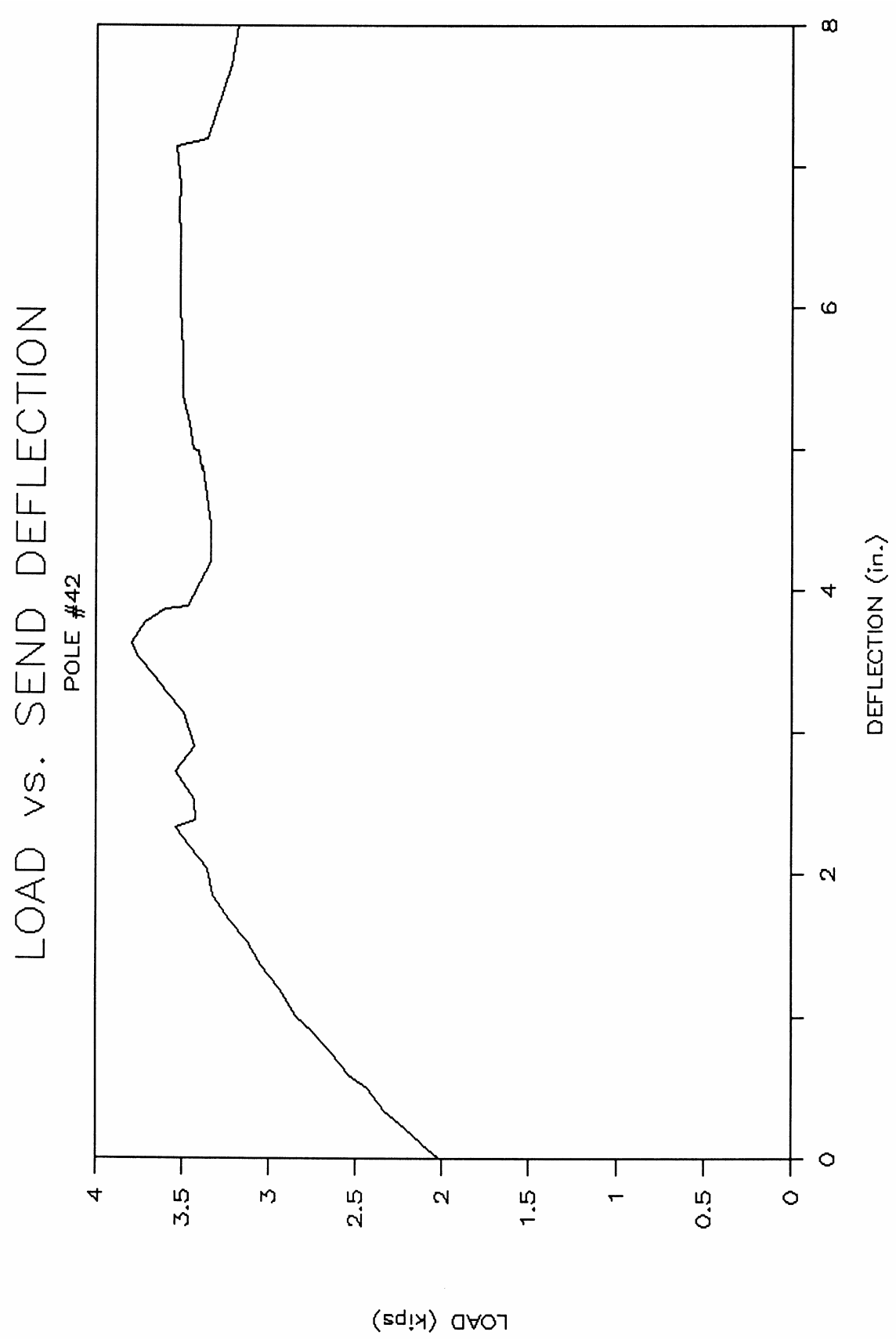
LOAD vs. SEND DEFLECTION
POLE #42
LOAD (kips)
4
3.5
3
2.5
2
1.5
1
0.5
0
0
2
4
6
8
DEFLECTION (in.)

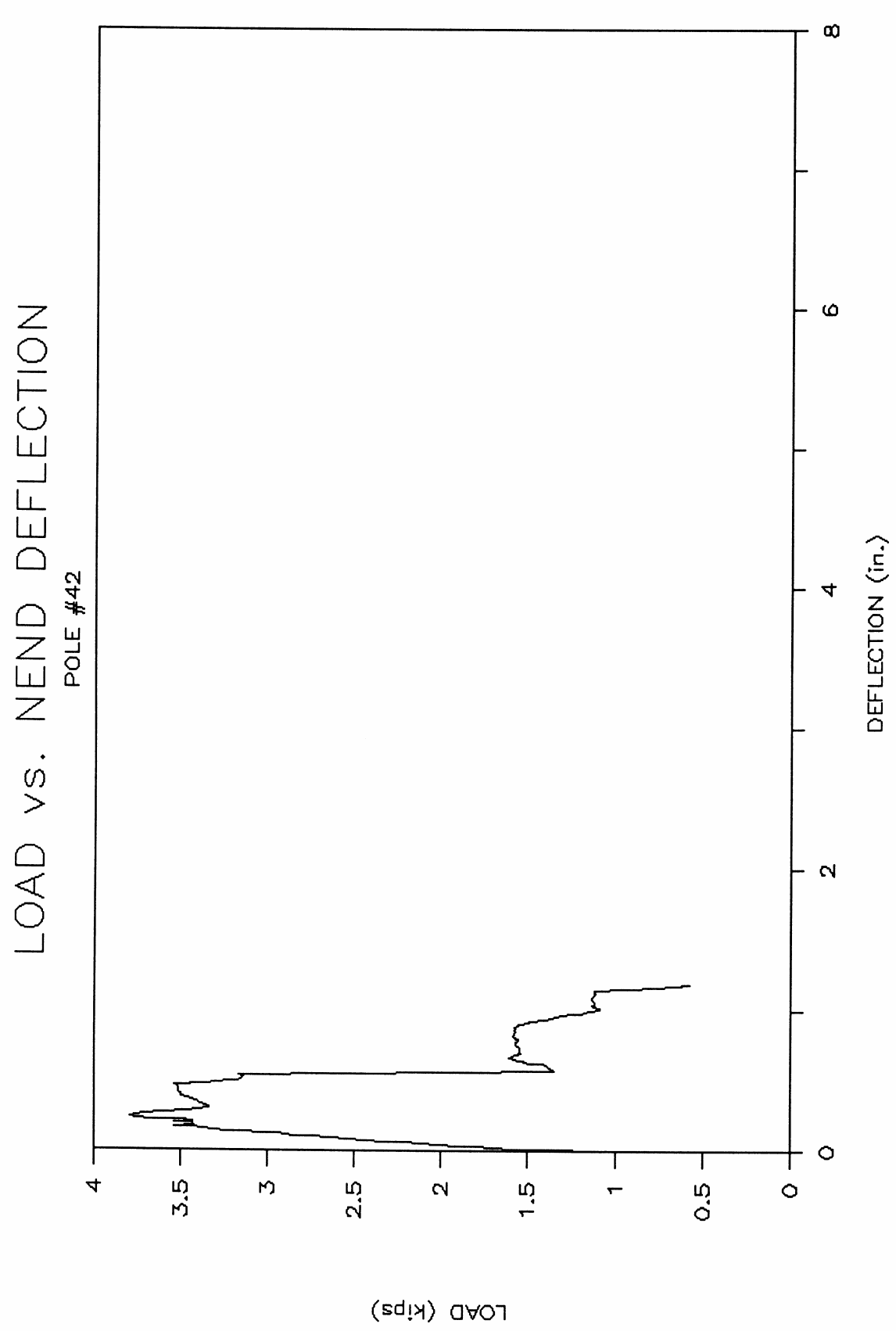
LOAD vs. NEND DEFLECTION
POLE #42
LOAD (kips)
4
3.5
3
2.5
2
1.5
1
0.5
0
0
2
4
6
8
DEFLECTION (in.)

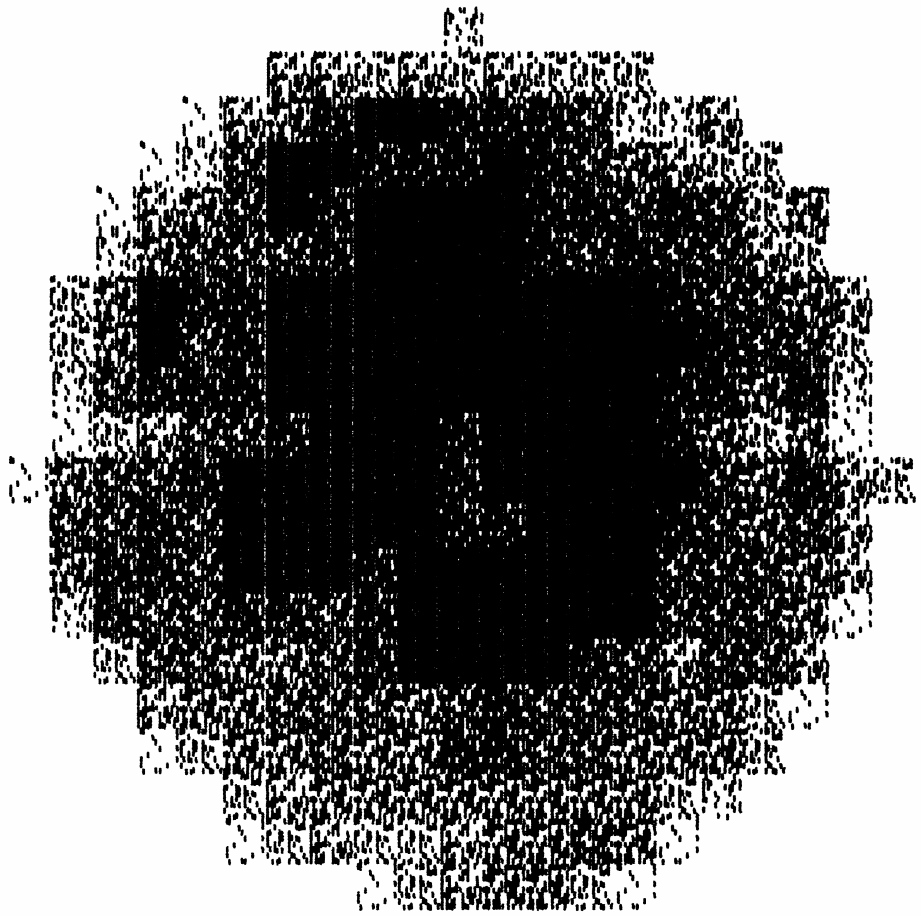

POLE IDENTIFICATION # 4213
IMAGED ON 11-17-1988
CIRCUMFERENCE (IN.) 22.25

<0.300
0.338
0.375
0.413
0.450
0.488
0.525
0.563
>0.600

SOURCE POSITION ERROR = -.0003
DETECTOR POSITION ERROR = +.0000

MIN+ MIN- MAX+ MAX- STRENGTH QUIT

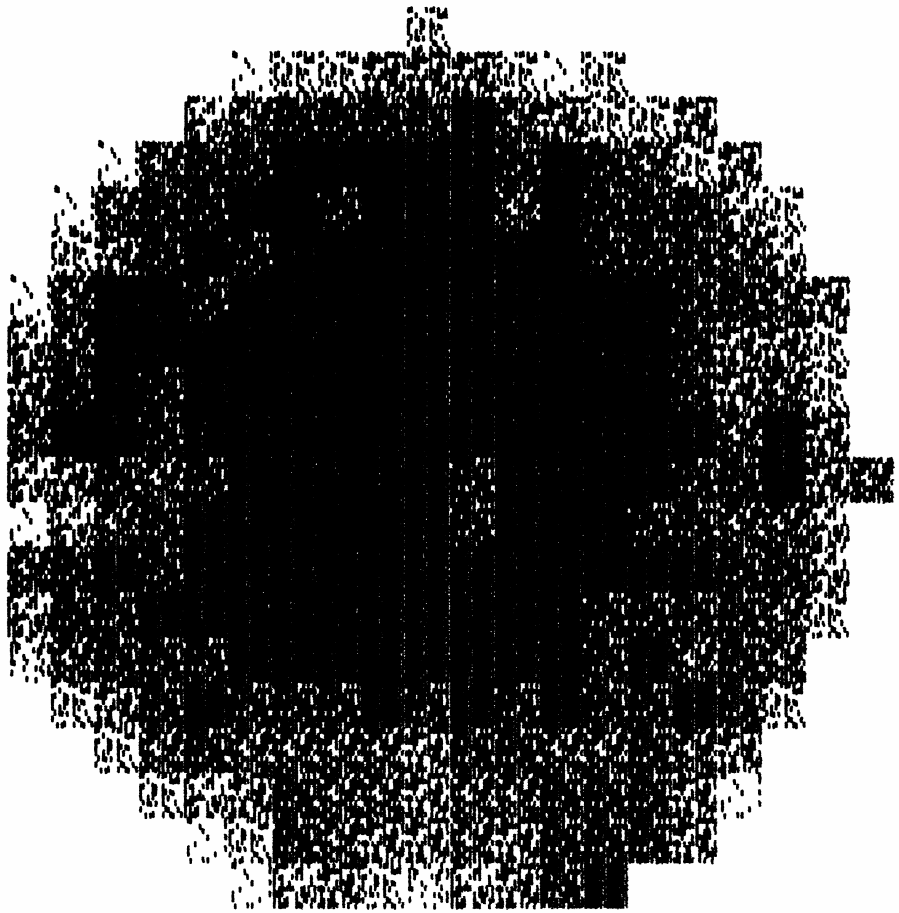

POLE IDENTIFICATION # 4212
IMAGED ON 11-17-1988
CIRCUMFERENCE (IN.) 22.5

<0.300
0.338
0.375
0.413
0.450
0.488
0.525
0.563
>0.600

SOURCE POSITION ERROR = -.0009
DETECTOR POSITION ERROR = +.0002

MIN+ MIN- MAX+ MAX- STRENGTH QUIT

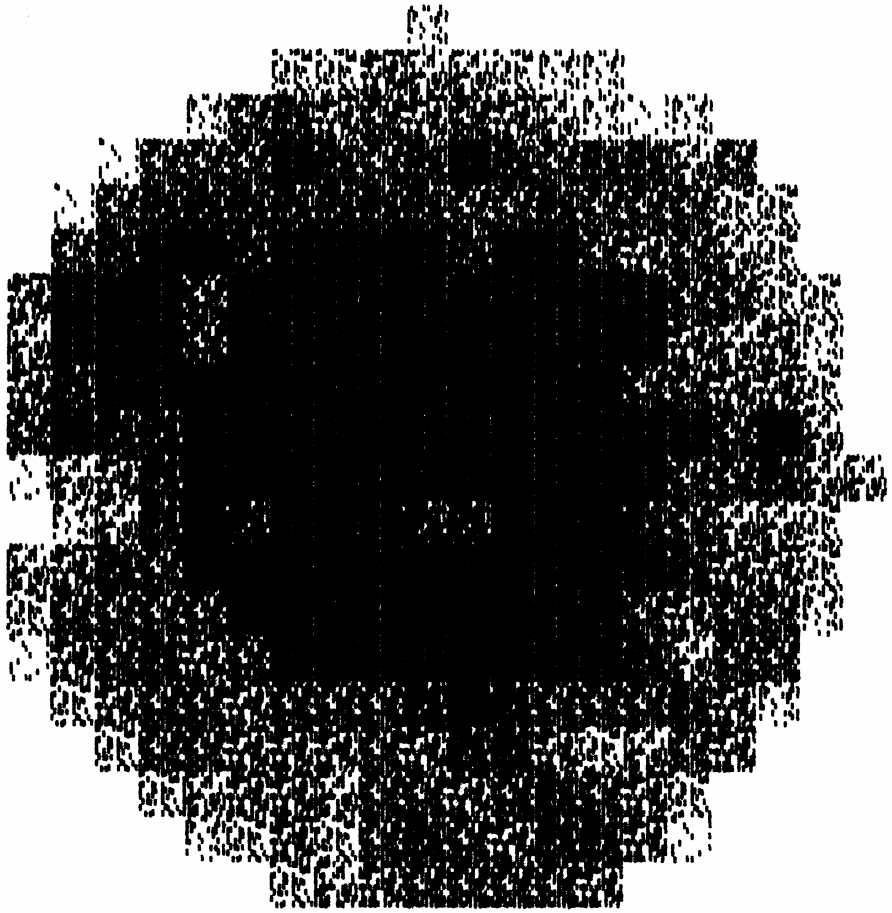

POLE IDENTIFICATION # 4211
IMAGED ON 11-17-1988
CIRCUMFERENCE (IN.) 22.25

<0.300
0.338
0.375
0.413
0.450
0.488
0.525
0.563
>0.600

SOURCE POSITION ERROR = -.0003
DETECTOR POSITION ERROR = +.0007

MIN+ MIN- MAX+ MAX- STRENGTH QUIT

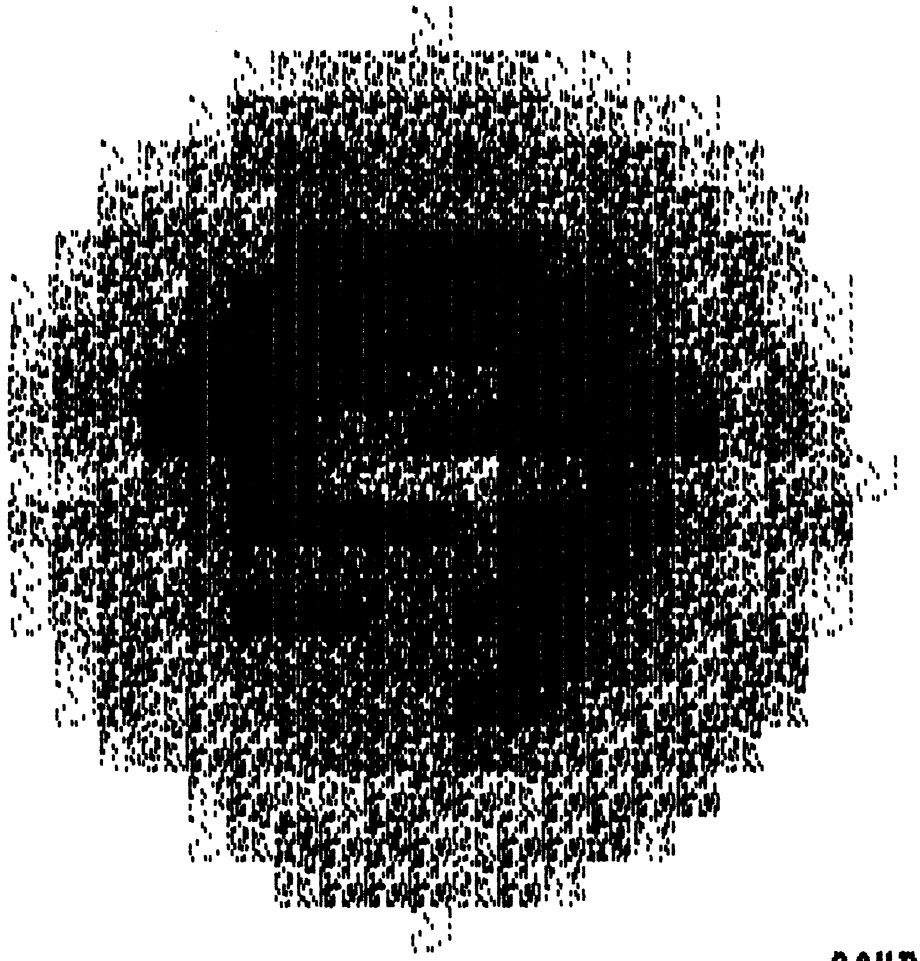

POLE IDENTIFICATION # 4200
IMAGED ON 11-17-1988
CIRCUMFERENCE (IN.) 22.5

<0.300
0.338
0.375
0.413
0.450
0.488
0.525
0.563
>0.600

SOURCE POSITION ERROR = -.0012
DETECTOR POSITION ERROR = +.0004

MIN+ MIN- MAX+ MAX- STRENGTH QUIT

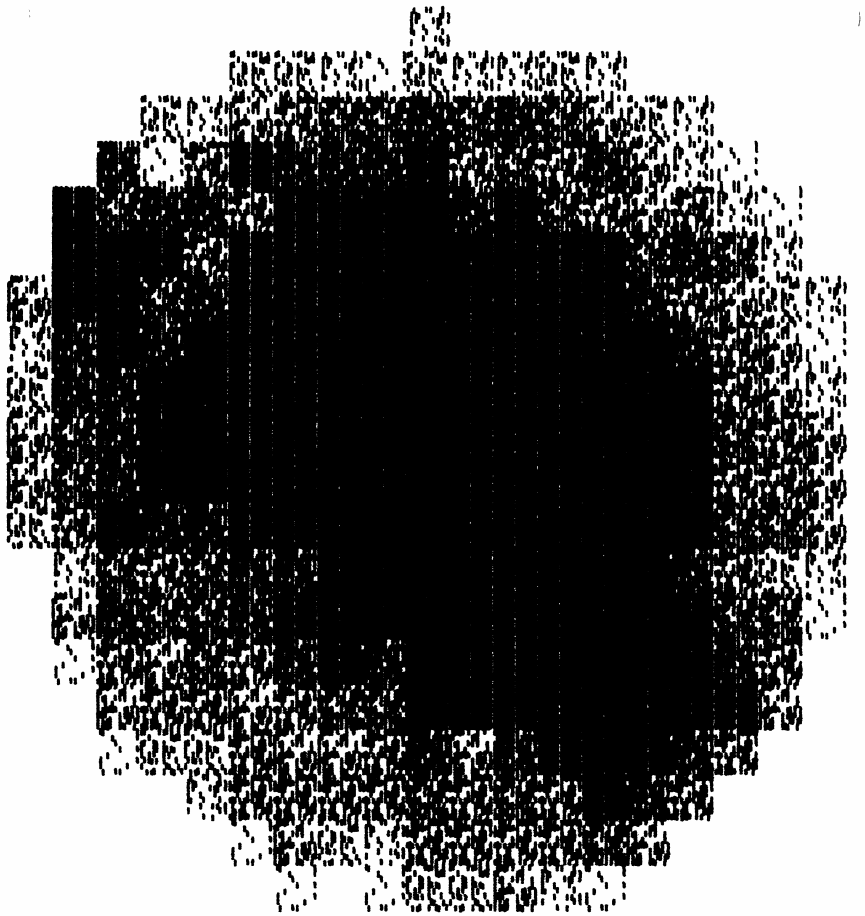

POLE IDENTIFICATION # 4201
IMAGED ON 11-17-1988
CIRCUMFERENCE (IN.) 23

<0.300
0.338
0.375
0.413
0.450
0.488
0.525
0.563
>0.600

SOURCE POSITION ERROR = -.0022
DETECTOR POSITION ERROR = +.0002

MIN+ MIN- MAX+ MAX- STRENGTH QUIT

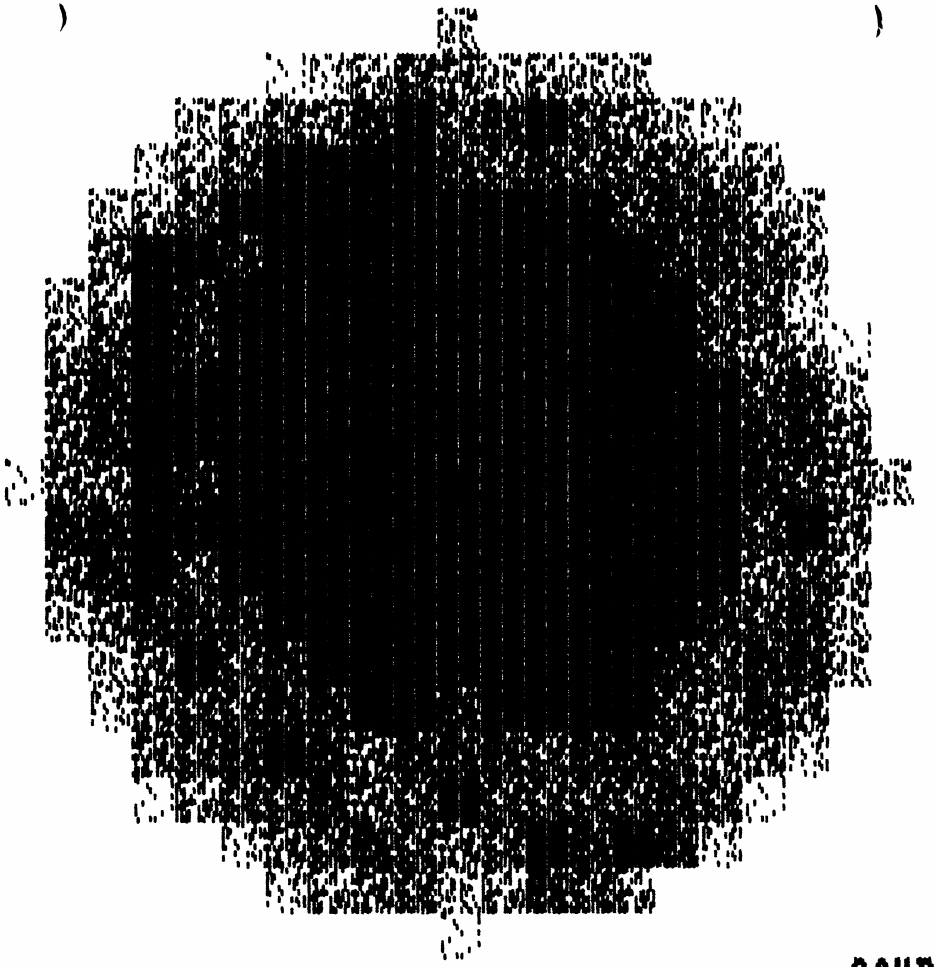

POLE IDENTIFICATION # 4202
IMAGED ON 11-17-1988
CIRCUMFERENCE (IN.) 23

<0.300
0.338
0.375
0.413
0.450
0.488
0.525
0.563
>0.600

SOURCE POSITION ERROR = -.0004
DETECTOR POSITION ERROR = +.0002

MIN+ MIN- MAX+ MAX- STRENGTH QUIT

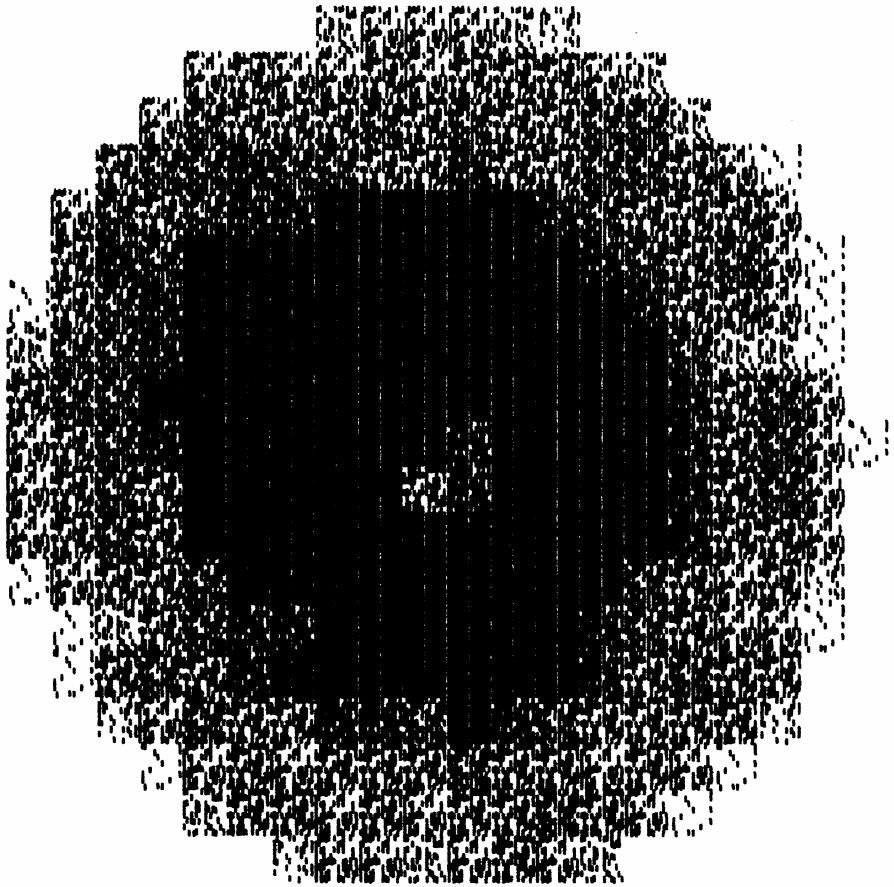

POLE IDENTIFICATION # 4203
IMAGED ON 11-17-1988
CIRCUMFERENCE (IN.) 23.25

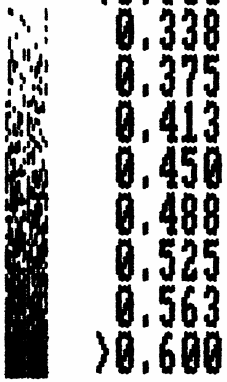

SOURCE POSITION ERROR = +.0004
DETECTOR POSITION ERROR = +.0011

MIN+ MIN- MAX+ MAX- STRENGTH QUIT

BIBLIOGRAPHY

1. Goodman, J.R., M.D. Vanderbilt, M.E. Criswell, J. Bodig, “Probability-Based Design of Wood Transmission Structures – Volume 1: Strength and Stiffness of Wood Utility Poles,” EPRI EL-2040 (September 1981).

2. Miller, W.H., "Design and Implementation of a Portable Computerized Axial Tomography System for Field Use, "Nuclear Instr. & Methods, A-270 (1988).

3. Miller, W.H., "The Design of a Portable CAT Scanner for Utility Pole Inspection, "Trans. of Am. Nuclear Soc., 52, 350 (June 1986).

4. Miller, W.H., "Non-Destructive Testing of Wooden Utility Poles Using a Prototype, Portable Computerized Axial Tomography Scanner," American Power Conference (April 1988).

5. EPRI – Technical Brief, RP 1352, Sheet No. 77 (1986), TB.ESD.16.8.86.

6. Bodig, Jozsef. “Innovative Strength Testing Using NDE Devices”, Innovative Wood Pole Management Using Nondestructive Strength Testing, Ft. Collins, CO, October 1986.

7. Bodig, J. and B.A. Jayne, Mechanics of Wood and Wood Composites, Van Nostrand Reinhold, New York (1982).

8. Toole, E.R., “Reduction in Crushing Strength and Weight Associated with Decay by Rot Fungi,” Wood Science, Vol. 3, No. 3 (1971).

9. Toole, E.R., “Effect of Decay on Crushing Strength,” Forest Products Journal, Vol. 19, No. 9 (1969).

10. Schniewind, A.P., Ohgama, T. Aoki, Tadashi Yamada, “Effect of Specific Gravity, Moisture Content, and Temperature on Fracture Toughness of Wood,” Wood Science, Vo. 15, No. 2 (October 1982).

11. Schniewind, Arno P. et al. Wood: Its Structure and Properties, “Mechanical Behavior and Properties of Wood” Educational Modules for Materials Science and Engineering (EMMSE) Project Materials Research Laboratory The Pennsylvania State University, University Park, PA

VITA

Howard David Thomas was born on a farm in Callaway County, Missouri which is located near the town of Mokane. He attended South Callaway RII schools and graduated in 1981. Upon high school graduation he enrolled at the University of Missouri – Columbia and he received his Bachelor of Science Degree in Civil Engineering in December of 1985. He has either been enrolled in graduate school or working in the civil engineering field since that time. He has been a licensed Professional Engineer since 1991 and is currently in the process of taking the certification test to become a licensed Architect. He is currently employed as the Ozark Unit Chief for the Design and Development Division of the Missouri Department of Conservation. In this position he supervises the professional design, construction and maintenance services provided to the department for the southern half of the state. He is married to a beautiful wife and has two lovely daughters.